SYNERGY NOT ANTAGONISM IN ANTIOXIDANT DEFENSES: THE UNANTICIPATED EFFECT OF ELECTRON DONORS ON CATALASE-PEROXIDASE FUNCTION

by

Elizabeth Ngwane Ndontsa

A dissertation submitted to the Graduate Faculty of
Auburn University
in partial fulfillment of the
requirements for the Degree of
Doctor of Philosophy

Auburn, Alabama
May 05, 2013

Keywords: peroxidase, catalase, catalase-peroxidase, ABTS, pH dependence, compound III

Approved by

Douglas C. Goodwin, Chair, Associate Professor of Chemistry and Biochemistry
Holly R. Ellis, Associate Professor of Chemistry and Biochemistry
German Mills, Associate Professor of Chemistry and Biochemistry
Christian R. Goldsmith, Associate Professor of Chemistry and Biochemistry

Abstract

     Catalase-peroxidases, also called KatGs, have raised considerable interest due to their role in the activation of isoniazid, an anti-tubercular pro-drug for *Mycobacterium tuberculosis*. KatGs are heme-dependent enzymes and are primarily known as H_2O_2 scavengers. As the name suggests, they catalyze the decomposition of H_2O_2 by catalatic and peroxidatic mechanisms using a single active site. Despite the progress made during the past decade in understanding the structure-function relationships of KatGs, very little is known about the connectivity/interplay between the catalatic and peroxidatic functions. The initial step for both catalytic processes is the heterolytic reduction of H_2O_2 to H_2O, giving rise to a two-electron oxidation of the ferric enzyme to a ferryl-porphyrin cation radical intermediate, compound I (i.e., $Fe^{IV}=O[porphyrin]^{\bullet+}$). At this point, the reduction of compound I to the ferric state differs for both the catalase and peroxidase activities. To complete the catalase reaction, compound I returns to the ferric state by oxidation of another H_2O_2 to form O_2 and H_2O. However, the peroxidase reaction is completed by the subsequent reduction of compound I to compound II (i.e., $Fe^{IV}=O$), and subsequently, to the ferric state at the expense of two equivalents of an exogenous electron donor. This yields H_2O and two equivalents of the corresponding radical of the donor. The ability of one activity to dominate over the other depends on several factors including: pH, the concentration of H_2O_2, and the availability of an appropriate exogenous electron donor. Catalase activity is optimal near neutral pH (i.e., pH ~ 7.5), whereas peroxidase activity is optimal under acidic conditions (i.e., pH ~ 4.5) and requires an exogenous electron donor. More so, peroxidase activity is favorable at

low H_2O_2 concentrations. Conversely, catalase activity can sustain high concentrations of H_2O_2 without the enzyme inactivation. Clearly, conditions which favor the peroxidase activity do not coincide with those that favor the catalase activity. Thus, the simplest way to understand the mechanism of both functions in KatG has often been to superimpose both the catalatic and peroxidatic mechanisms. Based on this mechanism, both activities should be mutually antagonistic and peroxidatic electron donors should inhibit the catalase activity. In fact, it has been established that the common peroxidatic electron donor *o*-dianisidine does inhibit the catalase activity of KatG from *Escherichia coli* at pH 7.5. Strikingly, in this dissertation, we report the dramatic stimulation of the catalase activity of KatG from *Mycobacterium tuberculosis* (MtKatG) by up to 14-fold, in the presence of several common peroxidatic electron donors. The stimulatory effect was most prominent under conditions favorable to peroxidase activity (i.e., acidic pH and low H_2O_2 concentrations). In particular, we observed that aromatic amines were better stimulators than other donors like pyrogallol and ascorbate. In the absence of a peroxidatic electron donor, we observed a "low-K_M" and "high-K_M" component for catalase activity at pH 5.0. The inclusion of peroxidatic electron donors increased the apparent k_{cat} for the "low-K_M" component at pH 5.0. During stimulated catalase activity, very little of the donor (0.008 eq./H_2O_2 consumed) accumulated in its oxidized state. This is far less than the amount expected for normal peroxidatic turnover where two equivalents of oxidized donor is anticipated for every equivalent of H_2O_2 consumed. Evaluation of the dominant enzyme intermediates by stopped-flow spectroscopy revealed that a compound III-like (i.e., $Fe^{III}\text{-}O_2^{\bullet-}[MYW]^{\bullet}$) intermediate dominated during electron donor-stimulated catalase activity of MtKatG, and this intermediate converted directly to the ferric state upon depletion of H_2O_2. In the absence of the donor, a similar species persisted and returned slowly to the ferric state, but only long after H_2O_2 was fully consumed.

Clearly, the catalase mechanism and the interrelationship between the catalase and peroxidase functions of KatG are much more complex than has been previously appreciated, and pH plays an important factor in both activities. Likewise, evidence is accumulating showing that pH also induce structural changes that markedly affect the catalase activity of KatG. Recent reports have shown that an invariant arginine residue (R418 in MtMatG numbering) is critical to the catalase activity, as it undergoes a conformational switch that is highly pH-dependent. KatG also possesses a unique covalent adduct (M255-Y229-W107 in MtKatG numbering) that is critical to its catalase activity. At pH 4.5, the arginine (R418) side chain is oriented away from the KatG-unique M255-Y229-W107 covalent adduct (i.e., "R" conformation). Whereas at pH 8.5, the side chain of this arginine is oriented toward the M255-Y229-W107 covalent adduct (i.e., "Y" conformation). The pH-dependence of the stimulatory effect and that of the R418 side chain and its role in catalatic turnover prompted us to evaluate the connection between the two. Substitution of R418 by alanine, R418A, produced an enzyme with almost no catalase activity at pH 7.0. However, catalase activity increased by nearly two orders of magnitude as pH was lowered to 5.0. Furthermore, at pH 5.0, peroxidatic electron donors such as 2,2'-azino-bis(3-ethyl-benzthiazoline-6-sulfonate) [ABTS] further stimulated the catalase activity of R418A by an order of magnitude. This was similar to the extent observed for wild-type and R418K KatG. Unlike the wild-type and R418K KatG, a greater amount of oxidized donor radical (i.e., $ABTS^{\bullet+}$) was produced per H_2O_2 consumed by R418A KatG. This was highly H_2O_2 concentration dependent such that far more donor radical accumulated at low H_2O_2 concentrations. Stopped-flow studies showed that a compound III-like intermediate dominated during electron donor-stimulated catalase activity of R418A and R418K KatG, and converted directly to the ferric state. Under these conditions, the time required for H_2O_2 consumption and return of the ferric state was

3 to 4 fold slower for R418A KatG than for wild-type and R418K KatG. However, in the absence of ABTS, the return of the ferric state lagged far behind the conclusion of H_2O_2 consumption by wild-type and both R418 variants. Even though the presence of ABTS seemed to resolve this problem for all three enzymes, it did so without a direct impact on the intermediates of the catalatic cycle. From our data we conclude that the stimulatory effect of electron donors is due to their ability to prevent the accumulation of intermediates which are inactive with respect to catalase activity. The R418A substitution, in addition to showing the conversion of the compound III-like intermediate to the ferric state, also appears to have a greater propensity for off-pathway electron transfers which produce catalase-inactive intermediates. Our results have potentially far reaching implications. The ability of peroxidatic electron donors to stimulate catalatic turnover instead of inhibition points toward a much more central role for peroxidase substrates in the unusual catalase mechanism of KatG. Clearly, the capacity of KatG to diffuse threats posed by H_2O_2 is far greater than first thought. The conditions which favor the stimulatory effect coincide with those observed during antimicrobial defenses such as the oxidative burst. This raises the importance of peroxidatic electron donors in accounting for the resistance of pathogens to H_2O_2 and stimulates the concern to investigate the identity and binding site of compounds which serve this capacity.

Acknowledgments

My sincere thanks go to my advisor Dr. Douglas Goodwin. He has been a great mentor, always treating his students with care and patience. The preparation of this dissertation would not have been possible without his encouragement and assistance. His contribution to my career and professional life will forever remain priceless.

My gratitude goes to my committee members, Dr. Holly Ellis, Dr. German Mills, and Dr. Christian Goldsmith, for their contribution and support. I am thankful to Dr. Angela Calderón for her time, suggestions, and corrections. I am also grateful to Dr. Eduardus Duin for his assistance.

I would also like to thank my research colleagues Dr. Robert Moore, Dr. Shalley Kudalkar, Dr. Yu Wang, Haijun Duan, and Olive Njuma for their wonderful support and friendly environment.

My greatest appreciations go to my family, relatives and friends, for their constant love and support throughout my studies.

I dedicate this work to my mum (Mrs. Helen Kana Ngwane), my dad (Mr. Andrew Ngwane Njimily), and my siblings for always loving and being there for me through the happy and tough moments I encountered during my graduate school career.

Table of Contents

List of Figures

List of Tables

Chapter one: Literature Review

1.1. Reactive Oxygen Species

Commonly abbreviated as ROS, reactive oxygen species are a class of oxygen containing molecules and ions formed as a result of partial reduction of dioxygen (*1-3*). These include oxygen radicals (*4*) such as superoxide ($O_2^{\bullet -}$), hydroxyl ($OH^{\bullet}$), peroxyl ($ROO^{\bullet}$), alkoxyl ($RO^{\bullet}$) radicals and nonradicals, such as hydrogen peroxide (H_2O_2), singlet oxygen ($^1O_2$), and ozone (O_3). There are several sources/mechanisms for generation of ROS in biological systems. These species are of great importance in biology because of their capacity to do great damage to biomolecules, and because they are formed as a result of oxidative metabolism. In terms of generation, the most common source begins with the incomplete reduction of oxygen during cellular respiration.

Historically, ROS in a biological context have been understood almost entirely in a negative light. However, more recently it has been demonstrated that some ROS have beneficial signaling functions (*5-8*). This, of course, depends on the ROS in question and its relative concentration. For example, $^{\bullet}OH$ at essentially any concentration is expected to induce damage in the biomolecules with which it reacts (*5*). Conversely, H_2O_2, at relatively low concentration, has been shown to serve an important role in signaling processes, such as the regulation of kinase-driven pathways (*5-9*). H_2O_2 signals can also fine-tune responses to growth factors and cytokines to control cell division, differentiation, and migration (*10*).

1.2.   Oxygen Structure and Reactivity

Aerobic respiration relies on dioxygen (O_2) as a terminal electron acceptor to generate by oxidative phosphorylation much of the ATP necessary for cellular activity. Electronically, O_2 exists as a triplet molecule in its ground state in that its $_{2p}$* antibonding orbital is occupied by two unpaired electrons (Fig. 1. 1) (*11*). In contrast to this, the vast majority of organic biomolecules are in a singlet ground state, and the reaction of triplet molecules with singlet molecules is spin forbidden (*12-15*). Therefore, the oxidation of any atom or molecule by O_2 requires that the incoming electrons be of parallel spin. However, to fulfill the Pauli Exclusion Principle, the pair of electrons in an atomic or molecular orbital must have opposite spins (i.e., +1/2 and -1/2). This implies that O_2 should accept its electrons one at a time. Thermodynamically, this half reaction (**1.1**) is unfavored since the reduction potential is negative (i.e., -0.33V).

$$O_2 + e^- \longrightarrow O_2^- \qquad\qquad (1.1)$$

However, if coupled to a favored half reaction, the overall reaction may be thermodynamically favored. This implies that the spin restriction of dioxygen is a kinetic barrier that prevents the oxidation of organic biomolecules regardless of thermodynamic considerations. Based on the fact that the spin restriction affects the kinetics of these reactions, it must manifest itself in the activation energy (*15*). In order to overcome this activation barrier, there are basically several alternatives: The first option involves a radical chain mechanism where the first products are $O_2^{\bullet-}$ with an organic free radical (in this case, the spin is conserved, i.e., S=1 both for reactants and products). However, these types of mechanisms are not commonly observed in enzymes. Next, it could also be envisioned that triplet dioxygen could convert to a singlet state upon binding to an organic biomolecule (i.e., transition state). However, this is unlikely because the spontaneous

Orbital
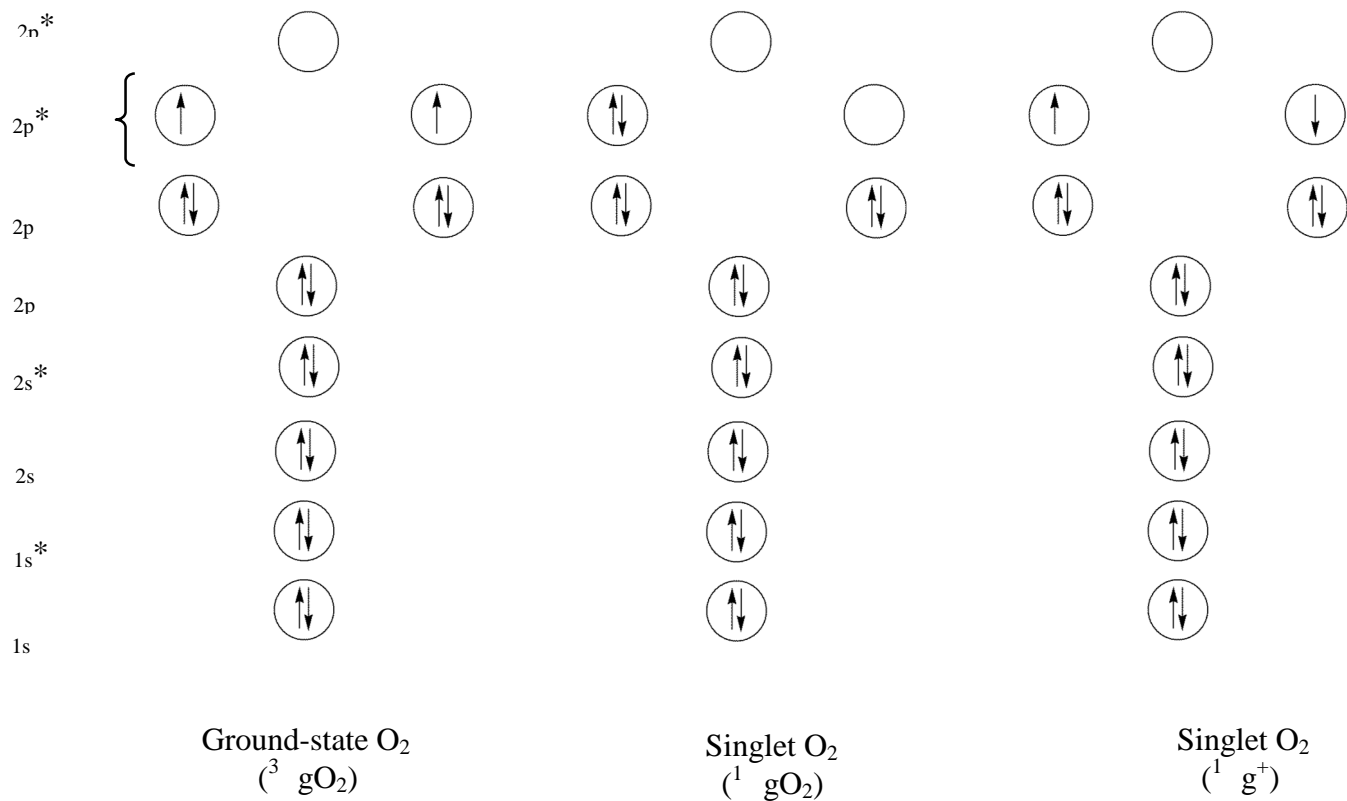
Figure 1.1. Molecular orbital diagram for dioxygen in its ground and excited singlet states.

conversion of triplet dioxygen to a singlet molecule is slow and can be estimated to occur at 10^{-7} s or longer (i.e., much longer than the lifetime of an excited triplet state) (*15*). Finally, spin conservation can also be achieved through transition metal ions with unpaired electrons where the metal serves as a donor, an example is shown below:

$$M^n + O_2 \longrightarrow M^{n+1} \cdot O_2^{\bullet-} \qquad (1.2)$$
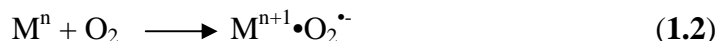
Such systems are widespread in enzymes, and this explains why oxidase enzymes and other enzymes which otherwise interact with O_2 contain transition metals. Examples of some transition metals commonly found in living systems include iron, copper, cobalt, and molybdenum. Among these, iron is by far the most commonly utilized. Interestingly enough, a great fraction of iron found in living organisms is associated with proteins in the form of heme, a prosthetic group which consists of protoporphyrin IX and iron where the iron is most commonly observed in either its (+2) or (+3) oxidation states. Despite its catalytic role in the "autoxidation" of biomolecules, iron is very toxic because "free iron" inside the cell can readily facilitate the generation of free radical species that can cause oxidative stress and cellular damage. In a similar way, although dioxygen serves as a vital source for ATP generation, it can be very toxic when it is converted to superoxide radical ($O_2^{\bullet-}$) through a single-electron reduction.

1.3. Superoxide: Reactivity and Chemistry

Nearly all aerobic organisms suffer threats from superoxide radical ($O_2^{\bullet-}$). Superoxide radicals are generated by a single-electron reduction of dioxygen either as a result of enzymatic catalysis or by "electron leaks" from various electron transfer processes (*16*). Superoxide is relatively stable in several organic solvents, but short-lived in aqueous solution. The latter is due to the rapid dismutation of $O_2^{\bullet-}$ to form hydrogen peroxide and O_2. Superoxide is the primary

ROS generated in the cell, but this initiates a cascade of subsequent reactions that form other ROS such as H_2O_2 and hydroxyl radical. Moreover, superoxide radicals can oxidize [4Fe-4S] cluster-containing enzymes such as aconitase or dihydroxy-acid dehydratase (*17*). In order to prevent the formation and accumulation of superoxide radicals, organisms have developed mechanisms to defend themselves against such species. Superoxide dismutases represent the most common and efficient mechanism by which cells limit the formation of superoxide.

The dismutation of $O_2^{\bullet-}$ to H_2O_2 can occur nonenzymatically, or it can be catalyzed by the enzyme superoxide dismutase (SOD). At pH 7.0, the rate constant for the

$$2O_2^{\bullet-} + 2H^+ \longrightarrow H_2O_2 + O_2 \qquad\qquad (\textbf{1.3})$$

uncatalyzed reaction is 5×10^5 $M^{-1}s^{-1}$. SOD produces a near four order of magnitude increase in rate, yielding a rate constant that is essentially at the diffusion limit (1.6×10^9 $M^{-1}s^{-1}$) (*17*). Unlike $O_2^{\bullet-}$, H_2O_2 is a neutral singlet molecule, and it is much more stable. Some benefits of H_2O_2 include its role in signaling processes (e.g., activation of transcription factors) and its use in defensive mechanisms against microbial invaders. Indeed, it is well known that H_2O_2 plays a central role in the host defenses of plants and animals (*4, 18-19*). Therefore, considering the benefits and chemistry of H_2O_2, can it be considered a safe haven? Clearly, the answer is no. To some extent, it is reactive itself, and large amounts of it can inactivate important enzymes. More importantly, H_2O_2 represents a threat because it can react further to yield more reactive and toxic compounds. For example, it can readily react with reduced transition metals such as iron or copper to generate the highly oxidizing hydroxyl radical ($^{\bullet}OH$) by Fenton chemistry. The hydroxyl radical is the most reactive of all ROS. With a reduction potential of 2.8 V, it can oxidize virtually any biological molecule, and it does so in most cases at diffusion-controlled

$$Fe^{2+} + H_2O_2 \longrightarrow Fe^{3+} + {}^{\bullet}OH + OH^- \qquad \text{(Fenton Reaction)}$$
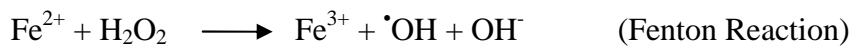
rates. Molecular damage observed by $^{\bullet}OH$-generating system induces lipid peroxidation, DNA/RNA base modification and strand breaks, protein oxidation and membrane destruction (*4*, *20-24*). Based on the fact that cells have no enzymatic mechanism to eliminate $^{\bullet}OH$, it is imperative that the agents that lead to its formation be strictly controlled. Thus, it is not surprising to find that transition metals, Fe in particular, are complexed with proteins during absorption and transport such that they are sequested from extensive interaction with O_2. Likewise, where electron transfer occurs in biological systems, O_2 is prevented from interacting inappropriately with those systems to a great extent. When interaction between transition metals and O_2 is necessary, those systems are designed to limit the release of potentially reduced O_2 species. The most prominent exception here is when $O_2^{\bullet-}$ generation is desired as a defense against microbial invaders. The NADPH oxidase of the oxidative burst mechanism is a prominent example.

Inspite of all these protective measures, production of $O_2^{\bullet-}$ and H_2O_2 cannot be entirely avoided. Therefore, there are biological strategies to deal with each of these. As mentioned above, SOD efficiently scavenges $O_2^{\bullet-}$. Surprisingly, across all of biology there are only two general mechanisms by which cells deal with H_2O_2, namely peroxidase and catalase.

1.4. Peroxidase

Peroxidases are enzymes that use peroxides (ROOH) as electron acceptors to catalyze a wide range of oxidative transformations. Their molecular weight ranges from 17 to 87 kDa and their polypeptide chain lengths from 153 to 753 amino acids. More often than not, they are observed as monomeric proteins. Peroxidases are widely spread in nature and are implicated in various important physiological and developmental processes. In prokaryotes and lower

eukaryotes (protists and fungi), peroxidases have been implicated in the virulence of pathogenic species (*25-30*). In mammals, they are involved in diverse biological processes ranging from bactericidal immune responses to hormone production and regulation (*31-32*). In plants, peroxidases are necessary for hormone regulation, lignin synthesis, defense against pathogenic organisms, and cross-linking of cell wall components (*33-35*). Peroxidases can be divided into two broad categories: those that are heme-dependent and the non-heme enzymes (*36*).

1.4.1.   Non-heme Peroxidases

The non-heme members are not evolutionary related and they contain either metals or specific metal-free prosthetic groups. They constitute five independent families among which the thiol peroxidases represent the largest and contain more than 1000 members classified in two different subfamilies (i.e., glutathione peroxidases and peroxiredoxines). The other non-heme families include alkylhydroperoxidase, non-heme haloperoxidase, and NADPH peroxidase.

The superfamily of glutathione peroxidases (GPx) contains eight members classified on the basis of primary structure similarities, specific substrate accessibility, and spatial expression (*37-38*). They are widely-spread in mammals and among them, GPx-8 has been the latest to be discovered. The selenium-containing GPx enzymes reduce H_2O_2 and organic hydroperoxides by using glutathione as an electron donor. However, other homologs of GPx prefer to use thioredoxin as the electron donor instead of glutathione. These are found primarily in invertebrates and plants and contain cysteine in the catalytic center (*39*). The mammalian isoforms GPx1-4 are selenoproteins with a selenocysteine (Sec) in the catalytic pocket (*40*).

1.4.2.   Heme-dependent Peroxidases

7

Heme-dependent peroxidases are the most abundant forms of peroxidases found in nature, and the majority of them contain heme *b* as the prosthetic group. They can be divided into two large superfamilies. Both superfamilies arose independently, thus, their primary, and tertiary and even the nature of their prosthetic group greatly differ. One superfamily is found in plants, bacterial and fungal species (*41*) whereas members of the other are found predominantly in animals (but sometimes present in fungi and bacteria) and are known as the peroxidase-cyclooxygenases (*42-43*). In addition to these two large superfamilies, there are also small heme peroxidases that can be classified into 3 different families: Di-heme cytochrome c peroxidase (DiHCcP), Dyp-type peroxidases (Dyp-Prx), and heme-haloperoxidases (HalPrx). All heme peroxidases catalyze the reduction of H_2O_2 to H_2O with concomitant one- or two-electron oxidation of a variety of organic and inorganic (e.g., halides) substrates.

1.4.2.1.   Peroxidase-Cyclooxygenase

Peroxidase-cyclooxygenases play an important role in the innate immune system of mammals and bacteria. The mammalian members include myeloperoxidase, eosinophil peroxidase, lactoperoxidase, and thyroid peroxidase (*44*). The first three are central to the production of hypohalous acids (hypohalide ions) and hypothiocyanate. They are a cornerstone of innate immunity and form a formidable defense against invading microorganisms. Conversely, thyroid peroxidase is central to the production of the metabolic regulatory hormone, thyroxine. The bacterial members are peroxinectins, peroxidasins, and primordial peroxidases. The mammalian members have been extensively characterized, and they have an assymetrical distorted heme with peculiar redox properties (*45-46*). This heme geometry together with the conserved distal and proximal residues is critical to the function of mammalian peroxidases

because it facilitates the binding and oxidation of small anionic substrates like halides (Cl, Br, I) and thiocyanate.

1.4.2.2. Small Family Heme Peroxidases

The small family of heme peroxidases contains 3 members namely: Di-heme cytochrome c peroxidase (DiHCcP), Dyp-type peroxidases (Dyp-Prx), and heme-haloperoxidases (HalPrx). All three members of this superfamily contain heme c as the cofactor which is covalently linked to the polypeptide chain. Among these, the di-heme cytochrome c peroxidase family is unique because it contains two heme groups (*47*). It reduces H_2O_2 peroxide to H_2O using cytochrome c or cupredoxin. The Dyp-type peroxidases are popular in biotechnology due to their ability to degrade various dispersive dyes. However, their physiological roles as well as their physiological electron donors remain unknown.

1.4.2.3. Plants, Fungal, and Bacterial Peroxidases

The non-animal superfamily consists of three major classes (*48*). Class I includes yeast cytochrome c peroxidase (CCP) and ascorbate peroxidase (AP). There are multiple isoforms of ascorbate peroxidases. One is the major form responsible for the removal of hydrogen peroxide in chloroplasts, whereas another does the same in the cytosol of higher plants. Finally, there are the bacterial enzymes called catalase-peroxidases. Class II enzymes contain four conserved disulfide bridges and two conserved calcium-binding sites. They consist of secretory fungal peroxidases such as lignin peroxidases (LiPs), manganese-dependent peroxidases (MnPs), and versatile peroxidases (VP). Finally, class III consists of secretory plant peroxidases such as horseradish peroxidase, and the guaiacol peroxidases. They also contain four conserved disulfide

bridges and two calcium ions. However, the placement of the disulfides differs from class II enzymes (*48-50*).

Generally, the catalytic mechanism of heme peroxidases involves two steps. The first step begins with the heterolytic reduction of hydrogen peroxide to form water and the ferryl-porphyrin π-cation radical intermediate, compound I (i.e., $Fe^{IV}=O[porphyrin]^{\bullet+}$) (*51*). In some cases, the radical is transferred by oxidation of a nearby amino acid (e.g., Trp 191 of cytochrome c peroxidase). To complete the peroxidase cycle, compound I returns to the ferric form by two sequential one-electron reductions at the expense of two equivalents of an exogenous electron donor. The enzyme is reduced first to a ferryl intermediate, compound II (i.e., $Fe^{IV}=O$), generating one equivalent of the donor radical, and the cycle is completed when compound II is reduced to the ferric state, generating a second equivalent of the donor radical and water (Fig. 1.2).

Structurally, there are features common to all three classes of the non-animal superfamily. They all contain a core ten-helix fold. Further, they all use heme *b* as a cofactor whose proximal ligand is an invariant histidine residue (*52*). The electronic character of the ligand is markedly influenced by a strictly conserved aspartate residue, which forms a strong hydrogen bond with the N_2 of the histidine imidazole. This strong hydrogen bond is purported to increase the anionic character of the histidine so as to enhance the stability of higher heme oxidation states and to help maintain the heme in a five-coordinate state. In addition, the distal pocket contains an invariant histidine which acts as a general base to facilitate the deprotonation of H_2O_2 and assist in the formation of compound I. Likewise, an adjacent arginine helps stabilize compound I by electrostatic interactions between the positive charge of its side chain
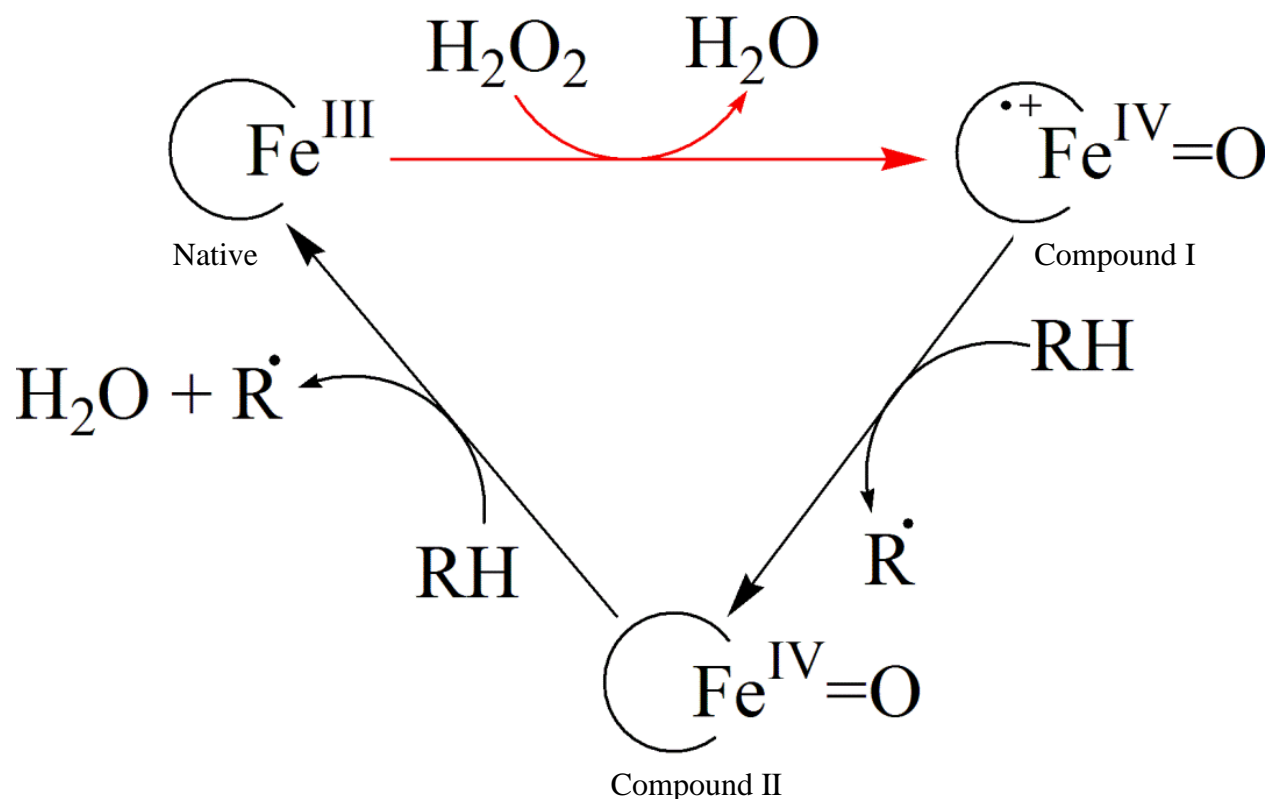
Figure 1.2. Catalytic cycle of monofunctional heme peroxidases. RH and R$^\bullet$ stand for reducing substrate and substrate's radical, respectively.

and the developing negative charge on the distal oxygen of the bound H_2O_2 during heterolytic O-O bond cleavge (*53-54*). The oxidation of several peroxidase susbtrates, including large aromatic compounds occurs at the exposed heme edge, a region accessible to solvent and comprising the heme methyl C18 and heme meso C20 protons (*55-57*).

1.5.   Catalase

The second strategy for disarming H_2O_2 is by catalase activity. Catalases are enzymes widely known for their ability to decompose large amounts of H_2O_2. They are ubiquituous and play an essential role in antioxidative mechanisms. Currently, more than 300 sequences are known, and they can either exist as heme or non-heme proteins (*58*). Among them are monofunctional catalases, bifunctional catalase-peroxidases, and manganese-containing catalases. Although they exhibit significant catalase activity, all three groups of catalases are unrelated on the basis of sequence and structure. The monfunctional (heme-containing) catalases are the most commonly found in nature and are widely characterized. The second less widespread group is the bifunctional (heme-containing) catalase-peroxidases, and is closely related by sequence and structure to plant peroxidases. Finally, the non-heme (manganese catalases) constitutes the third group.

1.5.1.   Non-heme Manganese Catalases

Manganese catalases are enzymes that contain a binuclear manganese complex within the active site instead of heme; and during catalysis, the metals cycle between Mn^{II}-Mn^{II}, and Mn^{III}-Mn^{III} oxidation states. They are widely distributed in eubacteria and archaea bacteria. The three-dimensional structures of two representatives have been determined: Mn-catalase from *Thermus*

thermophilus (*59*) and *Lactobacillus plantarum* (*60*). These enzymes are homohexamers with approximately 30 kDa per subunit, and each with a bridged Mn-center located within a conserved tightly packed four-helix bundle domain. The ligands for the dimanganese center are highly conserved and include a bridging glutamate residue, which anchors the two ions in the binuclear cluster, and each metal ion is further coordinated by one histidine and one glutamate bound to opposite faces (*61*). The mechanism for hydrogen peroxide dismutation in manganese catalases is substantially different from that observed in the heme-dependent catalases. There are no reactive intermediates involved during catalysis and both molecules of water are formed in one step (*62-63*). In addition, there is no temporal order in the oxidation and reduction stages and no free radical intermediates exist during turnover.

$$H_2O_2 + \{Mn_2(III, III)\} \longrightarrow O_2 + \{Mn_2(II, II) + 2H^+\}$$

$$H_2O_2 + \{Mn_2(II, II) + 2H^+\} \longrightarrow 2H_2O + \{Mn_2(III, III)\}$$
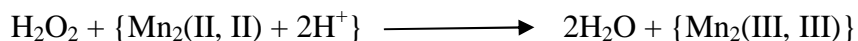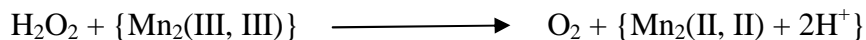
1.5.2. Heme-dependent Catalases

Typical (i.e., monofunctional heme-dependent) catalases are homotetrameric enzymes. They are ubiquitous in aerobic organisms, and their primary role centers on the protection of organisms from cytotoxic H_2O_2 or other reactive oxygen species derived therefrom. The size of typical catalases ranges from 200-340 kDa with four heme prosthetic groups (*64*). They are divided into three clades on the basis of amino acid sequence and structure (*65*).

The clade 1 catalases consist of approximately 500 residues per subunit with heme *b* as the prosthetic group. They are primarily plant enzymes with a subgroup found in bacteria. The clade 2 catalases are larger, close to 750 residues per subunit with heme *d* as the most common prosthetic group. This heme *d* is derived from heme *b* through a specific self-modification during

the first cycles of enzymatic activity (*66-67*). Finally, clade 3 enzymes have many features similar to clade 1. They use heme *b* and are of similar size. However, clade 3 enzymes stand out in their use of NADPH as a second redox active cofactor. NADPH binds 20 Å from the heme iron in a highly conserved environment and is not a compulsory cofactor for catalase turnover. The biological and biochemical roles of NADPH binding are not well understood. However, it is proposed that its binding prevents the formation of catalase-inactive intermediates (*62-68*). The subunits from all 3 clades have a core structure (~ 460 residues) with great similarity regardless of the organism. This highly conserved three-dimensional arrangement is known as the *catalase fold*. It comprises two globular domains (i.e., the -barrel and -helical domains) connected to each other by a long protein segment called the wrapping loop. This loop contains the helix that bears the heme proximal tyrosine residue. The central feature of the *catalase fold* is the -barrel domain. It consists of an anti-parallel eight-stranded -barrel, which includes at least six inserted -helices. The first half of the barrel (1- 4) typically consists of the residues that make the heme distal side, while the second half (5- 8) contributes to the NADP(H) binding side for those enzymes like human erythrocyte catalase which bind the nucleotide. Based on structural arrangements, the -barrel domain is preceded by an extended N-terminal arm, followed by the wrapping loop, and then by the -helical globular domain. The large subunit size of clade 2 catalase is due to the presence of an extra C-terminal domain that has approximately 150 residues. In contrast to the *catalase fold*, the C-terminal domain is not as well conserved. It contains a "flavodoxin-like" topology with no binding pockets for NADPH (Fig. 1.3, A and B).

The overall reaction of monofunctional catalases is the degradation of two molecules of hydrogen peroxide to two molecules of water and one molecule of dioxygen (Fig. 1.4). The cycle is performed as a two-step catalytic mechanism where H_2O_2 is used both as an oxidant and a
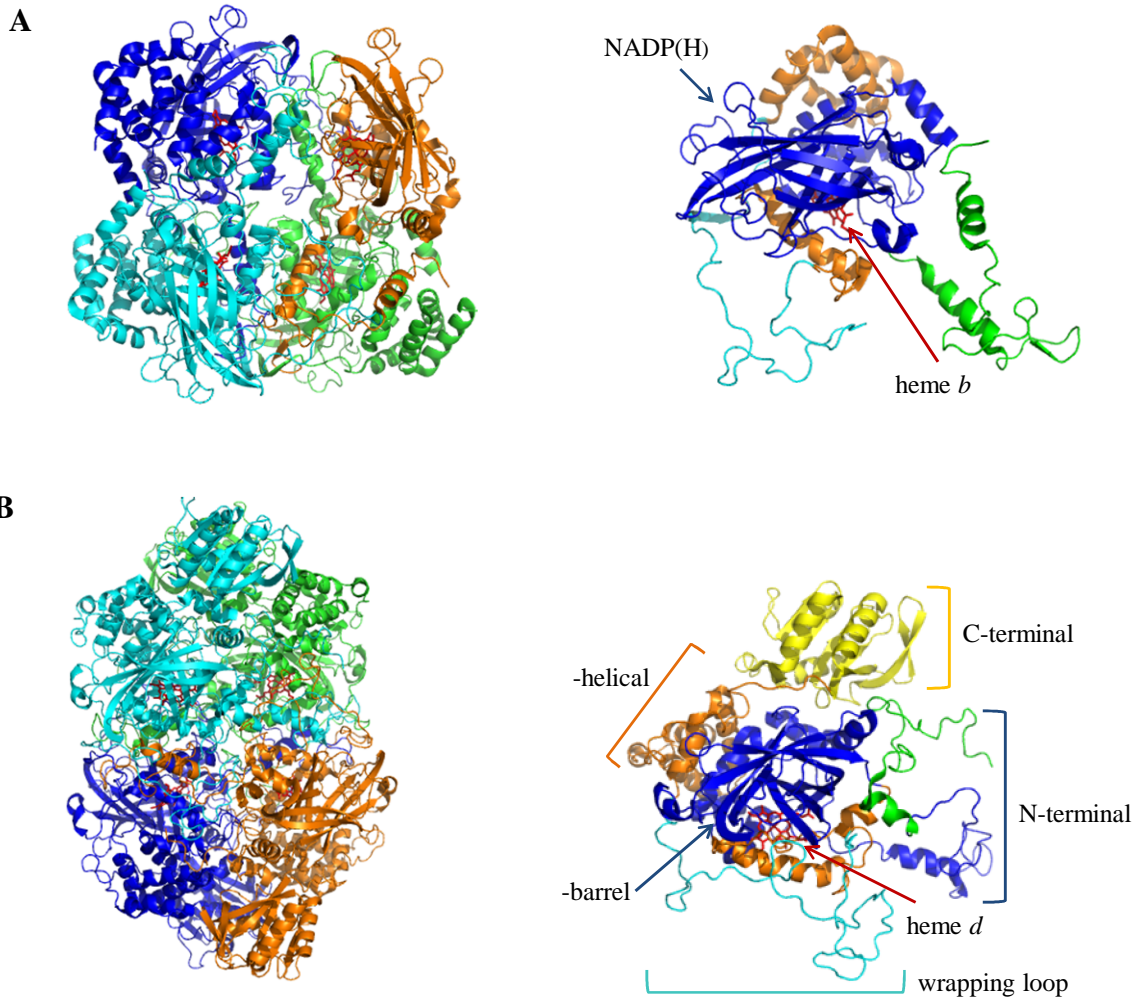
Figure 1.3. Catalase structures. Views of the subunits (right) and of the tetrameric molecules (left) of (A) human erythrocyte catalase (HEC) and of (B) catalase from *Escherichia coli* (HPII), as representative examples of small (clade 3) and large (clade 2) catalases, respectively. These structures were taken from PDB accession domains 1QQW and 1IPH, respectively.

$$\text{Fe}^{III} \xrightarrow[\quad]{\quad H_2O_2 \quad\quad H_2O \quad} {}^{\bullet+}\text{Fe}^{IV}=O$$

$$O_2 + H_2O \qquad H_2O_2$$

Native

Compound I
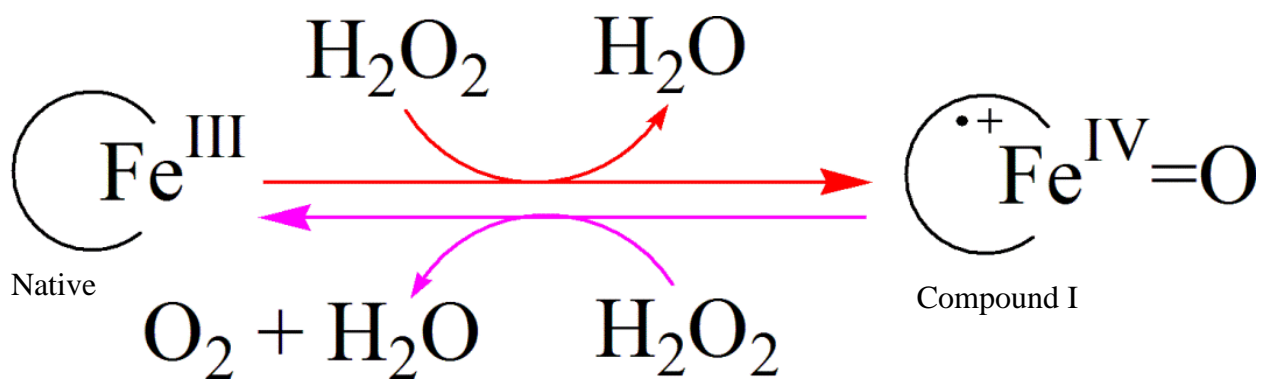
Figure 1.4. Catalytic cycle of monofunctional catalases.

reductant. The first step involves the heterolytic reduction of H_2O_2 to H_2O, resulting in two-electron oxidation of the ferric enzyme to a ferryl-porphyrin -cation radical intermediate. As with heme peroxidases, this is referred to as compound I (i.e., $Fe^{IV}=O[porphyrin]^{\bullet+}$) (*51*). In the second step (i.e., *catalatic* step), the second molecule of hydrogen peroxide reduces compound I, regenerating the ferric enzyme and releasing a second H_2O and one O_2. In some cases, compound I can undergo an intramolecular one-electron reduction, resulting in a *catalatically* inactive species (compound II, $^{\bullet+}AA[porphyrin]Fe^{IV}$-OH), where the protein (AA) donates the electron that quenches the porphyryl radical. This causes a decrease in the catalase activity over time, since the compound II intermediate returns very slowly to the ferric enzyme. This is where NADPH (in the catalases which bind it) is proposed to act. It is proposed to prevent the formation of this catalase-inactive species (*62-68*).

A common characteristic to all monofunctional catalases is their ability to decompose H_2O_2 over a wide pH range (i.e., pH: 5-10). This proterty is in contrast to bifunctional catalase-peroxidases (i.e., enzymes that also show catalase activity) as they tend to have a narrow pH range for H_2O_2 degradation. Within the active site, there are four invariant residues found in all monofunctional catalases: the distal residues histidine, asparagines, and serine and the proximal heme iron ligand tyrosine (*62*). Hydrogen peroxide binds at the distal heme pocket and forms a hydrogen bond network with the distal histidine, while the conserved distal asparagine serves to stabilize and polarize the peroxide. On the other hand, the role of the proximal heme iron ligand tyrosine is to modulate the heme iron reactivity and to stabilize higher heme oxidation states (*69*). In some cases, the proximal tyrosine can participate in redox reaction through its involvement with unusual modifications. For example, in *Escherichia coli* HPII, the N of the

17

imidazole ring of the distal histidine forms a covalent bond with the C of the proximal tyrosine (*70*).

Another feature of all the heme-dependent monofunctional catalases is that access to the active site heme is restricted by a long narrow channel. This channel allows passage of H_2O_2 and other very small molecules (ethanol, peracetic acid, etc.) (*71*). In contrast to heme peroxidases, the heme edge of catalases is not accessible to larger molecules like the typical aromatic electron donors which support peroxidatic turnover. This is purported to facilitate *catalatic* turnover by preventing heme reduction by molecules other than H_2O_2. This explains why catalases are very poor in performing the peroxidase activity, since most peroxidase electron donors are large and require an open access to the heme edge for facile electron transfer. For example, in *Saccharomyces cerevisiae* catalase A, it was shown through classic molecular interactions potentials, molecular dynamics, and activated molecular dynamic calculations (*72*), that water can be a competitive inhibitor of catalase by blocking the access of hydrogen peroxide to the active site.

1.6.   Catalase-peroxidases

Up to this point, we have considered the degradation of H_2O_2 by the peroxidase and catalase mechanisms. Interestingly, across all types of catalases, none of them is effective in peroxidase turnover. Likewise, peroxidases are uniformly poor catalases. However, across all of nature there is one class of enzymes known as catalase-peroxidases (KatG) which can efficiently degrade H_2O_2 through both the catalase and peroxidase mechanisms. Across all the superfamilies of heme-dependent and non-heme dependent catalases and peroxidases, the capability to perform both functions at significant turnover levels is found only in KatG. The fact that KatG is the only

member within its superfamily to show reasonably high catalase activity at neutral pH has brought great interest in understanding how its structure accounts for its novel bifunctional capability.

Catalase-peroxidases are found in bacterial and lower eukaryotic organisms (*73*). Based on sequence, overall structure, and active site homology, KatG enzymes are clearly from the superfamily of plants, fungal and bacterial peroxidases. Specifically, they are obvious members of class I together with ascorbate and cytochrome c peroxidases (*74-76*). Interestingly, they use a single active site to catalyze the degradation of hydrogen peroxide by catalatic and peroxidatic mechanisms.

The KatG active site uses heme *b* as its prosthetic group (*77-80*). The arrangements of amino acids that surround the heme cavity are well conserved. The proximal and distal sides of heme are occupied by the conserved Asp-His-Trp, and Trp-His-Arg triads, respectively. The proximal histidine is coordinated to the heme cofactor as the fifth ligand, and it is hydrogen bonded to the carboxylate side chain of the nearby aspartate residue, which also is hydrogen bonded to the nitrogen atom of the indole group of the proximal tryptophan residue (Fig. 1.5). These hydrogen bond networks at the proximal side have been shown to maintain the stability of the heme architecture (*81*). The distal histidine serves as a general base to facilitate the deprotonation of H_2O_2 and assist in the formation of compound I intermediate (*82-84*). Likewise, the distal arginine helps stabilize compound I by electrostatic interactions between the positive charge of its side chain and the developing negative charge on the distal oxygen of the bound H_2O_2 during heterolytic O-O bond cleavage (*82*). The roles of theses distal and proximal side residues in KatG are similar to those observed in other heme peroxidases (*52-54*).
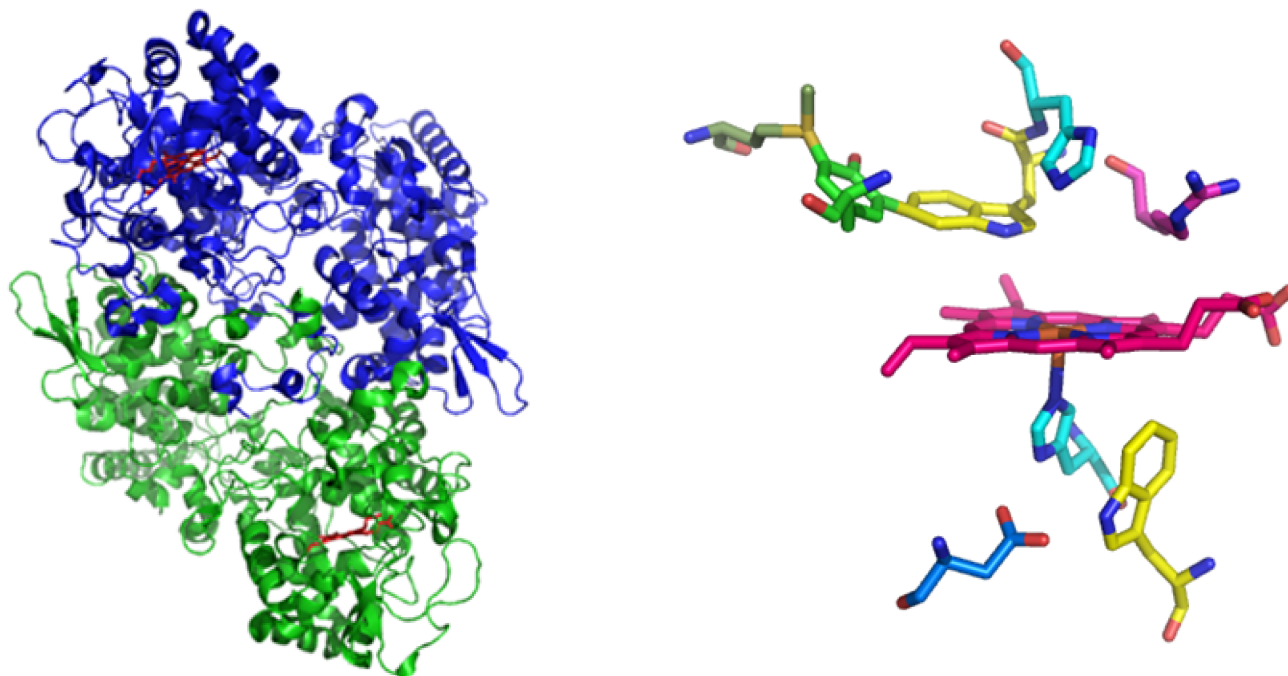
Figure 1.5. Three-dimensional structure of catalase-peroxidase from *Mycobacterium tuberculosis*. Views of the dimer (left) and active site (right). Amino acids are coded as follows: Tryptophan-Yellow, Histidine-Cyan, Arginine-Magenta, Aspartate-Tv_blue, Tyrosine-Green, Methionine-Palegreen. Amino acid oxygen and nitrogen elements are colored in red and blue, respectively. Structure was taken from PDB accession domain 2CCA.

Aside from active site similaries, KatG possesses several unique features that distinguish it from other heme peroxidases. First of all, other heme peroxidases are monomeric enzymes while catalase-peroxidases are isolated as homodimers, and in one case (*E. coli* HPI) as a homotetramer. Second, each subunit of KatG has a size of approximately 80 kDa and is divided into two domains (*77-80*). Both domains have a fold which is that of a typical plant peroxidase, hence, this structure is proposed to have arisen from a gene duplication and fusion event (*85*). The N-terminal domain is the only one of the two with the ability to bind heme, and therefore, it represents the only functioning active site on each subunit. Despite its inability to bind heme, the C-terminal domain, located approximately 30 Å from the active site, serves to maintain the active coordination environment for the heme and appears as a platform to direct conformational adjustments in the N-terminal domain (*86-89*).

More so, the N-terminal domain itself bears interhelical loops that are considerably longer than the analogous structures in other plant peroxidases due to insertions that contain approximately 35 amino acids each (*77-80*). Among these, the large loop 1 (LL1) bears an invariant tyrosine residue which is involved in a novel covalent adduct (MYW) including a methionine and an active site tryptophan. The MYW adduct is in close proximity to the heme prosthetic group and has been observed in crystal structures of KatG by mass spectrometric peptide mapping (*77-80, 90-93*). Substitution of any of these three amino acid residues by sited-directed mutagenesis abolishes the catalase activity but retains the peroxidase activity (*82-83, 93-97*). Substitution of either tyrosine or tryptophan prevents cross-linking, whereas exchange of methionine to cysteine allows the autocatalytic covalent bond formation between tyrosine and tryptophan, but still produces a catalase-negative variant.

In KatG enzymes, the degradation of hydrogen peroxide can either be accomplished through the catalase or peroxidase pathways. The ability to display such a unique behavior lies on their structural properties. By virtue of its structure, KatG is a peroxidase. However, it represents the only member within the peroxidase-catalase superfamily with appreciable catalase activity. In contrast to other heme peroxidase, KatG has a much more restricted access channel to the active site due to the presence of its interhelical loops (LL1 and LL2). This forms a potential barrier to large aromatic substrates and results in a low peroxidase activity. Indeed, recent discoveries have shown that deletion of a substantial portion of LL1 produces an enzyme with peroxidase activity that rivals that of horseradish peroxidase (*88*). Likewise, monfunctional catalases are poor peroxidases because their heme active site is restricted by a long narrow channel, which prevents the passage of common aromatic electron donors that support peroxidase turnover. Structurally, KatG bears no resemblance to monofunctional catalases. However, its unique ability to possess appreciable catalase activity results from the presence of the MYW covalent adduct, a structural feature absent from other members of the peroxidase-catalase superfamily (*77-80, 90-93*).

Based on the fact that both activities are facilitated within the same active site, the historical and most simple approach to understand the interplay between these two functions has been to superimpose the catalytic cycles of monofunctional catalases and peroxidases on the same scheme (Fig. 1.6), (*82, 87, 95, 98-106*). A consequence of this arrangement is that the activities are mutually competitive and diverge at compound I. That means, compound I could either be reduced by hydrogen peroxide (catalase) or by an exogenous electron donor (peroxidase). But in any case one would preclude the other. There has been good evidence to support such a scheme. First, the catalase and peroxidase activities of KatG have sharply distinct
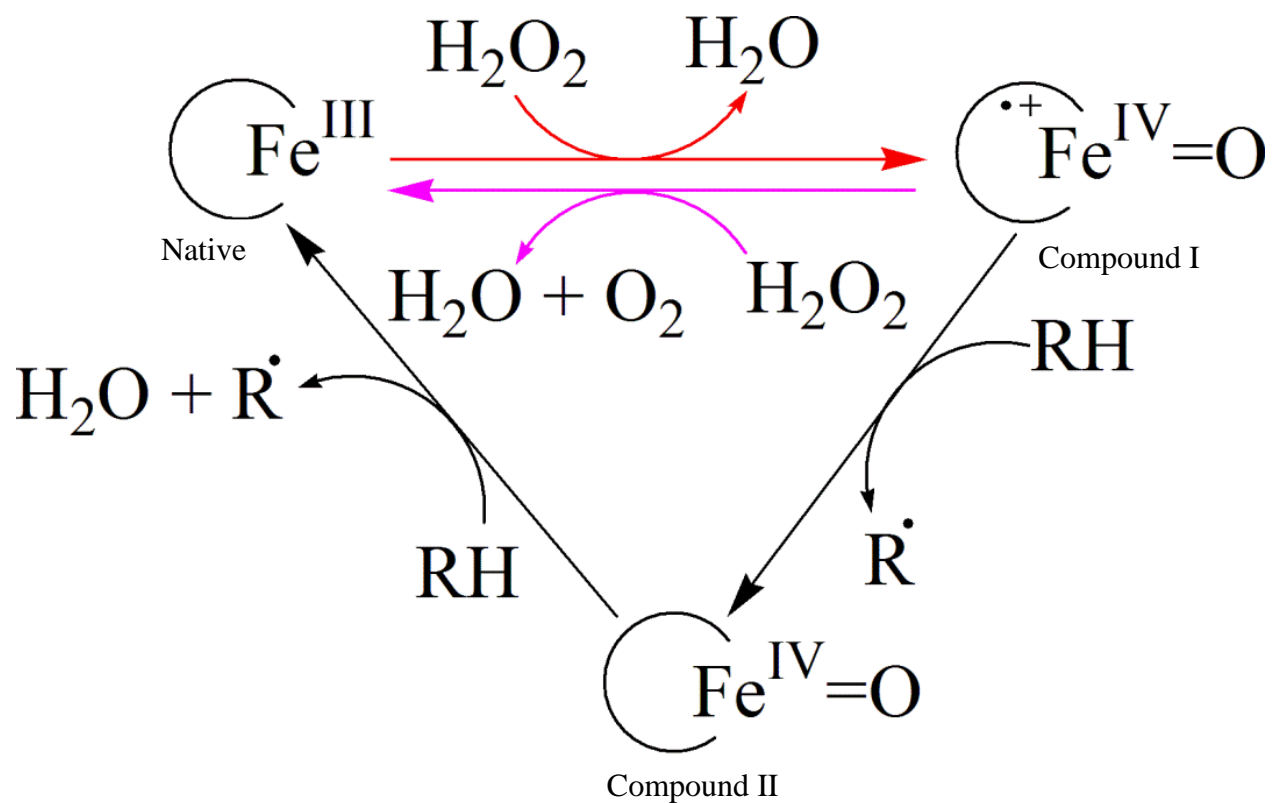
Figure 1.6. Classical reaction mechanism for catalase-peroxidases. RH and R$^{\bullet}$ represent the reducing substrate and substrate's radical, respectively.

conditions which produce optimal turnover. The catalase activity is optimal under neutral pH. However, the peroxidase turnover is optimal under acidic conditions and requires an exogenous electron donor. Second, substitutions by site-directed mutagenesis which eliminate catalase activity almost always enhance peroxidase activity. Third, an early study of isolated KatG from *E. coli* showed that a classical electron donor, *o*-dianisidine inhibited catalase activity at pH 7.5 (*107*). As for which activity dominates, this appears to be a function of pH and the availability of an exogenous electron donor. Indeed, it is widely accepted that peroxidase activity is optimum under far more acidic conditions (pH   4.5) than catalase activity (pH   6.5) (*82, 98, 104, 108*).

However, in several respects the historical conception of KatG catalase and peroxidase mechanisms and their interplay is unsatisfactory. Indeed, the mechanism for catalase turnover for KatG has been the subject of intense investigation. Evidence is accumulating for a mechanism of H_2O_2 degradation by KatG that is a much greater contrast to typical catalases than first appreciated (*94, 99, 109-121*). This mechanism (Fig. 1.7) is centering on a $Fe^{III}\text{-}O_2^{\bullet-}$ heme intermediate analogous to oxyhemoglobin and a protein-based radical centered at the novel Met-Tyr-Trp covalent adduct (*96, 112-113, 115, 121-123*). Several experiments including optical stopped-flow and rapid freeze quench EPR have revealed the presence of this species during steady-state turnover of the enzyme in the presence of H_2O_2 (*94, 96, 115, 121-122*). Isotopic labeling experiments of all the 21 tyrosine residues in *M. tuberculosis* KatG supported that the tyrosine involved in the MYW covalent adduct is the radical site (*121*).

Description of the catalatic cycle that centers on the $Fe^{III}\text{-}O_2^{\bullet-}$ heme species begins with the formation of compound I in the presence of hydrogen peroxide just as it occurs with monofunctional catalases. However, the KatG mechanism diverges from typical catalases with a subsequent intramolecular electron transfer that converts compound I to a ferryl/protein radical

24
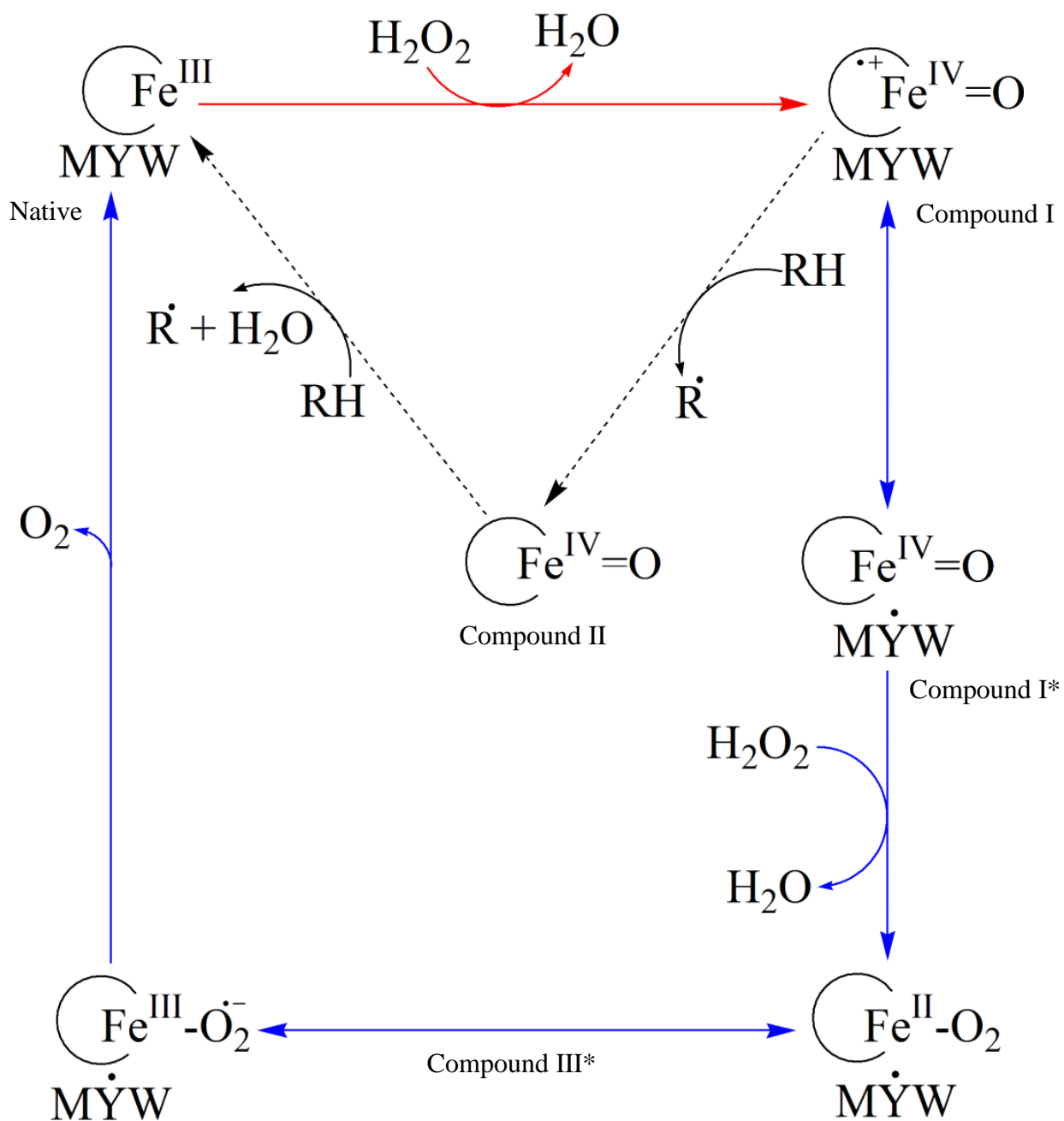
Figure 1.7. Current proposed mechanism for the catalatic cycle of catalase-peroxidases.

intermediate with the radical centered on the Met-Tyr-Trp adduct, $Fe^{III}-O_2^{\bullet-}[MYW]^{\bullet+}$ (*94, 113, 115, 117, 121, 123*). This is referred to as compound I*. Reaction of a second equivalent of hydrogen peroxide leads to the formation of a $Fe^{III}-O_2^{\bullet-}$ complex, a species designated as compound III* and the release of water. The analogous formation of compound III ($Fe^{III}-O_2^{\bullet-}$) in typical peroxidases is very common and occurs easily at high concentrations of H_2O_2 and low concentrations of electron donor (*112, 124*). However, typical peroxidases do not have the $MYW^{\bullet}$ adduct radical adjacent to the heme as does compound III* of KatG. For this reason the $Fe^{III}-O_2^{\bullet-}$ complex in typical peroxidases is largely inactive (*112, 125-126*). In contrast intramolecular electron transfer in KatG compound III* from the heme center to the $MYW^{\bullet}$ adduct radical returns the enzyme to its ferric state with the concomitant release of O_2 (*112-113, 121-122*). Though compound III of typical peroxidases is largely inactive, the complex can slowly degrade to produce ferric enzyme and O_2. This accounts for the detectable but very poor catalase activity of typical peroxidases. Whether hydrogen peroxide oxidation follows a compound III* intermediate or a single two-electron step (such as in monofunctional catalases), the nature of interplay between the catalase and peroxidase activities of KatG enzymes is still not well understood. The traditional view of interplay would suggest that they are mutually antagonistic. Even with the more recently determined catalytic scheme (Fig. 1.7), the same would be anticipated. In fact, very little is known about the participation of electron donors in KatG catalysis. For example, an earlier study of isolated KatG from *E. coli* showed that a classical electron donor *o*-dianisidine, inhibited catalase activity at pH 7.5 (*107*). The research described in this dissertation makes an important step toward understanding the function of electron donors in KatG function. Our discovery suggests that these compounds have a far more prominent and important role to play than has been generally appreciated.

1.7.   Biomedical Ramifications

KatG enzymes have been implicated as virulence factors in several pathogens including *Xanthomonas compestris*, *Yersinia pestis*, *Escherichia coli* O157:H7, *Legionella pneumophila*, and *Magnaporthe grisea* (*127-133*). Thus, the ability to understand the connectivity between its catalatic and peroxidatic functions would not only serve as a good model in the fields of enzyme engineering and drug target, but would also be of critical importance to understand factors associated to its virulence. Another important aspect that has increased the interest in the study of catalase-peroxidases is their role in the activation of isoniazid, a frontline anti-tubercular agent in *Mycobacterium tuberculosis* (*134-136*). The mechanism of activation is not yet fully known. However, the rapidly increasing rate of isoniazid drug-resistance, as a result of mutations that affect the *katG* gene has raised considerable interest in the study of KatG (*137-138*).

Chapter two: Stimulation of KatG Catalase Activity by Peroxidatic Electron Donors, *Arch. Biochem. Biophys* **525**, 215-222 (2012)

2.1. Introduction

Catalase-peroxidase (KatG) enzymes are capable of H_2O_2 decomposition by catalatic and peroxidatic mechanisms using a single active site. By sequence, overall structure, and virtually superimposable active sites, KatGs clearly belong to Class I of the peroxidase-catalase superfamily along with cytochrome *c* and ascorbate peroxidases (*74-76*), (Fig. 2.1). Structures from the more distantly related Class II (e.g., lignin peroxidase) and Class III (e.g., horseradish peroxidase) enzymes show that even these are highly similar at the active site level (*52, 139*). Interestingly, KatG is the only member of the entire superfamily with appreciable catalase activity, showing apparent second order rate constants (~1 x 10^6 $M^{-1}s^{-1}$) that rival those of typical (i.e., monofunctional) catalases (*140-141*), enzymes with which KatG shares no structural similarity (Fig. 2.2).

Although there is great similarity between KatG and other peroxidases, the bifunctional enzymes do possess several unique features. Among them, the active site-bearing N-terminal domain of KatG has interhelical loops (LL1, LL2, and LL3) that are considerably longer than the analogous structures in other superfamily members (*77-80*). Large Loop 1 (LL1) bears an invariant tyrosine residue that participates in a novel covalent adduct (MYW) involving a methionine and an active site tryptophan. The MYW adduct has been observed in KatG crystal structures and by mass spectrometric peptide mapping (*77-80, 90-93*). The tryptophan in the
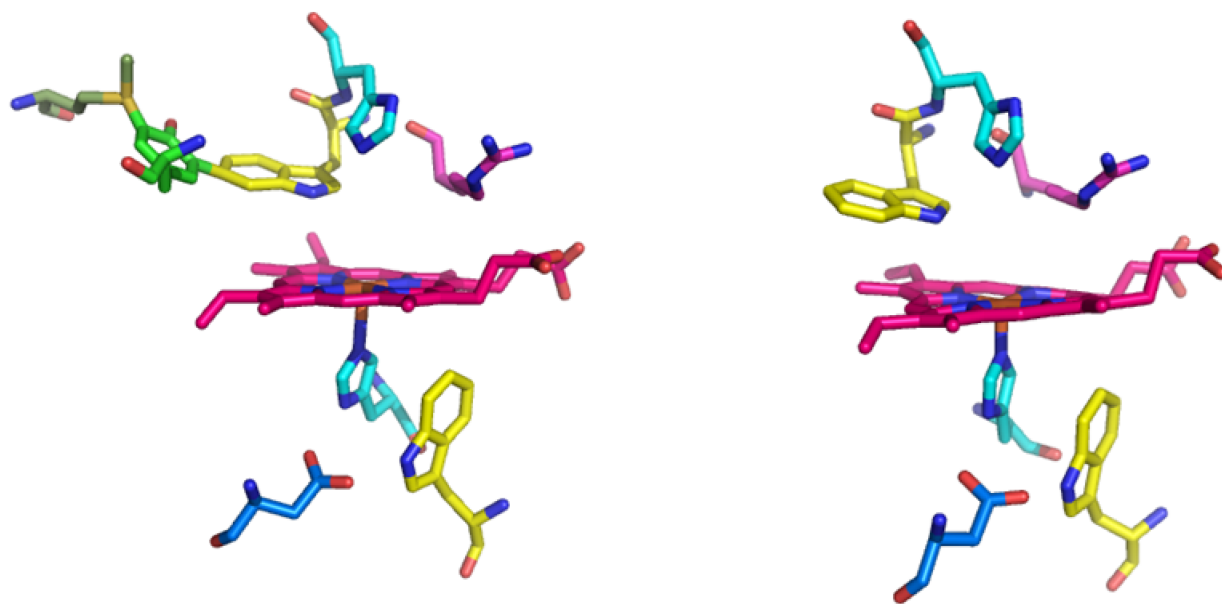
Figure 2.1. Active site structures of catalase-peroxidase (left) and cytochrome c peroxidase (right). Amino acids are colored as follows: Tryptophan-Yellow, Histidine-Cyan, Arginine-Magenta, Aspartate-Tv_blue, Tyrosine-Green, Methionine-Palegreen. Amino acid oxygen and nitrogen elements are colored in red and blue, respectively. Structures were taken from PDB accession domain 2CCA and 1BEM, respectively.
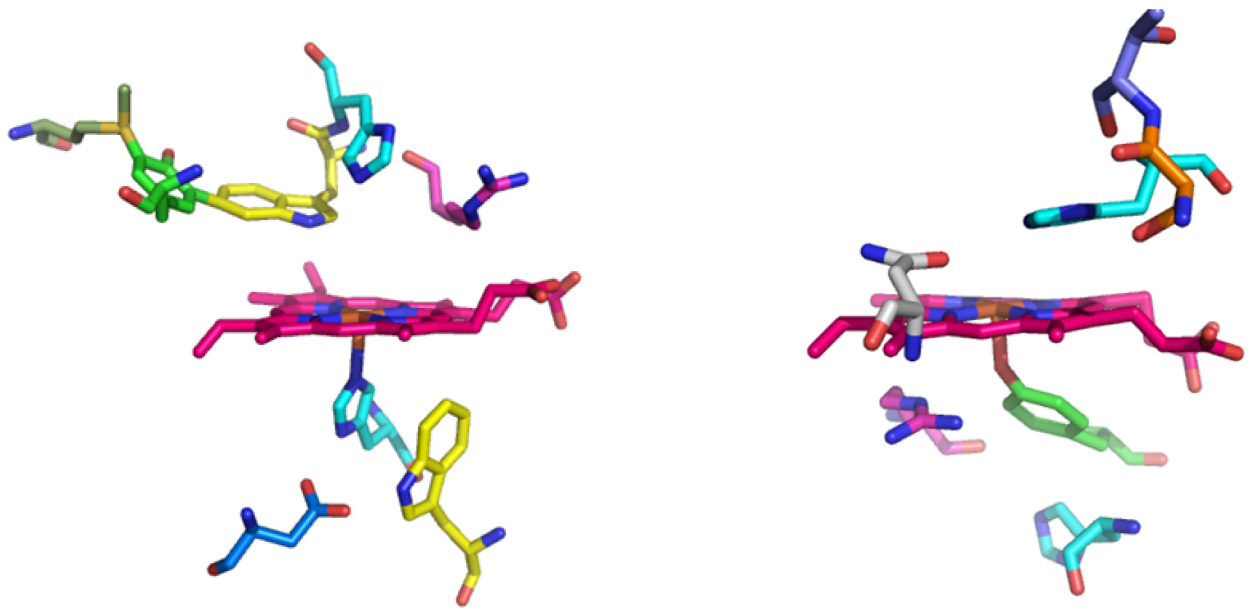
Figure 2.2. Active site structures of catalase-peroxidase (left) and monofunctional catalase (right). Amino acids are colored as follows: Tryptophan-Yellow, Histidine-Cyan, Arginine-Magenta, Aspartate-Tv_blue, Tyrosine-Green, Methionine-Palegreen, Serine-Orange, Threonine-Slate, Asparagine-Gray. Amino acid oxygen and nitrogen elements are colored in red and blue, respectively. Structures were taken from PDB accession domain 2CCA and 1IPH, respectively.

adduct (W107 by *M. tuberculosis* numbering) is in close proximity to the heme prosthetic group, which has been shown to facilitate the oxidative chemistry necessary for forming the adduct (*93*). Substitution of any of these residues by site-directed mutagenesis produces KatG variants that lack catalase activity but retain peroxidase activity (*82-83, 93-97*).

Though they are structurally unrelated, typical (i.e., monofunctional) catalases and typical peroxidases all begin their catalytic cycles with the heterolytic reduction of H_2O_2 to H_2O, resulting in two-electron oxidation of the ferric enzyme to a ferryl-porphyrin   cation radical intermediate, compound I (i.e., $Fe^{IV}=O[porphyrin]^{\bullet+}$). In some cases (most notably cytochrome *c* peroxidase), the radical is transferred by oxidation of a nearby amino acid. A typical mechanism for the return of a peroxidase to its ferric state is by two sequential one-electron reductions at the expense of two equivalents of an exogenous electron donor. Two equivalents of donor radical are generated, and the enzyme is reduced first to the ferryl intermediate, compound II (i.e., Fe^{IV}-OH), and then to the ferric state. In contrast, the typical catalase compound I returns to the ferric state by the two-electron oxidation of a second equivalent of H_2O_2 to produce O_2.
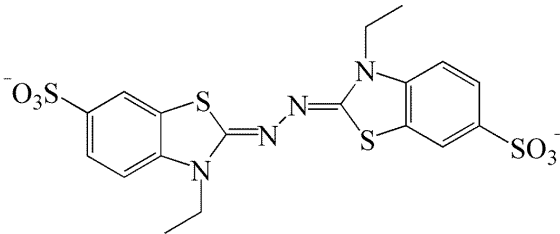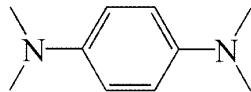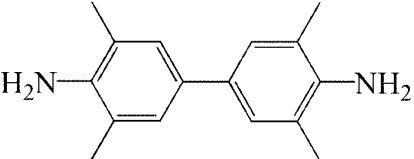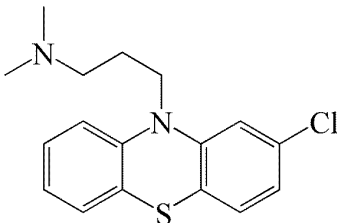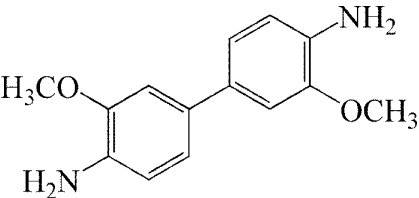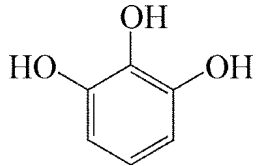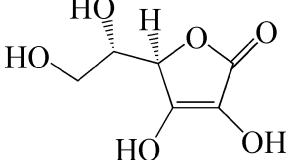
There has been considerable interest and discussion surrounding the catalase mechanism of KatG and the role of the covalent adduct (*94, 99, 111-121*), particularly over what occurs following formation of compound I (i.e., $Fe^{IV}=O[porphyrin]^{\bullet+}$). One mechanism posits that a compound I* intermediate derived from adduct oxidation (i.e., Fe^{IV}-OH[MYW]$^{\bullet+}$) reacts with the second equivalent of H_2O_2 to form Fe^{III}-$O_2^{\bullet-}$[MYW]$^{\bullet+}$ (*112-113, 115, 121*). This intermediate (compound III*) is similar to the compound III (Fe^{III}-$O_2^{\bullet-}$) that is easily formed in the other peroxidases in response to excess H_2O_2 (*112, 124*). Compound III is inactive with respect to peroxidase activity and accounts for the paltry "pseudocatalase" activity observed in other members of the peroxidase-catalase superfamily (*112, 125-126*). Conversely in KatG, compound

III*, due to the additional MYW$^{\bullet+}$ oxidizing equivalent, has been proposed to facilitate a second intramolecular electron transfer where the heme intermediate reduces the adduct radical leaving a Fe^{III}-O$_2$ complex which easily dissociates yielding the resting enzyme and O$_2$ (*112-113, 121-122*).

In spite of the hallmark multifunctionality of KatG, the nature of the interplay between the catalase and peroxidase activities of the enzyme is not well understood. Generally, it has been assumed that the two should be mutually competitive with the two cycles diverging at the intermediate which reacts with the second equivalent of H$_2$O$_2$. That is, either H$_2$O$_2$ or an exogenous (typically aromatic) electron donor will serve as the source of electrons to return the enzyme to its starting state. Indeed, an early study on *E. coli* KatG showed that the common peroxidatic electron donor *o*-dianisidine did inhibit catalase activity at pH 7.5 (*107*). As for which activity dominates, this has been taken to be a function of the presence and identity of an exogenous electron donor, the relative concentrations of H$_2$O$_2$, and the pH of the reaction.

In this work, we report the surprising stimulation of KatG catalase activity by several well-known peroxidatic electron donors (Table 2.1). Further, the most substantial effect was observed under conditions most favorable to peroxidase activity. Due in large part to the stimulatory effect of the donors themselves, the vast majority of H$_2$O$_2$ consumption by KatG was dedicated toward catalatic turnover (i.e., O$_2$ production) rather than the accumulation of the oxidized products of the electron donors. Stopped-flow studies using multiple turnover conditions showed that a heme intermediate with features characteristic of a Fe^{III}-O$_2$$^{\bullet-}$ complex dominated during steady-state turnover and returned directly to the ferric state once H$_2$O$_2$ was depleted.

Table 2.1. Structure of common peroxidatic electron donors.

Electron donor	Structure
ABTS, 2,2'-azino-bis(3-ethylbenzthiazoline-6-sulfonic acid)	
TMPD,N,N,N',N'-tetramethyl-*p*-phenylenediamine	
TMB, 3,3',5,5'-tetramethylbenzidine	
CPZ, chlorpromazine	
o-dianisidine	
Pyrogallol	
Ascorbate	

These data point toward an integral role for peroxidatic electron donors in KatG catalase activity with implications for the mechanism of O_2 production by the enzyme. Given the ability of electron donors to substantially expand the conditions under which robust catalase activity is observed, the participation of as yet unidentified physiological electron donors for KatG may have important consequences for catalytic H_2O_2 degradation *in vivo*, particularly for organisms like *M. tuberculosis* whose only catalase active enzyme is KatG (*73*).

2.2. Materials and Methods

2.2.1. Materials

3,3',5,5'-tetramethylbenzidine dihydrochloride hydrate (TMB), *N,N,N',N'*-tetramethyl-*p*-phenylenediamine dihydrochloride (TMPD), L-ascorbic acid, 3,3'-dimethoxybenzidine (*o*-dianisidine), 2,2'-azino-bis(3–ethylbenzthiazoline-6-sulfonic acid) (ABTS), hydrogen peroxide (30%), imidazole, ampicillin, hemin, chloramphenicol, chlorpromazine (CPZ), pyrogallol, calcium chloride hydrate and sodium dithionite were purchased from Sigma-Aldrich (St. Louis, MO). Tetracycline hydrochloride, mono- and dibasic sodium phosphate, sodium chloride, sodium acetate trihydrate, potassium chloride, magnesium chloride, and magnesium sulfate were purchased from Fisher (Pittsburgh, PA). *Pfu* polymerase, Herculase polymerases, T4 DNA ligase, and *E. coli* (XL-1 Blue) were obtained from Agilent (La Jolla, CA). All restriction enzymes were purchased from New England Biolabs (Beverly, MA). All oligonucleotide primers were purchased from Invitrogen (Carlsbad, CA). Benzonase nuclease, Bugbuster®, nickel–nitrilotriacetic acid (Ni–NTA) resin were obtained from Novagen (Madison, WI). Isopropyl- -D-thiogalactopyranoside (IPTG) was obtained from Gold Biotechnology (St. Louis, MO). Buffer exchange columns (10DG) and Macro-Prep High Q resin were purchased from BioRad

(Hercules, CA). Centrifugal filter units (50 kD cutoff) were acquired from Millipore (Billerica, MA). All buffers and media were prepared using water purified through a Barnstead EASYpure II system (18.2 MΩ/cm resistivity).

2.2.2. *E. coli C41 (DE3) pHPEX3*

The pHPEX3 plasmid, constructed as previously described (*142*), was used to transform *E. coli* C41 (DE3) cells made competent by a standard CaCl$_2$ procedure (*143*). Transformants (i.e., *E. coli* C41 [DE3] pHPEX3) were selected on the basis of tetracycline resistance (20 µg/ml), and competent cells of the new strain were generated according to the same CaCl$_2$ procedure (*143*). Competent cells were used immediately for transformation by a standard heat-shock protocol by pMRLB11, a pET23b plasmid bearing the gene for *M. tuberculosis katG,* obtained from the TB Vaccine Testing and Research Materials Contract at Colorado State University. Transformants were selected on the basis of tetracycline (20 µg/ml) and ampicillin (100 µg/ml) resistance.

2.2.3. *Expression of MtKatG*

Protein expression was carried out using Luria-Bertani broth supplemented with tetracycline (20 µg/ml) and ampicillin (100 µg/ml). Cells were grown at 37 ºC with agitation (250 rpm) to mid-log phase (OD$_{600}$ = 0.4 – 0.5) at which point expression was induced by addition of 1 mM IPTG. At the time of induction, the culture medium was also supplemented with 8 µM hemin. Four hours after induction, cells were harvested by centrifugation (2,700 × *g*), and the cell pellets were stored at -80 ºC.

2.2.4. *Purification of MtKatG*

Cell pellets were resuspended in Bugbuster® reagent (Novagen, Madison, WI) supplemented with phenylmethylsulfonyl fluoride. The mixture was homogenized with a Dounce homogenizer followed by addition of benzonase nuclease (25 U/µL), and incubated at 4 ℃ with gentle stirring for 1 h. The cell lysate was then centrifuged for 20 min (2,700 × g, 4 ℃). The supernatant was loaded onto a Ni-NTA column by recirculating the solution through the column bed overnight (1 mL/min). The column was washed with 50 mM Tris, pH 8.0, followed by a second wash with Buffer A (50 mM phosphate, pH 7.0; 200 mM NaCl). Subsequent washes were carried out using Buffer A supplemented with 2 mM, 20 mM, and 50 mM imidazole. The protein was then eluted off the column with Buffer A supplemented with 100 mM imidazole. The final eluent (100 mM imidazole) was concentrated by ultrafiltration with a 30 kD molecular cutoff filter (Amicon, Billerica, MA). Following concentration, excess imidazole was removed using a 10 DG size exclusion column (BioRad, Hercules, CA) equilibrated with Buffer B (50 mM phosphate, pH 7.0; 50 mM NaCl). To prepare samples for anion exchange chromatography, protein was concentrated using a centrifugal filter (MW cutoff = 50 kD) and diluted using buffer C (50 mM phosphate, pH 7.0). The protein was then separated by anion exchange using a Macro-Prep High Q resin pre-washed with buffer D (50 mM phosphate 0.5 M NaCl) and then equilibrated with buffer C. Protein separation was accomplished using a linear gradient from 100% buffer C/0% buffer D to 0% buffer C/100% buffer D. Fractions were evaluated for purity by SDS-PAGE. Relevant fractions were pooled and concentrated by ultrafiltration using a 30 kD molecular cutoff filter (Amicon, Billerica, MA). The protein was then diluted by a factor of six using 5 mM phosphate buffer, pH 7.0, aliquoted, and stored at -80 ℃. The final purified MtKatG showed an optical purity ratio (i.e., RZ value) A_{408}/A_{281} of 0.64, with Soret, β, and α bands at 408, 500, and 633 nm, respectively. The apparent second order rate constant for the

catalase activity of the purified enzyme was 1.1×10^6 $M^{-1}s^{-1}$. These properties are highly similar to those reported elsewhere for MtKatG (*93, 96, 141*).

2.2.5. *UV-visible absorption spectra*

Spectral readings for KatG were taken by scanning the samples in a quartz cuvette between 800 and 250 nm using a Shimadzu UV-1610 spectrophotometer (Columbia, MD). All spectral measurements were carried out at room temperature in 100 mM phosphate buffer, pH 7.0. The holoenzyme concentration was determined by the pyridine hemichrome procedure of Falk (*144*).

2.2.6. *Peroxidase activity assays*

Peroxidase activity was evaluated by monitoring the production of ABTS radical ($\varepsilon_{417} = 34.7$ mM^{-1} cm^{-1}) (*145*) over time following initiation of reactions with H_2O_2. In a similar manner, oxidation of TMB to its radical ($TMB^{\bullet+}$) ($\varepsilon_{652} = 39$ mM^{-1} cm^{-1}) (*146*) or *o*-dianisidine oxidation ($\varepsilon_{460} = 11.3$ mM^{-1} cm^{-1}) were monitored spectrophotometrically. All assays contained 20 nM KatG, and were carried out at room temperature in 50 mM acetate buffer, pH 5.0 on a Shimadzu UV-1601 spectrophotometer (Columbia, MD). At a constant ABTS concentration, hyperbolic responses to increasing H_2O_2 concentration and *vise versa* were typically observed. Thus, curve fitting to a standard Michaelis-Menten equation was used to determine the *apparent* kinetic parameters K_M, k_{cat}, and k_{cat}/K_M. For all places where these terms are applied, apparent K_M only refers to the concentration of substrate required to reach ½ of the maximum rate, k_{cat} is the maximum rate divided by the concentration of holo-MtKatG as estimated by heme

concentration, and k_{cat}/K_M is appropriately regarded as the catalytic efficiency and corresponds to the slope of the tangent line to rates obtained at low concentrations of substrate (i.e., $< K_M$).

2.2.7. *Extent of ABTS oxidation vs. H_2O_2 consumption*

Reactions containing 0.1 mM ABTS, 20 nM MtKatG, and varying concentrations of H_2O_2 (1 – 5 mM) were allowed to proceed to completion (at least 10 minutes). Adding more ABTS or KatG to completed reactions did not result in any additional $ABTS^{\bullet+}$ production, but adding more H_2O_2 did, indicating that the reactions stopped due to H_2O_2 limitation. At the conclusion of each initial reaction, a sample was withdrawn and diluted to maintain absorbance values in correspondence with Beer's Law. Then, the absorbance was recorded at 417 nm, and the $ABTS^{\bullet+}$ concentration was estimated (accounting for dilution). This concentration was compared against the concentration of H_2O_2 consumed in each reaction.

2.2.8. *Catalase activity assay by H_2O_2 decomposition*

Catalase activity was evaluated by monitoring the decrease in H_2O_2 concentration with time at 240 nm ($\varepsilon_{240} = 39.4$ M^{-1} cm^{-1}) (*147*). All assays contained 20 nM KatG and were carried out at room temperature either in 50 mM acetate and/or 100 mM phosphate at the target pH of the reaction. We did not use this method to monitor catalase activity in the presence of peroxidatic electron donors because of the intense absorption of these molecules in the UV.

2.2.9. *Catalase activity by O_2 production*

Catalase activity was also monitored polarigraphically for O_2 production using a Clark-type O_2 sensitive electrode (Hansatech Pentney, Norfolk, England). Unless otherwise indicated,

this was the method employed for measurement of catalase activity. Calibration was achieved using N_2 saturated solution to establish a zero O_2 level within the reaction chamber prior to experimental measurements. All reactions contained 5 nM KatG (unless otherwise specified) and were carried out at room temperature (23 ºC) in either 50 mM acetate and/or 100 mM phosphate buffer at the corresponding pH of the reaction. Data collection was started with buffer, KatG, and electron donor (when present) in the reaction chamber for 20 seconds to establish a baseline, at which point H_2O_2 was injected to initiate O_2 production.

2.2.10. Analyses of steady-state kinetic data

At pH 5.0 there were two distinct phases in the response of MtKatG catalase activity to H_2O_2 concentration (whether measured by O_2-sensitive electrode or UV-vis). At low H_2O_2 concentrations (i.e., below 2 mM), we observed a hyperbolic response, but at higher concentrations (i.e., 2.0 – 50 mM), we observed a linear response. Others have reported a large apparent K_M for H_2O_2 (~225 mM) for MtKatG at pH 5 (*141*), and a linear response of activity to H_2O_2 concentrations ranging from 2 – 50 mM would be consistent with that observation. Two phases would suggest the operation of two mechanisms for H_2O_2 disproportionation by MtKatG at pH 5.0, each with its own kinetic parameters. Accordingly, our fitting equation contained two components, one to account for each phase (equation (**2.1**)),

$$\frac{v_o}{[E]_T} = \frac{k_{cat}[S]}{K_M + [S]} + k_{app}[S] \qquad (\textbf{2.1})$$

where k_{cat} and K_M are the apparent kinetic parameters that best fit the hyperbolic (i.e., low $[H_2O_2]$) component, and k_{app} is the slope of the linear (i.e., high $[H_2O_2]$) component and would correspond to the k_{cat}/K_M for a second H_2O_2 disproportionation mechanism.

Under other conditions (e.g., higher pH or in the presence of most electron donors), only a single hyperbolic phase was observed, calling for a standard Michaelis-Menten equation to obtain an apparent K_M and k_{cat} (equation (**2.2**)).

$$\frac{v_o}{[E]_T} = \frac{k_{cat}[S]}{K_M + [S]}$$
(**2.2**)

The primary effect of ABTS on the H_2O_2-dependent kinetic parameters of O_2 production was a hyperbolic increase in the observed k_{cat}, ($k_{cat(o)}$). As such, these values were fit to equation (**2.3**) to obtain an apparent K_D for ABTS. Here $k_{cat(u)}$ is the apparent k_{cat} in the absence of any ABTS, and $k_{cat(s)}$ is the maximum stimulatory contribution of ABTS to the k_{cat} parameter.

$$k_{cat(o)} = \frac{k_{cat(s)}[ABTS]}{K_D + [ABTS]} + k_{cat(u)}$$
(**2.3**)

2.2.11. Stopped-flow analysis

Optical stopped-flow methods were used to observe the dominant heme intermediates of MtKatG under multiple turnover conditions. We used a PC-upgraded SX18.MV from Applied Photophysics (Leatherhead, UK) for all measurements. All reactions were carried out in the single-mixing mode using diode array detection. The intense absorption spectra of electron donor radical oxidation products often obscured a clear view of spectral characteristics due to the heme. To circumvent this challenge, we used ascorbate to rapidly reduce these accumulating free radical products generated during the consumption of H_2O_2. This approach has been successfully applied to single-turnover stopped-flow experiments with plant peroxidases (*148-149*), and we report here the effective application of the strategy to identify heme intermediates which accumulate in the steady-state under multiple turnover conditions. Indeed, our results showed that ascorbate effectively scavenges the peroxidase substrate radicals generated during H_2O_2

consumption. Importantly, the data show that although ascorbate is able to act as a direct electron donor to KatG, its capacity to do so in the presence of donors like TMB at the concentrations used is very limited. By far, the primary action of ascorbate in the system was to reduce substrate-derived radicals rather than to react directly with KatG.

MtKatG (6 µM) was placed in syringe A in the presence of 5 mM phosphate buffer, pH 7.0. A second syringe (syringe B) contained varying concentrations of H_2O_2 in 100 mM buffer at the target pH for the reaction. Ascorbate, when included, was also placed in syringe B at a concentration of 0.2 mM. The aromatic peroxidase electron donor (TMB, TMPD, or ABTS), when included, was also placed in syringe B at a concentration of 0.2 mM.

2.3.   Results

We evaluated the effect of ABTS, a classical peroxidase electron donor, on the catalase activity of MtKatG anticipating that it would be an inhibitor. Instead, its inclusion produced a dramatic and concentration-dependent *stimulation* of O_2 production at pH 5.0 (Fig. 2.3). When ABTS was absent or present at lower concentrations (i.e., 1.0 – 10.0 µM), an unusual bipartite response to H_2O_2 concentration was observed. For example, in the absence of ABTS there was a linear increase in rates of O_2 production from 2.0 mM to 50 mM H_2O_2 (Fig. 2.4). This was consistent with the high apparent K_M for H_2O_2 (225 mM) previously reported for this KatG at low pH (*141*), with the slope of the fit line corresponding to the apparent second order rate constant for the reaction. However, linear fitting of the 2 mM – 50 mM data consistently returned positive Y-intercepts (470 ± 30 s^{-1}). Upon monitoring reaction rates at lower H_2O_2 concentrations (0.1 - 1.0 mM), we observed a sharp deviation from linearity, indicating two components of the H_2O_2 dependence of MtKatG catalase activity. The data were fit to equation **2.1** to account for

41
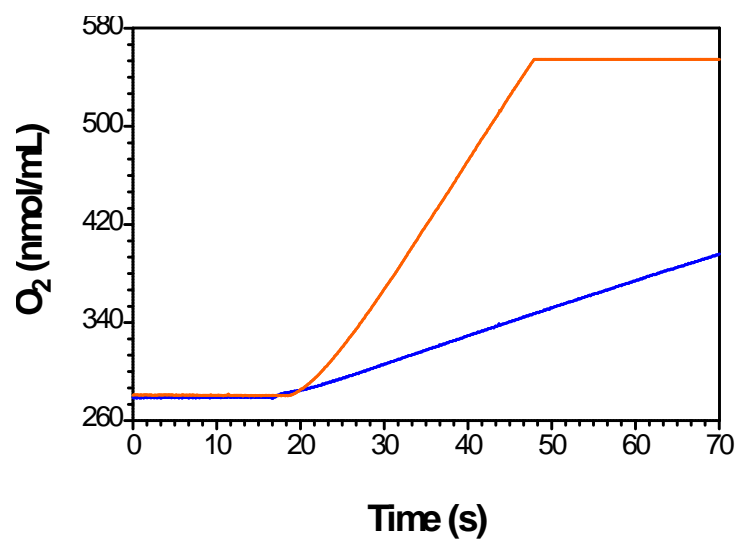
Figure 2.3. Effect of ABTS on O_2 production by MtKatG. Catalase activity was measured by O_2 production with (orange) and without (blue) 0.1 mM ABTS. All reactions contained 2 mM H_2O_2 and were carried out using 5 nM KatG and 50 mM acetate buffer, pH 5.0, at 23 °C.

the hyperbolic and linear components at low and high H_2O_2 concentrations, respectively. Without ABTS, the apparent k_{cat} corresponding to the hyperbolic phase was 570 ± 60 s^{-1} (Table 2.2). This was in good agreement with the *Y*-intercept obtained from the linear extrapolation of the higher H_2O_2 concentration data (Fig. 2.4).

Two components in the rates of O_2 production were also observed when low concentrations of ABTS (1 to 10 µM) were included (Fig. 2.5). The slope corresponding to the second component appeared to decrease while the amplitude of the hyperbolic phase increased due primarily to increase in the apparent k_{cat} parameter. At higher ABTS concentrations (0.05 – 1 mM), only one hyperbolic phase was observed, and accordingly, the data were fit to equation **2.2** (Fig. 2.6). Across the entire ABTS concentration range, the apparent K_M for H_2O_2-dependent O_2 production remained near 0.6 mM ($\pm$ 0.2 mM), but the apparent k_{cat} increased hyperbolically starting from 570 s^{-1} (without ABTS) and increasing toward a maximum of 6,000 s^{-1} (Fig. 2.7). Least squares fitting of the data to equation **2.3** uncovered an apparent K_D of 0.12 mM for ABTS in its stimulation of catalase activity.

The stimulatory effect of ABTS was pH dependent (Fig. 2.8A and 2.8B). Catalatic O_2 production in the absence of an electron donor was optimal at pH 7.5, consistent with the pH dependence of the k_{cat}/K_M of KatGs reported elsewhere (*108, 141*) and expected based upon the concentration of H_2O_2 (1 mM) used in these experiments. In the presence of 0.1 mM ABTS, the pH profile for O_2 production was similar to that without ABTS, provided the pH was 7.0 or greater. However, below 7.0, rates of O_2 production diverged, becoming greater in the presence of ABTS and lower in its absence. The pH optimum for ABTS-stimulated O_2 production was between 4.5 and 5.0. This bore some similarity to the pH dependence of MtKatG peroxidase activity whose optimum we observed at pH 4.0.

Table 2.2. Effect of peroxidatic electron donors on catalatic kinetic parameters.

	Catalase Kinetic Parameters[a]			
	Component 1			Component 2
Electron donor[b]	k_{cat} (s^{-1})	K_M (mM)	$k_{app(1)}$ (M^{-1}s^{-1})	$k_{app(2)}$ (M^{-1}s^{-1})
None	570 ± 60	0.8 ± 0.2	$(7.1 \pm 0.9) \times 10^5$	$(1.8 \pm 0.2) \times 10^4$
Ascorbate	520 ± 30	0.13 ± 0.3	$(3.9 \pm 0.8) \times 10^6$	$(1.7 \pm 0.1) \times 10^4$
Pyrogallol	630 ± 20	0.20 ± 0.03	$(3.2 \pm 0.4) \times 10^6$	$(1.91 \pm 0.07) \times 10^4$
ABTS	3300 ± 60	0.83 ± 0.05	$(4.0 \pm 0.1) \times 10^6$	- -
TMB	5220 ± 70	0.70 ± 0.05	$(7.4 \pm 0.1) \times 10^6$	- -
o-Dianisidine	5600 ± 100	0.49 ± 0.05	$(1.2 \pm 0.1) \times 10^7$	- -
ABTS (1.0 mM)	6040 ± 80	0.56 ± 0.04	$(1.1 \pm 0.1) \times 10^7$	- -
TMPD	7012 ± 60	1.2 ± 0.1	$(6.0 \pm 0.2) \times 10^6$	- -
CPZ	7940 ± 120	1.1 ± 0.1	$(7.2 \pm 0.4) \times 10^6$	- -

[a]All activities were measured by O_2 production using a Clark-type electrode in 50 mM acetate buffer, pH 5.0, at 23 ºC.
[b]Unless otherwise specified, the concentration of each electron donor was 0.1 mM.
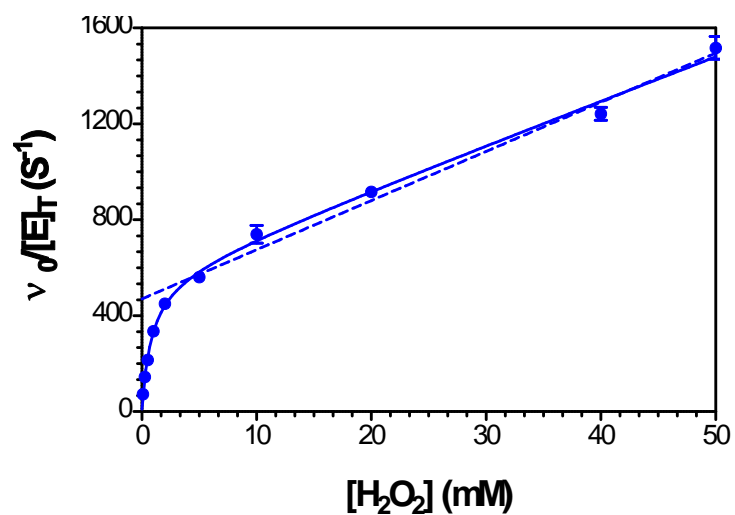
Figure 2.4. Effect of H_2O_2 concentration on O_2 production by MtKatG. Linear regression was carried out for points obtained from 2 to 50 mM H_2O_2 (dashed line). The solid line was obtained by nonlinear least squares fitting of all points to equation (**2.1**). All reactions were carried out using 5 nM KatG and 50 mM acetate buffer, pH 5.0, at 23 ^{o}C.
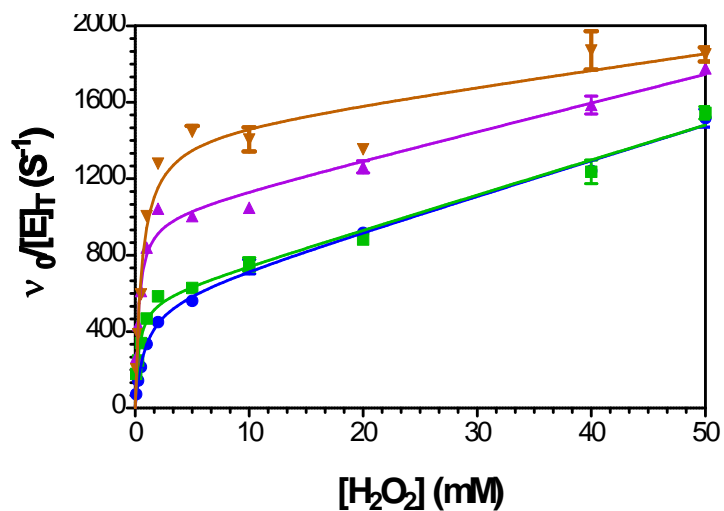
Figure 2.5. The effect of H_2O_2 concentration on the rate of O_2 production by MtKatG in the presence of 0 mM ( ), 0.001 mM ( ), 0.005 mM (   ), and 0.01 mM (   ) ABTS. Each set of points was fit to Equation (**2.1**) to obtain the fit lines. All reactions were carried out using 5 nM KatG and 50 mM acetate buffer, pH 5.0 at 23 ^{o}C.
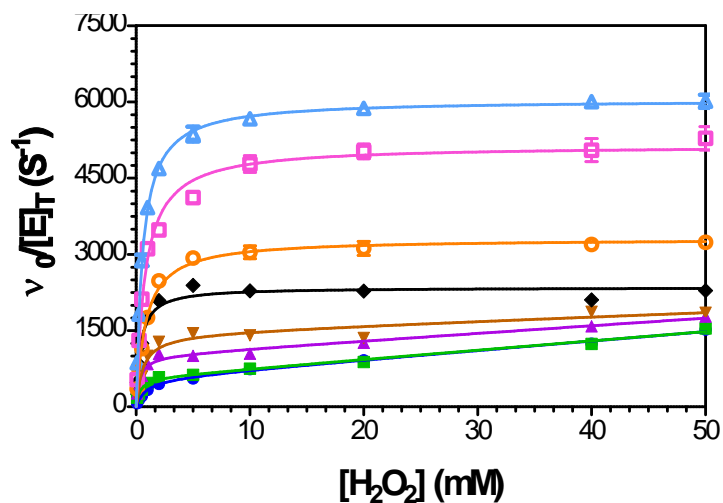
Figure 2.6. Effect of ABTS concentration on catalase activity of MtKatG. Rates of O_2 production were measured as a function of H_2O_2 concentration in the presence of 0 mM ( ), 0.001 mM ( ), 0.005 mM ( ), 0.01 mM ( ), 0.05 mM ( ), 0.1 mM ( ), 0.5 mM ( ), and 1.0 mM ( ) ABTS. All reactions were carried out using 5 nM KatG and 50 mM acetate buffer, pH 5.0 at 23 °C.
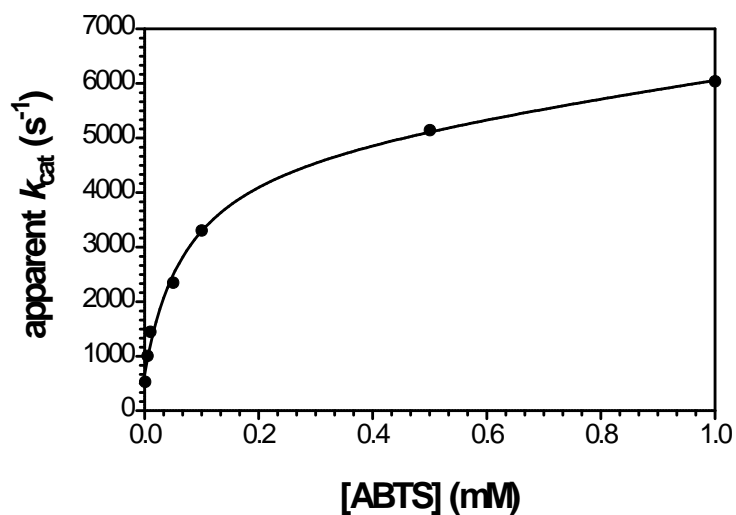
Figure 2.7. Effect of the peroxidase electron donor ABTS on the apparent k_{cat} for catalase activity of MtKatG. Catalase activity was measure by O_2 production and kinetic parameters with respect to H_2O_2 were calculated from non-linear least squares fitting of the data presented in Figure 2.6 to equation (**2.1**), (**2.2**) as appropriate. The observed k_{cat} values were fit to equation (**2.3**) to obtain an apparent K_D for ABTS.
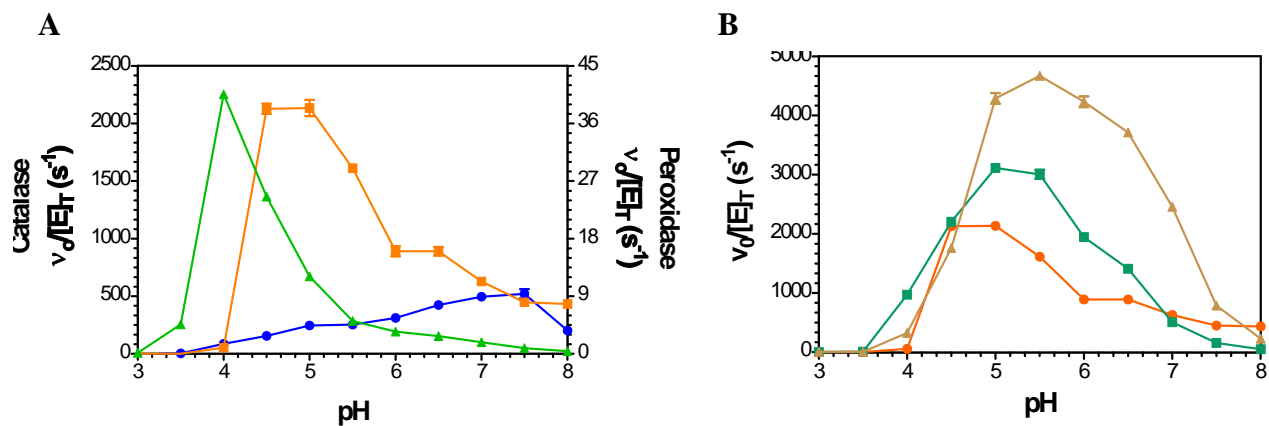
Figure 2.8. Effect of pH on MtKatG catalase activity in the presence and absence of electron donor ABTS. Catalase activity (as measured by O_2 production) was evaluated without any added ABTS ( ) and with 0.1 mM ABTS ( ). Peroxidase activity was also measured using 0.1 mM ABTS ( ), (Panel A). Panel B shows the pH dependence of catalase activity stimulated by 0.1 mM TMB ( ), 0.1 mM TMPD ( ), and 0.1 mM ABTS ( ). All reactions contained 1.0 mM H_2O_2 and were carried out at 23 ^{o}C.

The extent of ABTS oxidation by MtKatG was measured under the same conditions that showed stimulation of O_2 production (Fig. 2.9). Each reaction was allowed to proceed until the H_2O_2 had been fully consumed. This was confirmed by the fact that of all reaction components only a second addition of H_2O_2 was able to affect additional ABTS$^{\bullet+}$ production. As expected, the extent of ABTS$^{\bullet+}$ production increased with increases in initial H_2O_2 concentration. However, less than one equivalent ABTS$^{\bullet+}$ was generated for every 125 equivalents H_2O_2 consumed, far less than the 2:1 ratio anticipated for typical peroxidase activity. Thus, even under conditions most favorable to peroxidase activity (i.e., pH ~ 4.5, presence of an efficient aromatic electron donor, and H_2O_2 concentration below 5 mM), the vast majority of H_2O_2 consumption was directed toward O_2 production, not *in spite* of the electron donor but *because* of it.

Despite their markedly different structures and oxidation potentials, other common peroxidase electron donors like 3,3',5,5'-tetramethylbenzidine (TMB), *N,N,N',N'*-tetramethylphenylenediamine (TMPD), chlorpromazine (CPZ), and *o*-dianisidine showed comparable abilities to stimulate O_2 production (Fig. 2.10). As with ABTS, the stimulatory effect was restricted to the first hyperbolic component corresponding to low H_2O_2 concentrations and was primarily observed in the k_{cat} parameter with all of them producing k_{cat} values for catalase activity in excess of 5000 s^{-1} (Table 2.2). Similar rates of O_2 production could be achieved in the presence of ABTS but only at a ten-fold higher concentration. Interestingly, little if any stimulatory effect was observed with ascorbate and pyrogallol. At 0.1 mM, they returned apparent k_{cat} values of 520 s^{-1} and 630 s^{-1}, respectively. Without any electron donor added, the k_{cat} was 570 s^{-1}. The effect of pH on the stimulatory activity of TMB and TMPD was very similar to that of ABTS on the low end, but both donors showed greater stimulatory capacity at
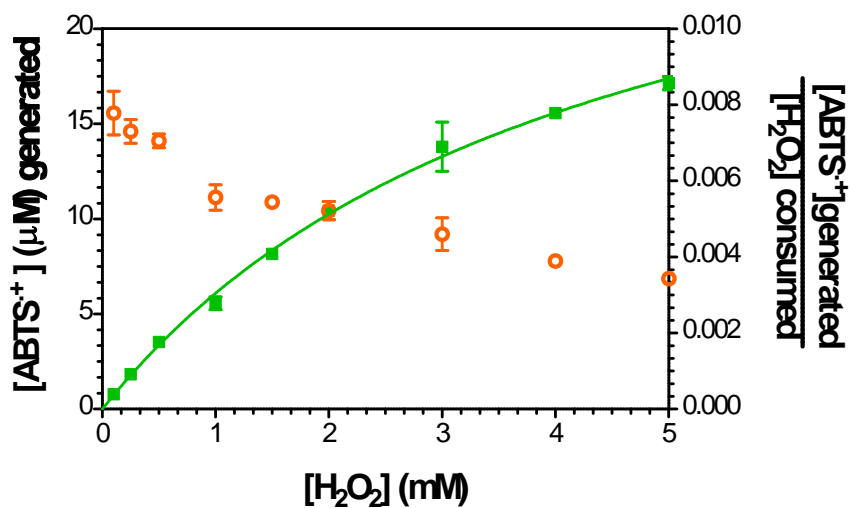
Figure 2.9. Extent of peroxidatic electron donor oxidation in comparison to H_2O_2 consumption by MtKatG. The extent (µM) of $ABTS^{\bullet+}$ accumulation ( ) and the ratio of $ABTS^{\bullet+}$ generated to H_2O_2 consumed ( ) are plotted as a function of initial H_2O_2 concentration. All reactions were carried out using 20 nM KatG and 0.1 mM ABTS in 50 mM acetate buffer, pH 5.0, at 23 ^{o}C.
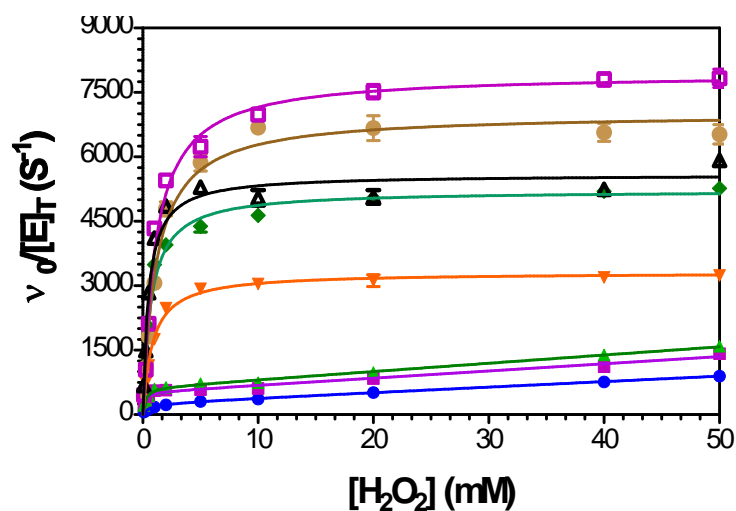
Figure 2.10. Enhancement of MtKatG catalase activity by various peroxidase electron donors. The catalase activity of MtKatG was measured without any peroxidase electron donor ( ), 0.1 mM pyrogallol ( ), 0.1 mM ascorbate ( ), 0.1 mM ABTS ( ), 0.1 mM TMB ( ), 0.1 mM o-dianisidine ( ), 0.1 mM TMPD ( ), or 0.1 mM chlorpromazine ( ). All reactions were carried out at 23 ^{o}C using 5 nM KatG and 50 mM acetate buffer, pH 5.0.

higher pH values with the optimum for TMB between 5.0 and 5.5 and that for TMPD at 5.5 (Fig. 2.8B).

To evaluate the dominant heme intermediate(s) present during electron donor-stimulated O_2 production, we used stopped-flow to react MtKatG with excess H_2O_2 in the presence and absence of the peroxidase substrate TMB. As described in Materials and Methods, we used an ascorbate-based method to suppress spectral interference due to the accumulation of $TMB^{\bullet+}$. This experiment was performed for verification purposes. Our aim was to compare the heme absorption spectra observed during the catalatic consumption of H_2O_2 in the presence and absence of peroxidase electron donors. The most effective electron donors for stimulating catalase activity were tetramethylbenzidine (TMB), tetramethylphenylenediamine (TMPD), o-dianisidine, and ABTS. During the stimulation of catalase activity, these electron donors were oxidized at least to some extent. Due to the very intense absorption characteristics of the free radical oxidation products of these electron donors, heme absorption spectra were obscured, particularly under multiple turnover conditions (i.e., excess H_2O_2). In order to minimize the interference from accumulated free radical products, we employed ascorbate to rapidly reduce the free radical oxidation products of these electron donors back to the parent compound.

It was critical to verify that the primary effect of ascorbate was the rapid reduction of electron donor radical products (e.g., $TMB^{\bullet+}$) rather than a direct reaction with the higher oxidation states of the MtKatG heme. Figure 2.11 shows the spectra recorded for MtKatG following mixing with 0.5 mM H_2O_2 and 0.1 mM TMB at pH 5.0. The spectra recorded show a rapid increase in absorbance across the visible range with the exception of a small decrease in absorption centered at 429 nm. As TMB does not absorb in the visible range and $TMB^{\bullet+}$ is known for absorption maxima at 370 and 650 nm, the decrease in absorbance at 429 nm was

53
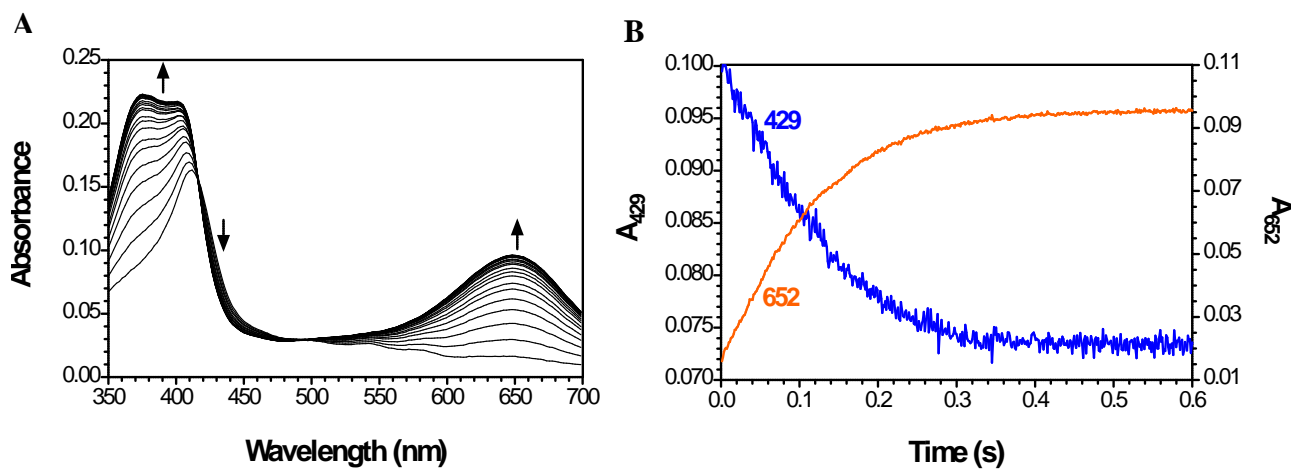
Figure 2.11. Reaction of MtKatG with 0.5 mM H_2O_2 in the presence of 0.1 mM TMB. The spectra displayed on the left started 1.26 ms after mixing and continued through 606 ms in 25.2 ms increments. The spectra on the right show the time course for changes in absorbance at 429 nm (blue) and 652 nm (orange). The directions of absorbance changes with time are indicated by the arrows. The final reaction contained 1.5 µM MtKatG and 50 mM acetate buffer, pH 5.0, and was carried out at 5.0 ^{o}C.

attributable to changes in heme absorption spectra during the reaction. Comparison of the time courses for changes in absorbance at 652 nm (due to $TMB^{\bullet+}$ accumulation) and 429 nm (due to changes in the MtKatG heme) demonstrated that both occurred simultaneously. The conclusion of $TMB^{\bullet+}$ accumulation corresponded with the cessation of changes to the heme absorption spectrum.

The effect of ascorbate on this reaction was evaluated by including it in syringe B with TMB and H_2O_2. Whether ascorbate was present or absent, the initial absorption spectra recorded at 1.26 ms were virtually identical and were consistent with domination by heme species (Fig. 2.12 -panel A). Conversely, the inclusion of ascorbate had a pronounced effect on spectra recorded at 0.5 s (Fig. 2.12-panel B). In the presence of ascorbate, the spectrum recorded at 0.5 s was dominated by heme, and its features were consistent with high spin ferric state. In the absence of ascorbate, contributions from $TMB^{\bullet+}$ and heme species were observed. Indeed, the difference between these spectra (spectrum at 0.5 s without ascorbate minus spectrum with ascorbate at 0.5 s) was consistent with that of $TMB^{\bullet+}$ alone (Fig. 2.12-panel D). Regardless of the presence or absence of ascorbate, the absorbance at 429 nm decreased over the course of the reaction (Fig. 2.12-panel C), indicating that changes in absorbance at this wavelength were due to changes in the heme itself. Moreover, the traces recorded at 429 nm in the presence and absence of ascorbate were virtually superimposable. Taken together, these data indicate that the primary action of ascorbate in this system is in the rapid reduction of $TMB^{\bullet+}$ rather than a direct reaction with MtKatG. Thus, the system was appropriate to evaluate the heme state during the consumption of H_2O_2 in the presence of TMB.

Accordingly, KatG was either reacted with 0.5 mM H_2O_2 alone, 0.5 mM H_2O_2/0.1 mM ascorbate, or 0.5 mM H_2O_2/0.1 mM ascorbate/0.1 mM TMB. Under the later conditions, the first
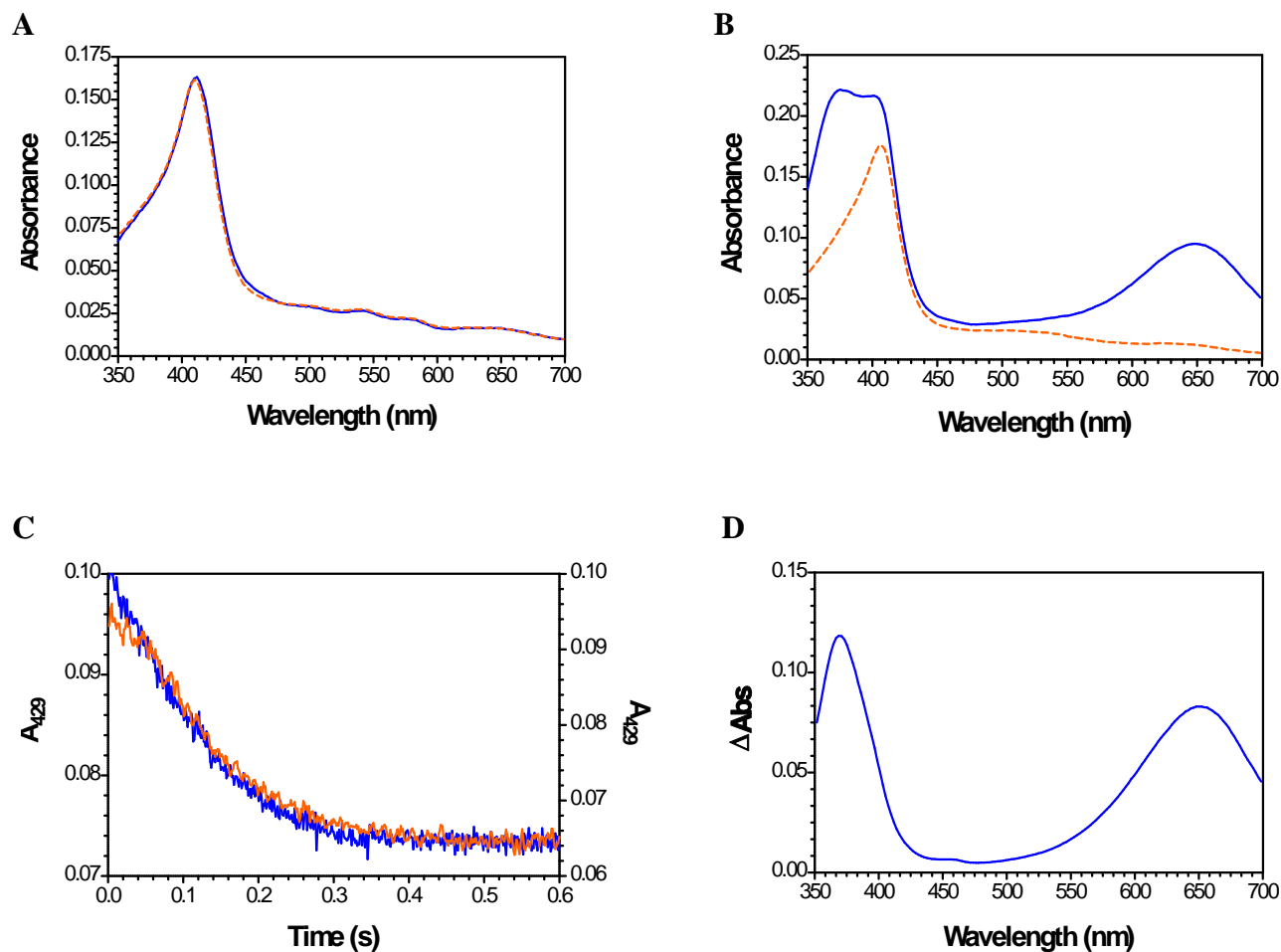
Figure 2.12. Effect of ascorbate on spectra recorded during MtKatG turnover in the presence of 0.5 mM H_2O_2 and 0.1 mM TMB. Panel A shows the spectra collected at 1.26 ms for MtKatG in the presence of 0.5 mM H_2O_2 and 0.1 mM TMB with (dashed line) and without (solid line) 0.1 mM ascorbate. Panel B shows spectra collected at 0.5 s from the same reactions with (dashed line) and without (solid line) 0.1 mM ascorbate. Panel C shows the time course of the reaction of MtKatG with 0.5 mM H_2O_2 and 0.1 mM TMB in the presence (orange) and absence (blue) of 0.1 mM ascorbate monitored at 429 nm. Panel D shows the difference spectrum for the spectra shown in panel B, i.e., spectrum recorded at 0.5 s in the absence of ascorbate (solid line) minus the spectrum recorded in the presence of 0.1 mM ascorbate (dashed line). Both reactions included 1.5 μM MtKatG and 50 mM acetate buffer, pH 5.0, and were carried out at 5.0 $^{\circ}$C.

heme spectrum recorded (1.26 ms) showed a λ_{max} in the Soret band at 413 nm and prominent β and α bands at 542 and 578 nm, respectively. Over the next 300 ms, there was a spectral shift to a species with maxima at 407, 500, and 633 nm (Fig. 2.13A [trace c] and 2.13B). The earliest spectra were consistent with a compound III-like intermediate (*124*) which was then rapidly converted to the ferric state.

In the absence of TMB (with or without ascorbate) the first recorded spectrum was similar to that observed in the presence of TMB with maxima at 413, 542, and 578 nm (Fig. 2.13C and 2.13E). However, over the next 300 ms little if any change in the Soret band was observed, and concomitantly, there was a broad and nondescript increase in absorbance at wavelengths greater than 520 nm. These spectral changes are highly similar to those observed during reaction of *Synechocystis* KatG and MtKatG with excess H_2O_2, particularly at acidic pH (*113, 115*). After 300 ms there was a slow conversion back to the ferric state as indicated by the shift of the Soret maximum to 408 nm and features at about 500 and 625 nm (Fig. 2.13D and 2.13F). This also was consistent with previously observed reactions of MtKatG with excess H_2O_2 at pH 6.0 (*113*). The return of MtKatG to its ferric state was the slowest in the presence of H_2O_2 alone (Fig. 2.13A [trace a]), slightly faster with the inclusion of ascorbate (Fig. 2.13A [trace b]), and two orders of magnitude more rapid when TMB was also present (Fig. 2.13A [trace c]).

The return of MtKatG to its ferric state indicated the complete consumption of H_2O_2 in these reactions. Inclusion of increasing concentrations of H_2O_2 in reactions containing MtKatG/TMB/ascorbate increased the time preceding the appearance of the ferric state (as monitored at 401 nm) (Fig. 2.14A). Indeed, a steady-state phase of H_2O_2 consumption became apparent in the traces obtained using 1.75 and 3.5 mM H_2O_2. The spectra recorded during this phase showed absorption maxima at 416, 542, and 580 nm, consistent with a compound III-like
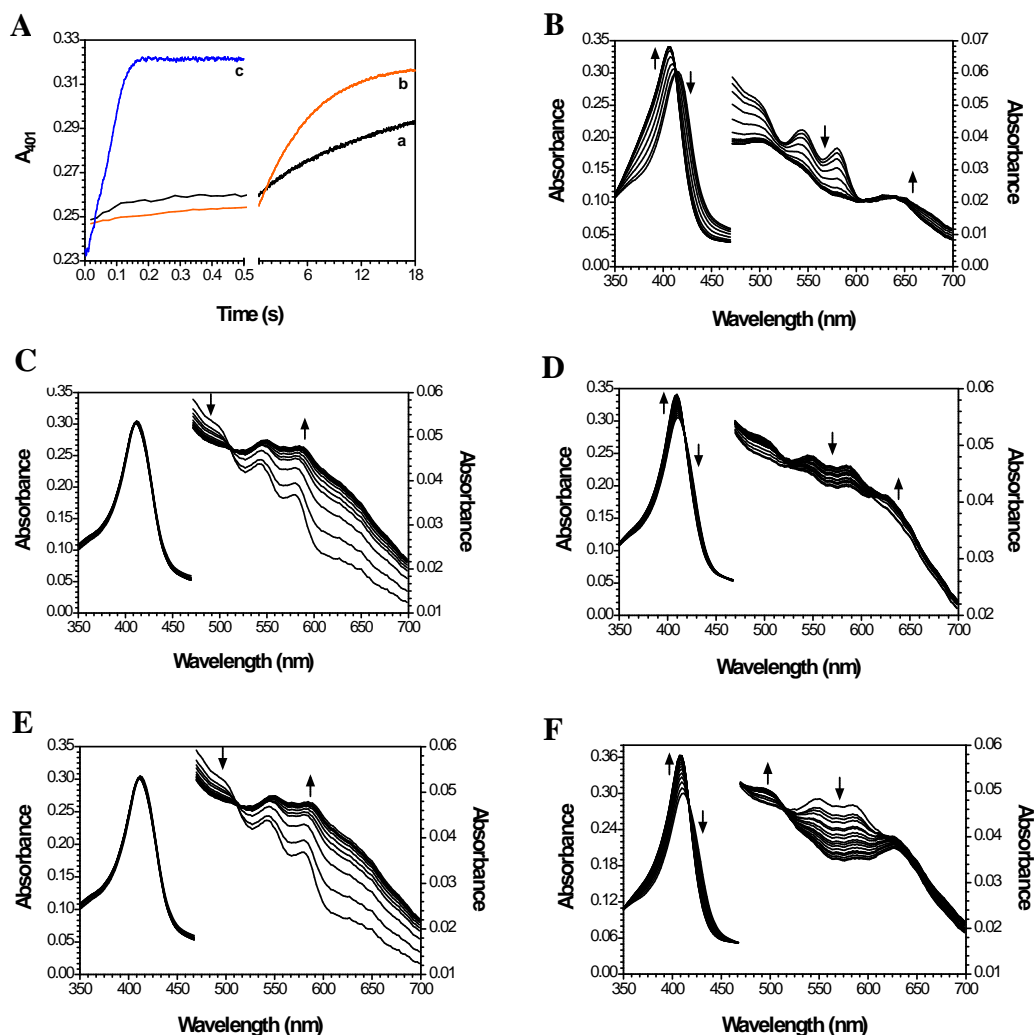
Figure 2.13. Heme spectra observed during MtKatG reactions with excess H_2O_2 in the presence and absence of the peroxidase electron donor TMB. The time courses for the return of the ferric state as monitored at 401 nm (Panel A) are shown for MtKatG reaction with 0.5 mM H_2O_2 alone (a), 0.5 mM H_2O_2 and 0.1 mM ascorbate (b), and 0.5 mM H_2O_2, 0.1 mM ascorbate and 0.1 mM TMB (c). Spectra recorded following MtKatG reaction with 0.5 mM H_2O_2, 0.1 mM ascorbate, and 0.1 mM TMB are shown in Panel B where the first spectrum was recorded at 1.26 ms and every 25.2 ms thereafter up to 278 ms. Spectra recorded following MtKatG reaction with 0.5 mM H_2O_2 alone are shown in panels C (1.26 - 278 ms) and D (0.302 - 18.3 s). Spectra recorded following MtKatG reaction with 0.5 mM H_2O_2 and 0.1 mM ascorbate are shown in panels E (1.26 - 278 ms) and F (0.302 - 18.3 s). For all spectra the direction of changes in absorption over the course of the reaction are shown with arrows. The final reaction all contained 3 μM MtKatG and 50 mM acetate buffer, pH 5.0. All reactions were carried out at 4 °C.
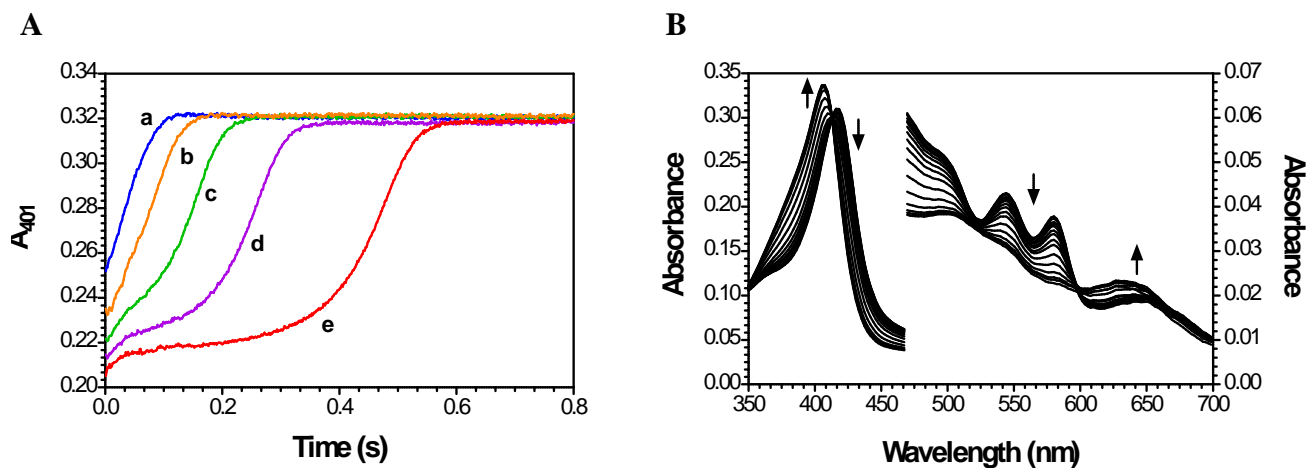
Figure 2.14. Effect of H_2O_2 concentration on the return of MtKatG to its ferric state. The accumulation of MtKatG in its ferric state was monitored by an increase in absorbance at 401 nm (Panel A). Reactions contained 3 μM MtKatG, 0.1 mM TMB, 0.1 mM ascorbate, and 0.25 mM H_2O_2 (a), 0.5 mM H_2O_2 (b), 1.0 mM H_2O_2 (c), 1.75 mM H_2O_2 (d), and 3.5 mM H_2O_2 (e). Spectra corresponding to the reaction with 3.5 mM H_2O_2 (Panel B) were recorded every 25.2 ms starting at 200 ms post-mixing up to 604 ms. The arrows indicate the direction of absorbance changes during the course of the reaction. Each reaction was carried out in 50 mM acetate buffer, pH 5.0, at 4 ^{o}C.

intermediate (*124*). This species appeared to convert to the ferric state without appreciable intermediary accumulation of another heme state (Fig. 2.14B).

An additional experiment was performed to evaluate the extent of TMB oxidation to TMB$^{\bullet+}$ during the turnover of MtKatG in the presence of H_2O_2 (Fig. 2.15). In this experiment all reactions contained 0.1 mM TMB. The steady-state turnover of the enzyme and its return to the ferric state upon H_2O_2 depletion were monitored in the presence of ascorbate with the emergence of the ferric state signified by a decrease in absorbance at 429 nm. Accumulation of TMB$^{\bullet+}$ was monitored at 650 nm in an identical experiment except that ascorbate was excluded from the reaction. In the each case, the return of the enzyme to its ferric state corresponded with the cessation of TMB$^{\bullet+}$ production. The concentration of TMB$^{\bullet+}$ observed at the end of each reaction was proportional to the initial concentration of H_2O_2, but that proportion was consistently near 1 equivalent TMB$^{\bullet+}$ generated for every 150 equivalents H_2O_2 consumed. Complementary with the results presented in Figure 2.9, the vast majority of H_2O_2 consumed was directed toward O_2 production (i.e., catalase activity). Counterintuitively, it was the presence of the peroxidase electron donor itself which contributed to such high rates of O_2 production in the first place. Notably, the results of this experiment and those reported in Figure 2.9 seem to indicate that the stimulation of O_2 production (i.e., catalase activity) occurs by a mechanism that produces little in the way of net accumulation of the oxidized electron donor.
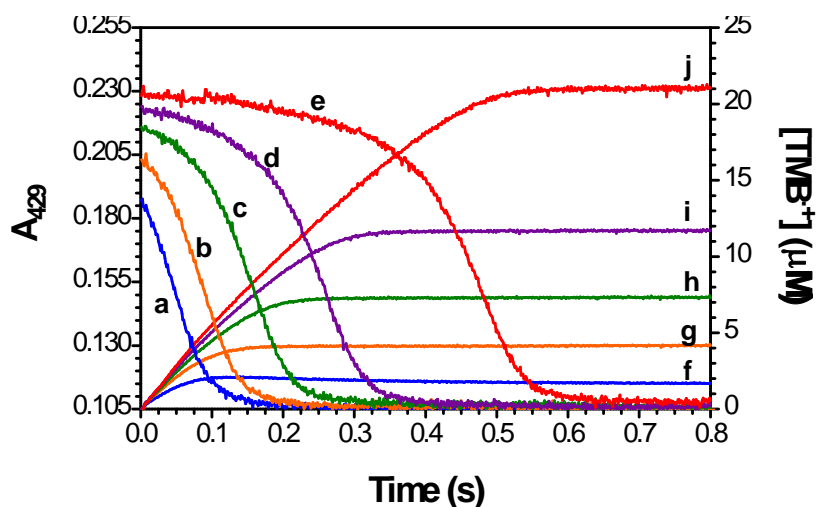
Figure 2.15. Effect of H_2O_2 on turnover of MtKatG and accumulation of TMB$^{\bullet+}$. Return of MtKatG to its ferric state was monitored by a *decrease* in absorbance at 429 nm in the presence of 0.25 (a), 0.5 (b), 1.0 (c), 1.75 (d), and 3.5 mM H_2O_2 (e). Ascorbate (0.1 mM) was included in these reactions to minimize interference from TMB$^{\bullet+}$. In order to measure accumulation of TMB$^{\bullet+}$, ascorbate was excluded from the reactions and *increases* in absorbance were monitored at 605 nm in the presence of 0.25 (f), 0.5 (g), 1.0 (h), 1.75 (i), and 3.5 mM H_2O_2 (j). Final reactions all contained 3.0 µM KatG, 0.1 mM TMB, 50 mM acetate buffer, pH 5.0, and were carried out at 4 °C.

2.4. Discussion

2.4.1. Implications for the nature of observed peroxidase activity and O_2 production by KatG

The stimulatory effect of peroxidatic electron donors on *catalatic* O_2 production by KatG is surprising. It has been generally assumed that the two activities should be mutually competitive. There is broad agreement that the peroxidase and catalase reaction cycles of KatG both begin with H_2O_2 reduction to access higher KatG oxidation states. The completion of each catalytic cycle requires oxidation of one or another substrate: either H_2O_2 for catalatic turnover or an exogenous (typically aromatic) electron donor for peroxidatic turnover. Though there is considerable debate as to how KatG accomplishes H_2O_2 oxidation to generate O_2, it is reasonable to suppose that the two-electron oxidation of H_2O_2 would preclude the oxidation of some other donor. Consistent with this, one of the earliest studies on *E. coli* KatG showed that the common peroxidase electron donor *o*-dianisidine inhibited catalase activity at pH 7.5 (*107*). Under limited circumstances (i.e., above pH 7.0), we also observed inhibition by TMB and TMPD, but under more acidic conditions the dominant effect of these compounds was to stimulate O_2 production by as much as 14-fold. This counterintuitive effect was most prominent below pH 6.0 where one typically observes the most robust peroxidase activity. Previous investigations of the pH dependence of KatG catalase activity have shown a substantial increase in the apparent K_M for H_2O_2 as the pH decreases below 7 (*108, 141*). In particular, for MtKatG, this parameter shifts from 2.5 mM at pH 7.0 to 225 mM at pH 5.0 (*141*). At first glance, ABTS appeared to restore at pH 5.0 the efficient catalase activity typically observed near pH 7.0. However, the two-component response of KatG to H_2O_2 suggested that a "low-K_M" catalase activity was already operating at pH 5.0. In the absence of an electron donor, its contribution to the total observed

activity was small, particularly at high H_2O_2 concentrations (i.e., k_{cat} = 570 s^{-1} vs.
k_{cat} = 10,500 s^{-1}), making it easy to miss. The electron donor appeared to exclusively stimulate the "low-K_M" component by increasing its k_{cat} parameter. If there was any effect on the "high-K_M" component, the electron donor was inhibitory.

This led to a second striking observation. Even under conditions most favorable to peroxidase activity (i.e., pH ~ 4.5, millimolar concentration of aromatic electron donor, and H_2O_2 concentration below 5 mM), the vast majority of H_2O_2 consumption was directed toward O_2 production rather than accumulation of the aromatic donor in its oxidized state. More importantly, the magnitude of the imbalance came about not *in spite* of the electron donor but *because* of it. Indeed, the accumulation of one equivalent of oxidized aromatic donor (e.g., TMB$^{•+}$) corresponded to the consumption of about 150 equivalents H_2O_2. It has been generally appreciated that the parameters for catalatic turnover are far greater than those recorded for peroxidase activity. For example, an apparent k_{cat} a value of 4000 s^{-1} for catalase (pH 7) and 20 s^{-1} for peroxidase (pH 4.5) are not at all atypical. Even evaluating activity at the same pH (5.0), we observed catalase turnover in the presence of 1 mM H_2O_2 alone was about 570 s^{-1} whereas peroxidase activity in the presence of 1 mM H_2O_2 and 0.1 mM ABTS was about 12 s^{-1} (accounting for canonical peroxidase stoichiometry, this would translate to about 6 turnovers per second). Supposing that the two activities are mutually competitive, one would expect catalase activity to be no more than 570 s^{-1}, and most likely less in the presence of ABTS. Instead, the conditions that showed an apparent peroxidase turnover of ~ 6 s^{-1} were simultaneously producing catalase turnover on the order of 2100 s^{-1}.

2.4.2. Implications for the mechanism (s) of KatG catalatic turnover

There has been considerable discussion surrounding the mechanism by which KatG accomplishes catalatic turnover, in particular the oxidation of H_2O_2 to produce O_2. Several intermediates have been proposed as the H_2O_2 oxidizing species, including a typical compound I (i.e., $Fe^{IV}=O[porphyrin]^{\bullet+}$), or a compound I* where an oxidizing equivalent is held on the protein in the form of an amino acid-centered radical such as a nearby tryptophan (e.g., Fe^{IV}-OH[W321]$^{\bullet+}$) (*115-117*), or the KatG-unique covalent adduct (i.e., Fe^{IV}-OH[MYW]$^{\bullet+}$) (*115*), or finally, a compound III-like intermediate derived from a reaction of the latter with an additional equivalent of H_2O_2 (i.e., Fe^{III}-$O_2^{\bullet-}$[MYW]$^{\bullet+}$) (*112-113, 115, 121*).

With the caveat that UV-visible absorption spectra should be interpreted with caution, it is notable that the dominant heme absorption spectrum we observed during electron-donor stimulated catalase activity had features consistent with a compound III (i.e., oxyperoxidase or Fe^{III}-$O_2^{\bullet-}$) intermediate (*124*). First, the greater prominence and persistence of this intermediate in the presence of TMB correlated with the much greater rates of catalatic O_2 production observed with this compound. This suggests that peroxidatic electron donors act to facilitate an existing rather than an alternative catalatic mechanism. This is corroborated by the fact that the Y229F variant of MtKatG shows no catalase activity even in the presence of peroxidatic donors. Furthermore, the appearance of a compound III-like intermediate is counter to what one would anticipate for canonical peroxidase turnover as electron donors typically prevent compound III accumulation. Because the rate-determining step in typical peroxidatic turnover is the reduction of compound II by the exogenous electron donor, compound II would be the expected dominant heme state (*124*). In our experiments using TMB, compound III-like spectral features dominated with no evidence of characteristics typically assigned to a compound II (i.e., Fe^{IV}-OH) state (*124*). Although we also detected compound III-like features in reactions of KatG with H_2O_2

alone, as have others (*113, 115*), TMB did not diminish but only seemed to enhance these features. Further, compound III-like features persisted until H_2O_2 was depleted at which time there was an apparent direct conversion to the ferric state. Conversely, without TMB the compound III-like features were most prominent only at the earliest time points and appeared to be washed out at later time points by an intermediate (s) with rather featureless spectral characteristics. Upon depletion of H_2O_2 no isosbestic points were detected above 450 nm, suggesting a more complex transition perhaps involving the conversion of multiple intermediates to the ferric state.

One possible explanation for such behavior would be the participation of more than one mechanism for catalase turnover where the presence of a peroxidatic electron donor simply shifts the balance toward one that proceeds via an intermediate with spectral characteristics typical of a peroxidase compound III, perhaps $Fe^{III}\text{-}O_2^{\bullet-}[MYW]^{\bullet+}$. The kinetics of O_2 production corroborated the possibility of coexistent mechanisms for catalatic turnover. At low pH and in the absence of electron donors, we observed two distinct components to the kinetic response of KatG to H_2O_2 concentration. One component was governed by a low apparent K_M and k_{cat} (0.8 mM and 570 s^{-1}, respectively), and the second component was consistent with a high apparent K_M as has been previously reported for MtKatG (k_{cat} 10,200 s^{-1}; K_M 225 mM) (*141*). Due to the large disparity in apparent k_{cat} values, in the absence of a peroxidatic electron donor, it is clearly the "high-K_M" mechanism that will dominate O_2 production as H_2O_2 concentration increases. However, the electron donors appeared to exert their stimulatory effect exclusively on the "low-K_M" component. Increasing ABTS from 1 to 10 µM ABTS produced a fourfold increase in the k_{cat} corresponding to this component with simultaneous decrease in the "high-K_M" component of the kinetics. At higher concentrations of ABTS (50 µM to 1 mM), the apparent k_{cat} corresponding to

the "low-K_M" mechanism continued its hyperbolic increase, maintaining an apparent K_M for H_2O_2 near 0.6 mM. Interestingly, at higher concentrations of ABTS, a contribution from the "high-K_M" component was not observed. It suggests that while the electron donors stimulated catalase turnover by the "low-K_M" mechanism, they may have inhibited catalase turnover by the "high-K_M" mechanism. Nevertheless, the net result was a substantial increase in O_2 production by virtue of the presence of electron donors.

The participation of more than one mechanism in catalatic O_2 production by KatG remains to be established, but several previously reported features of KatG structure and function are indicative of a divided nature and suggest that it is a reasonable possibility. EPR spectra of the enzyme in its resting ferric state are consistent with multiple high-spin coordination states, and the population distribution between these states is highly sensitive to pH (*104, 118, 150-151*). Structures solved for KatG show clear conformational heterogeneity particularly with respect to arginine 418 (MtKatG numbering) with the distribution between these conformations strongly dependent on pH and heme oxidation state (*99, 118*). Calculations of the electronic structure of KatG compound I* have shown spin density distributed primarily between the MYW covalent adduct and the proximal tryptophan (W321 in MtKatG) with relative populations dependent upon the ionization state of the adduct tyrosine and its association with arginine 418 (*120*), both of which are pH-dependent phenomena. Finally, the optical spectra corresponding to the dominant heme intermediate represented during catalatic H_2O_2 decomposition at low pH is reminiscent of a compound III (i.e., $Fe^{III}-O_2^{\bullet-}$) intermediate with absorption features at 416, 545, and 580nm (*113, 115*). However, at substantial higher pH an intermediate with considerable different features (418 and 520 nm) has also been observed (*113, 115*).

2.4.3. *Potential mechanism for electron donor participation in catalatic activity*

The mechanistic role of peroxidatic electron donors in KatG catalase activity remains to be established, but substantial catalase activity due to the electron donor (rather than in spite of it) combined with minimal accumulation of the donor in its oxidized state suggests three possibilities. First, the stimulatory effect may not depend on the redox properties of the donor *per se*, rather its binding facilitates, perhaps through an induced conformational change, an otherwise slow step of the catalatic cycle (e.g., compound I to I* or compound I* to III*). Such a scenario would account for the more prominent appearance of compound III* in the presence of the electron donor, the minor accumulation of the electron donor in its oxidized state, and the two-component kinetics we observed at pH 5.0. However, the difficulty with such a proposal is that a wide variety of structures are able to afford essentially the same effect. For example, CPZ, TMB, ABTS, and TMPD are all stimulators of catalase activity, but have little in the way of structural similarity.

A second possibility is that the stimulatory effect requires the electron donors to redox cycle much as a cofactor might. For example, one could envision a scenario where the electron donor serves as a surrogate for the MYW adduct itself. This capitalizes on what these compounds do hold in common, and it would explain the minimal accumulation of these compounds in their oxidized states. However, because ascorbate does not appear to hinder the stimulatory effect of other electron donors (e.g., TMB), such a mechanism would require that the radical species be tightly bound and sequestered by KatG. Here again, the structural diversity of stimulators would argue against a highly specific binding site. Furthermore, as mentioned previously, electron donors are unable to restore appreciable catalase activity to Y229F KatG under any conditions.

Finally, one might postulate that peroxidatic electron donors serve a role similar to NADPH for some of the typical catalases, where accumulation of compound II, an inactive intermediate for those enzymes, is prevented (*152-153*). One forseeable consequence of the compound III*-dependent catalatic mechanism proposed for KatG (*112-113*) is that inactive versions of compound I* would result from oxidation of the KatG protein at some position other than the MYW adduct. Indeed, there is ample evidence for oxidation of several tryptophanyl residues upon the reaction of KatG with peracetic acid (*116-117, 154*), a substrate that does not allow for catalatic turnover of the enzyme. Exogenous electron donors could return nonproductive compound I* states to the ferric state, retaining KatG in its active catalatic cycle. If this were an infrequent occurrence, it would explain the relatively minor accumulation of electron donors in their oxidized states, but several points argue against such a mechanism. First, O_2 production traces show constant rates over the time range evaluated in the presence and absence of peroxidatic donors. There is evidence neither for the progressive loss of activity in the absence of a donor nor its prevention by the inclusion of such a compound. Finally, the extent to which the oxidized electron donor accumulates would correspond to prevention of an inactivation event once roughly every 100 turnovers. With such a partition ratio toward inactivation, KatG would be more sensitive to H_2O_2-dependent inactivation than HRP, an enzyme which by comparison shows almost no catalase activity (*155*).

In all three possibilities, it seems clear that any observed "peroxidase" activity may appropriately be viewed as a failure of the enzyme to execute catalase turnover. More importantly, it represents a failure of the electron donor itself to properly facilitate such turnover.

2.4.4. *Physiological implications for KatG-dependent defenses against H_2O_2*

Peroxidase electron donors dramatically expand the capacity of KatG to decompose H_2O_2, not because they increase peroxidase activity but because they stimulate catalase activity. With MtKatG, catalatic turnover approaching 8,000 s^{-1} was observed at acidic pH, and this was achieved with relatively low concentrations of H_2O_2 (i.e., 1 mM) and electron donor (i.e., 0.1 mM). Although high rates of catalatic turnover (~10,000 s^{-1}) can be obtained at acidic pH in the absence of an electron donor, much higher concentrations of H_2O_2 are required to do so. For example, with MtKatG similar rates of catalase activity without electron donor would require around 500 mM H_2O_2 (*141*).

This may have important ramifications for understanding how KatG-bearing bacteria and fungi respond to the challenges presented by H_2O_2 produced by whatever mechanisms are associated with their environments. Examples include but are not limited to plant and human pathogens (e.g., *Magnaporthe grisea* and *M. tuberculosis*, respectively) in the face of host-generated reactive oxygen species and soil microorganisms (e.g., *Pseudomonas putida*) during the oxidative metabolism of organopollutants. Interestingly, with the latter it has recently been reported that *p*-phenylenediamine increases by nearly a factor of ten the catalase activity of *P. putida* cultures (*156*). As a final example, we have found a similar effect of electron donors on the catalase activity of the plasmid-encoded catalase-peroxidase (KatP) from enterohemorrhagic *E. coli* strain O157:H7. This particular organism is well known for its remarkable acid tolerance (*157-158*), and a strong connection between antioxidant capacity (including that afforded by hydroperoxidases) and acid tolerance has recently been noted (*159*).

In conclusion, peroxidatic electron donors are the subject of several perennial unanswered questions surrounding KatG function. The identity of physiological electron donor(s) for KatG remains unknown. Our results indicate that a broad range of artificial donors

can act to stimulate the catalase activity of KatG to a substantial degree, but none of them is expected to be present at significant concentrations under typical physiological conditions. Given the potential magnitude of the stimulatory effect, the greater range of conditions where appreciable catalatic activity can be sustained, and the kinds of organisms/biological processes where such a stimulatory effect may impart a considerable advantage, the identification of the physiological donor(s) is important matter to be resolved. Furthermore, though sites have been proposed (*78*) and a binding site for isoniazid has been identified in one KatG (*160*), the binding site(s) for peroxidatic electron donors in the KatG structure have yet to be identified. Our discovery that these compounds do not contribute primarily to canonical peroxidase activity but rather synergistically stimulate catalase activity elevates the binding site(s) of these compounds as a central feature for unraveling the mechanisms by which KatG accomplishes its unusual catalatic turnover.

Chapter three: Peroxidatic Electron Donors and the Stimulation of KatG Catalase Activity: Insights from the Arginine Switch

3.1.   Introduction

Catalase-peroxidase (KatG) is a bifunctional heme-dependent enzyme found in bacteria and lower eukaryotes (*161*). Accumulating evidence shows that shows KatG is integral to the defense of these organisms against toxic levels of H_2O_2 (*2, 162*). KatG function appears to be especially important for plant and animal pathogens (*163-165*), as these organisms are likely to encounter copious quantities of H_2O_2 produced by host defensive responses (e.g., oxidative burst). Among these, the function of KatG in *Mycobacterium tuberculosis* (MtKatG) is especially important for two reasons. First, KatG is the only catalase-active enzyme carried by *M. tuberculosis* (*166*). Second, KatG from this organism activates the front-line antitubercular agent, isoniazid (*134*). A large percentage of isoniazid resistant strains of *M. tuberculosis* carry mutations which alter KatG function (*167-168*). The mechanism by which isoniazid is activated by KatG, and the molecular basis for how KatG mutations interfere with activation are the subjects of ongoing investigation (*138, 160, 169*).

As its name suggests, KatG is an efficient catalyst for the disproportionation of H_2O_2 into H_2O and O_2 (i.e., it is a catalase). Using the same active site KatG is able to catalyze H_2O_2 reduction to H_2O concomitant with the oxidation of a structurally diverse range of exogenous electron donors (i.e., it is a peroxidase). Strikingly, KatG bears no structural resemblance to typical (i.e., monofunctional) catalases, but instead resides in the same superfamily as

cytochrome c peroxidase (CcP) and ascorbate peroxidase (APx), and even horseradish peroxidase (HRP) (*74, 76*). Indeed, the active sites of CcP, APx, and KatG are virtually superimposable (*77-79, 170-171*), yet KatG is the only member of the entire superfamily that possesses appreciable catalase activity.

Despite their striking similarities, KatG does possess structural features that distinguish it from the other members of its superfamily. First, it contains three large loops (LL1, LL2, and LL3) which extend the connections of the D and E helices, F and G helices, respectively (*77-79, 172*). LL1 bears an invariant tyrosine residue (Y229 by MtKatG numbering) which participates in a unique methionine-tyrosine-tryptophan covalent adduct (*77-79, 90,173*). Substitution of any of the residues of the adduct invariably produces KatG variants with negligible catalase activity but peroxidase activity comparable and in some cases superior to that of the wild-type enzyme (*82, 93-97*). Second, both LL1 and LL2 contribute to a much more restricted access channel to the active site heme (*78, 174*). This channel allows passage of H_2O_2 to the heme iron, but presents a substantial steric barrier for most peroxidatic electron donors. As a consequence, the peroxidase activity of KatG is much lower than that observed for other peroxidases like horseradish peroxidase (HRP) in which electron donors have relatively open access to the heme edge for facile electron transfer (*52, 175*). Indeed, we have recently shown that deletion of a substantial portion of LL1 (including the invariant tyrosine) produces a KatG with no catalase activity and peroxidase activity the rivals that of HRP (*88*).

Robust catalase activity from what is structurally a peroxidase raises two critical questions. First, what is the catalatic mechanism employed by KatG? This question has been the subject of intense investigation, but evidence is accumulating for a mechanism which is distinct from that carried out by typical (i.e., monofunctional) catalases (*112-113, 115, 121, 123, 176*).

The first step is common to all heme-dependent catalases and peroxidases; H_2O_2 oxidizes the ferric heme of KatG to form compound I (i.e., $Fe^{IV}=O[porphyrin^{\bullet+}]$). However, a subsequent intramolecular electron transfer from the MYW adduct reduces the porphyrin radical, generating compound I* (i.e., $Fe^{IV}=O[MYW^{\bullet}]$). Reaction of compound I* with a second equivalent of H_2O_2 produces compound III* (i.e., $Fe^{III}-O_2^{\bullet-}[MYW^{\bullet}]$). Finally, the MYW adduct radical accepts an electron from the $Fe^{III}-O_2^{\bullet-}$ heme resulting in the formation of the ferric enzyme and release of O_2 (Fig. 1.7).

What, then, is the place of peroxidase activity and the peroxidatic electron donor in KatG catalysis? As both catalase and peroxidase catalytic mechanisms involve the H_2O_2-dependent formation of compound I, all that differs is the route by which the ferric state of the enzyme is regenerated. As outlined above, catalatic turnover requires the oxidation of the second H_2O_2, but with peroxidases, an exogenous (usually aromatic) electron donor is oxidized instead. Typically, compound I is reduced by one electron to produce compound II ($Fe^{IV}=O$) and the corresponding radical of the electron donor. A second single-electron transfer returns the enzyme to the ferric state and produces a second equivalent of the donor radical. By this formulation one would anticipate that peroxidase and catalase activities should be mutually antogonistic, and in particular, peroxidatic electron donors should inhibit catalase activity. Indeed, the first published report on a catalase-peroxidase showed that the classical peroxidase electron donor o-dianisidine did inhibit the catalase activity of KatG at pH 7 (*107*). However, we have recently shown that a number of peroxidatic electron donors stimulate catalase activity of KatG by over an order of magnitude (*177*). Interestingly, this synergistic effect is most prominent at lower pH (i.e., ~pH 5), a condition that coincides with antimicrobial defenses like the oxidative burst. Clearly, the

interrelationship between the catalatic and peroxidatic mechanisms is more complex than has been previously appreciated.

Critical to the catalatic activity of KatG is an invariant arginine residue (R418 in MtKatG) whose conformation is highly pH dependent (*99, 118, 178-179*). Structures solved for *Burkholderia pseudomallei* KatG (BpKatG) at pH 8.5 show the guanidinium moiety of this arginine associated with the tyrosyl phenoxide anion of the MYW covalent adduct (the so-called "Y" conformation). At pH 4.5, the arginine side chain is oriented away from the MYW adduct and toward a surface exposed cleft between the N- and C-terminal domains (i.e., the "R" position). At pH 6.5, corresponding roughly to the optimum pH for catalase activity, this arginine equally populates the "R" and "Y" conformational states (*99, 118*). Although the catalatic activity of KatG is sharply diminished upon replacement of this arginine, the mechanism by which it facilitates catalatic turnover is still being investigated. It has been proposed that the position of the arginine facilitates compound I formation in its "R" state, and reduction of compound I in its "Y" state. Thus, the equal distribution between these states (at pH 6.5) is optimum for catalatic turnover, where one equivalent of H_2O_2 must produce compound I, and a second equivalent must return the enzyme to its ferric state. More recently, it has been shown that the R418L variant of MtKatG readily allows accumulation of the MYW adduct in its radical state (*176*). The low catalatic activity of the variant is assigned to a greatly diminished rate of conversion of compound III* back to the ferric state (*176*).

The pH dependence of this stimulatory phenomenon and that of the R418 side chain and its role in catalatic turnover prompted us to investigate the connection between the two. We evaluated the effect of peroxidatic electron donors on the catalatic function of R418A, R418K, and wild-type MtKatG by steady-state as well as stopped-flow methods. Our data suggest that

peroxidatic electron donors prevent the accumulation of intermediates that are inactive with respect to catalase activity. Further, the disruption of the arginine 418 guanidinium interaction with the tyrosyl-OH of the MYW adduct (either by pH or by site-directed mutagenesis) promoted the formation of inactive intermediates by way of the compound I* intermediate.

3.2. Materials and Methods

3.2.1. Materials

3,3',5,5'-tetramethylbenzidine dihydrochloride hydrate (TMB), *N,N,N',N'*-tetramethyl-*p*-phenylenediamine dihydrochloride (TMPD), L-ascorbic acid, 3,3'-dimethoxybenzidine (*o*-dianisidine), 2,2'-azino-bis(3–ethylbenzthiazoline-6-sulfonic acid) (ABTS), hydrogen peroxide (30%), imidazole, ampicillin, hemin, chloramphenicol, chlorpromazine (CPZ), pyrogallol, calcium chloride hydrate and sodium dithionite were purchased from Sigma-Aldrich (St. Louis, MO). Tetracycline hydrochloride, mono- and dibasic sodium phosphate, sodium chloride, sodium acetate trihydrate, potassium chloride, magnesium chloride, and magnesium sulfate were purchased from Fisher (Pittsburgh, PA). *Pfu* polymerase, Herculase polymerases, T4 DNA ligase, and all *E. coli* (XL-1 Blue) were obtained from Agilent (La Jolla, CA). Phusion High-Fidelity PCR Master Mix with GC Buffer and all restriction enzymes were purchased from New England Biolabs (Beverly, MA). All oligonucleotide primers for site-directed mutagenesis as well as sequencing were purchased from Invitrogen (Carlsbad, CA). Benzonase nuclease, Bugbuster®, nickel–nitrilotriacetic acid (Ni–NTA) resin were obtained from Novagen (Madison, WI). Isopropyl- -D-thiogalactopyranoside (IPTG) was obtained from Gold Biotechnology (St. Louis, MO). Buffer exchange columns (10DG) and Macro-Prep High Q resin were purchased from BioRad (Hercules, CA). Centrifugal filter units (50 kD cutoff) were acquired from

Millipore (Billerica, MA). All buffers and media were prepared using water purified through a Barnstead EASYpure II UV ultrapure water system (18.2 M /cm resistivity).

3.2.2. *Mutagenesis*

Site-directed mutagenesis was carried out by applying the "Round-the-horn" approach (*180*) to the construct we use for the expression of wild-type MtKatG. This construct, pMRLB11, is a pET23b-derived plasmid bearing the *M. tuberculosis katG* gene and was obtained from the TB Vaccine Testing and Research Materials Contract at Colorado State University. The forward primers designed for R418A and R418K MtKatG construction were 5'-C*GCA*GATATGGGTCCCGTTGCGAGATACCTTG-3', and 5'-C*AAG*GATATGGGTCCCGTTGCGAGATACCTTGG-3', respectively. The nucleotide substitutions designed to produce the mutation are highlighted in bold italics. This approach allowed us to use the same reverse primer to generate both mutants (5'-TGGATCAGCTTGTACCAGGCCTTGGCGAACTC-3'). All primers were modified to include 5'-phosphoryl groups, allowing for the blunt-end ligation of the PCR products. PCR for generation of the R418K mutant was carried out using Herculase polymerase in manufacturer supplied buffer. Due to difficulty obtaining the R418A mutant, its PCR reaction was carried out using Phusion High-Fidelity polymerase in GC Buffer-containing Master-Mix and 3% DMSO. All PCR products were treated with *Dpn* I to remove starting template and then ligated using T4 DNA ligase. Ligation products were used to transform *E. coli* (XL-1 Blue) by a standard heat shock protocol. Transformants were selected using ampicillin-containing media, and candidate plasmids were screened by *PshA* I digestion as successful mutation would eliminate a unique *PshA* I restriction site. Successful candidates were sent for full DNA sequence analysis (Davis

76

Sequencing, Davis CA) to verify that the intended mutation was present and that no unintended mutations were present.

3.2.3. Protein expression and purification

E. coli C41 (DE3) bearing the heme protein expression plasmid, pHPEX3 (*142*), were transformed with the expression constructs for R418K and R418A KatG and transformants were selected on the basis of tetracycline/ampicillin resistance. Expression of wild-type MtKatG and both R418 variants were carried out as previously described (*177*). As with wild-type MtKatG, the R418A and R418K variants were expressed in a soluble form. Thus, their purifications were carried out as reported previously (*177*). The final purified R418K and R418A KatG had optical purity ratios A_{408}/A_{281} (i.e., R_z values) of 0.61 and 0.57, respectively. The apparent kinetic parameters for both catalase and peroxidase activities are shown in Table 3.1 and are in good agreement with those reported previously for KatG from *B. pseudomallei* and *Synechocystis* (*99, 118, 178*).

3.2.4. UV-visible spectra and activity assays

Spectra were recorded as previously described (*177*). The molar absorptivity of wild-type, R418K, and R418A enzymes were determined using the pyridine hemichrome assay (*144*). Peroxidase activity was evaluated as previously described (*177*) using three different substrates (ABTS, TMB, and *o*-dianisidine) by monitoring the production of ABTS$^{\bullet+}$ ($\varepsilon_{417} = 34.7$ mM^{-1} cm^{-1}) (*145*), TMB radical ($\varepsilon_{652} = 39$ mM^{-1} cm^{-1}) (*146*) and *o*-dianisidine oxidation ($\varepsilon_{460} = 11.3$ mM^{-1} cm^{-1}) (*181*), respectively.

Unless otherwise specified, catalase activity was evaluated by monitoring O_2 production over time using a Clark-type O_2 sensitive electrode (Hansatech, Pentney, Norfolk, England) as previously described (*177*). In specified experiments, catalase activity was evaluated spectrophotometrically by monitoring a decrease in H_2O_2 concentration over time at 240 nm ($_{240}$ = 39.4 M^{-1} cm^{-1}) (*147*).

3.2.5. *Analyses of steady-state kinetic data*

In our laboratory we typically observe one of three kinetic responses to substrate concentration by KatG and its variants. If, as is often the case, we observe a standard rectangular hyperbolic increase in rate with increasing substrate concentration, we fit the data using the standard Michaelis-Menten equation (equation **3.1**) to obtain the *apparent* kinetic parameters k_{cat}, K_M, and k_{cat}/K_M.

$$\frac{v_o}{[E]_T} = \frac{k_{cat}[S]}{K_M + [S]}$$

(**3.1**)

In all situations where these terms are applied, k_{cat} is the asymptotic maximum rate divided by the concentration of holo-enzyme as estimated by heme concentration. The apparent K_M is not intended to refer to anything more than the concentration of substrate necessary to produce ½ of the maximum rate, and k_{cat}/K_M is considered the catalytic efficiency.

In some instances, we observe enzyme activity that approaches a maximum followed by a decrease as substrate concentrations increase further. To account for substrate-dependent inhibition and obtain an unobscured estimate of the kinetic parameters, the data are fit to equation **3.2**. The apparent K_I corresponds to a macroscopic apparent dissociation constant accounting for the inhibitory properties of the substrate.

Table 3.1. Catalase and peroxidase kinetic parameters for MtKatG and R418 variants.

Activity (substrate)		KatG Protein		
	Parameter	MtKatG	R418K	R418A
Catalase (pH 7.0)[a]				
	k_{cat} (s^{-1})	7736 ± 82	5112 ± 50	268 ± 46
	K_M (mM)	7.0 ± 0.3	4.6 ± 0.2	34 ± 13
	k_{cat}/K_M (M^{-1}s^{-1})	1.1×10^6	1.1×10^6	7.9×10^3
Peroxidase[b] (H$_2$O$_2$)[c]				
	k_{cat} (s^{-1})	13.5 ± 0.3	16.3 ± 1.0	10.5 ± 0.1
	K_M (mM)	0.24 ± 0.03	0.30 ± 0.04	0.0025 ± 0.0001
	k_{cat}/K_M (M^{-1}s^{-1})	5.6×10^4	5.5×10^4	4.2×10^6
Peroxidase (ABTS)[d]				
	k_{cat} (s^{-1})	29.2 ± 0.2	25.1 ± 0.4	27.4 ± 0.3
	K_M (mM)	0.14 ± 0.01	0.11 ± 0.01	0.14 ± 0.01
	k_{cat}/K_M (M^{-1}s^{-1})	2.1×10^5	2.3×10^5	2.0×10^5
Catalase (pH 5.0)[e]				
	k_{cat} (s^{-1})[f]	570 ± 30	330 ± 30	150 ± 3
	K_M (mM)[f]	0.8 ± 0.1	1.6 ± 0.4	0.29 ± 0.04
	k_{cat}/K_M (M^{-1}s^{-1})	7.1×10^5	2.0×10^5	5.2×10^5
	k_{app} (M^{-1}s^{-1})	$(1.8 ± 0.1) \times 10^4$	$(9.5 ± 0.7) \times 10^3$	-

[a]Activity was determined by H$_2$O$_2$ consumption observed at 240 nm at 23 °C in 100 mM phosphate buffer, pH 7.0.
[b]All peroxidase activity assays were performed at 23 °C in 50 mM acetate buffer, pH 5.0.
[c]Peroxidase parameters with respect to H$_2$O$_2$ were determined using 0.1 mM ABTS.
[d]Peroxidase parameters with respect to ABTS were determined using 1.0 mM H$_2$O$_2$.
[e]Activity was determined by O$_2$ production at 23 °C in 50 mM acetate buffer, pH 5.0.
[f]Kinetic parameters for the low-K_M component.
[g]Apparent second-order rate constant for the high-K_M component.

$$\frac{v_o}{[E]_T} = \frac{k_{cat}[S]}{K_M + [S] + {[S]^2}/{K_I}} \qquad (3.2)$$

Finally, for the catalase activity of MtKatG and the R418K variant, we observed two distinct components in response to H_2O_2 concentration. Accordingly, we use equation **3.3** to fit the data. Where k_{cat} and K_M are the apparent kinetic parameters that best fit the hyperbolic (i.e.,

$$\frac{v_o}{[E]_T} = \frac{k_{cat}[S]}{K_M + [S]} + k_{app}[S] \qquad (3.3)$$

low K_M) component, and k_{app} is the slope of the linear (i.e., high K_M) component and would correspond to the k_{cat}/K_M for a second H_2O_2 disproportionation mechanism.

3.2.6. *Extent of ABTS oxidation vs. H_2O_2 consumption*

The extent of ABTS oxidation was measured by setting up reactions containing 0.1 mM ABTS, 20 nM enzyme, and varying concentrations of H_2O_2 (i.e., 0.1 – 5 mM) and allowing them to proceed to completion (at least 10 minutes) as previously described (*177*). We also used a stopped-flow method to evaluate the quantity of $ABTS^{\bullet+}$ generated during H_2O_2-dependent enzyme turnover (see below).

3.2.7. *Stopped-flow kinetic studies*

Heme intermediates formed by wild-type, R418K, and R418A MtKatG under steady-state conditions were observed using a PC-upgraded SX18.MV rapid reaction analyzer from Applied Photophysics (leatherhead, UK). As described previously (*177*), in order to more clearly observe absorption due to heme intermediates, we included ascorbate to scavenge the radical oxidation products of peroxidatic electron donors (e.g., $ABTS^{\bullet+}$). Single-mixing experiments were set up such that 6 µM KatG (or one of its variants) was placed in syringe A in 5 mM

phosphate buffer, pH 7.0. Syringe B contained 0.2 mM ascorbate, 0.2 mM ABTS, and varying concentrations of H_2O_2 in 100 mM acetate buffer, pH 5.0. As mentioned above, we also applied stopped-flow to determine the quantity of ABTS radical generated during the consumption of a range of H_2O_2 concentrations. These experiments were set up in the same way except that ascorbate was excluded from syringe B. In these experiments, $ABTS^{\bullet+}$ was quantified by monitoring absorbance at 645 nm using a molar absorptivity of 13,500 M^{-1} cm^{-1} (*145*).

3.3. Results

We previously reported the stimulatory effect of several classical peroxidatic electron donors on the catalatic activity of MtKatG (*177*). Electron donors appeared to have the most dramatic effect at low pH and low concentrations of H_2O_2 (i.e., ~ 1 mM). These are conditions where catalase activity is typically relatively low and peroxidatic activity is optimal. It is well established that KatG, particularly R418 (MtKatG numbering), undergoes a pH-dependent conformational shift (*99, 118*). In order to evaluate any connection between R418 and the stimulatory effect of electron donor at low pH, we produced the MtKatG variants R418A and R418K and evaluated the effect of peroxidatic electron donors on their ability to act as catalases.

We successfully expressed and isolated the R418A and R418K variants and the spectral properties of the isolated enzymes were consistent with one another and with the wild-type enzyme (Table 3.2). We also evaluated catalase and peroxidase activities of all three proteins under typical assay conditions (Table 3.1). In every respect, wild-type and R418K MtKatG showed highly similar steady-state kinetic parameters. However, R418A showed a greatly diminished catalase activity (>95% decrease in k_{cat}). The peroxidase activity was unaffected by either substitution with the exception of a 100-fold decrease in the apparent K_M of R418A KatG

Table 3.2. UV-visible absorption characteristics of KatG variants.

Protein	Absorption Features			
	Soret ( )	CT[a] 2	CT 1	RZ[b]
MtKatG	408	500	633	0.64
R418K KatG	408	500	633	0.61
R418A KatG	407	501	632	0.57

[a]CT = charge transfer transition. CT 1 is usually near 640 nm, and CT 2 is usually near 500 nm.
[b]RZ = Reinheitzahl ratio. Ratio of absorbance at the Soret $_{max}$ versus absorbance at 280 nm.
All spectra were recorded using a Shimadzu UV 1601 spectrophotometer (Columbia, MD) at 23 ^{o}C using 100 mM phosphate buffer, pH 7.0.

for H_2O_2. These results are highly similar to those obtained for the analogous variants of KatG enzymes from other organisms (*99, 118, 178*).

The correspondence between the catalase activities of the wild-type enzyme and the R418K variant was also observed at pH 5.0 (Table 3.1). As we have observed for the wild-type enzyme (*177*), there were also two components to the response of R418K KatG to increasing H_2O_2 concentration. A hyperbolic phase at low H_2O_2 concentration (< 10 mM) (k_{cat} = 330 s^{-1}; K_M = 1.6 mM) gave way to a linear component at higher H_2O_2 concentration (k_{app} = 9.5 × 10^3 M^{-1} s^{-1}). Interestingly, R418A KatG showed only a single hyperbolic response to H_2O_2. Its parameters were most similar to the initial hyperbolic phases observed for wild-type and R418K KatG (Fig. 3.1-panel A). Furthermore, though the k_{cat} values were essentially the same for R418A at pH 7 and at pH 5, the apparent K_M for H_2O_2 for this variant was considerably lower at pH 5.0. Accordingly, the apparent second-order rate constant for R418A KatG catalase activity was 65 fold greater at pH 5.0 than it was at pH 7.0.

As with wild-type KatG, the inclusion of ABTS dramatically stimulated O_2 production by R418K and R418A KatG (Fig. 3.1-panel B). The stimulatory effect was most prominently and consistently observed in the apparent k_{cat} parameter (Table 3.3). Interestingly, at a concentration of 0.1 mM ABTS, a similar enhancement of k_{cat} was observed for all three enzymes (6 – 8 fold) (Fig. 3.2). Although other peroxidatic electron donors also stimulated O_2 production by R418K and R418A MtKatG, both variants were more selective. In particular, the benzidine derivatives TMB and *o*-dianisidine failed to produce appreciable stimulation of O_2 production for either variant (Fig. 3.2).
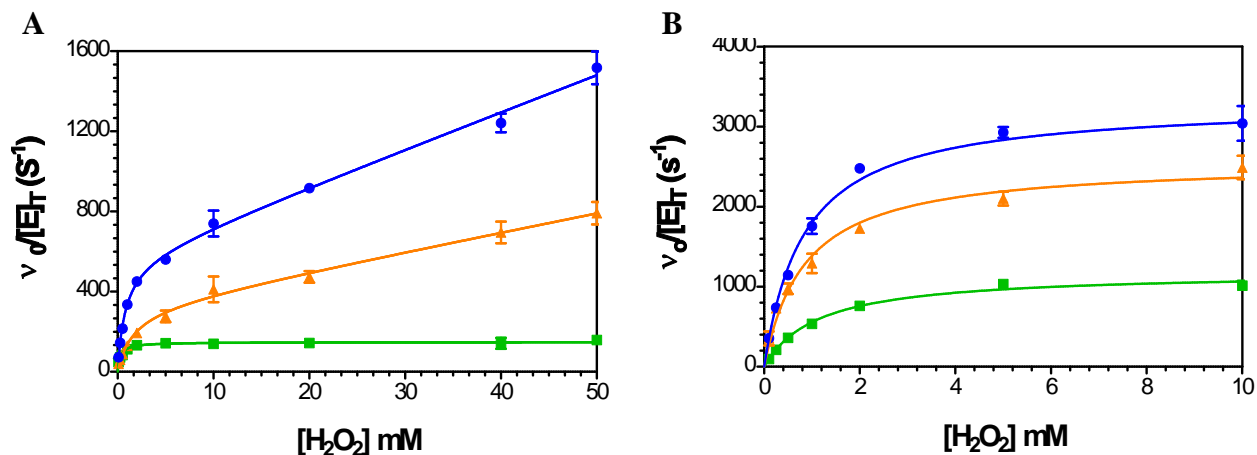
Figure 3.1. Effect of ABTS on O_2 production by wild-type MtKatG and its R418 variants. Catalase activity was evaluated for wild type ( ), R418K ( ), and R418A ( ) KatG in the absence of any electron donor (Panel A) and in the presence of 0.1 mM ABTS (Panel B). All assays monitored O_2 production by Clark-type electrode and were carried in 50 mM acetate buffer, pH 5.0, at 23 °C. The data in panel A were fit with equation **3.3** (wild-type and R418K) or equation **3.1** (R418A) to account for two kinetic components or one, respectively. The data obtained for all three enzymes in panel B were fit using equation **3.1**.

Table 3.3. Effect of electron donors on catalase kinetic parameters at pH 5.0.

Electron Donor		KatG Protein		
	Parameter	MtKatG	R418K	R418A
None				
	k_{cat} (s^{-1})	570 ± 30	330 ± 30	148 ± 3
	K_M (mM)	0.8 ± 0.1	1.6 ± 0.4	0.29 ± 0.04
	k_{cat}/K_M (M^{-1}s^{-1})	7.1×10^5	2.1×10^5	5.1×10^5
ABTS				
	k_{cat} (s^{-1})	3300 ± 60	2560 ± 40	1184 ± 0.1
	K_M (mM)	0.83 ± 0.05	0.85 ± 0.06	1.1 ± 0.1
	k_{cat}/K_M (M^{-1}s^{-1})	4.0×10^6	3.0×10^6	1.1×10^6
CPZ				
	k_{cat} (s^{-1})	7940 ± 120	2382 ± 24	1960 ± 60
	K_M (mM)	1.1 ± 0.1	0.36 ± 0.02	4.8 ± 0.5
	k_{cat}/K_M (M^{-1}s^{-1})	7.2×10^6	6.6×10^6	4.1×10^5
TMPD				
	k_{cat} (s^{-1})	7010 ± 60	2700 ± 80	1150 ± 40
	K_M (mM)	1.2 ± 0.1	0.79 ± 0.07	1.0 ± 0.1
	k_{cat}/K_M (M^{-1}s^{-1})	6.0×10^6	3.4×10^6	1.1×10^6
TMB				
	k_{cat} (s^{-1})	5220 ± 70	490 ± 20	82 ± 6
	K_M (mM)	0.70 ± 0.05	0.07 ± 0.02	3.1 ± 0.9
	k_{cat}/K_M (M^{-1}s^{-1})	7.4×10^6	7.0×10^6	2.6×10^4
o-dianisidine				
	k_{cat} (s^{-1})	5600 ± 100	540 ± 30	93 ± 5
	K_M (mM)	0.49 ± 0.05	0.13 ± 0.04	4.1 ± 0.8
	k_{cat}/K_M (M^{-1}s^{-1})	1.2×10^7	4.2×10^6	2.3×10^4
pyrogallol				
	k_{cat} (s^{-1})	630 ± 20	820 ± 30	250 ± 10
	K_M (mM)	0.20 ± 0.03	0.30 ± 0.04	0.30 ± 0.04
	k_{cat}/K_M (M^{-1}s^{-1})	3.1×10^6	2.7×10^6	8.3×10^5
ascorbate				
	k_{cat} (s^{-1})	520 ± 30	530 ± 20	140 ± 10
	K_M (mM)	0.13 ± 0.03	0.36 ± 0.04	0.25 ± 0.6
	k_{cat}/K_M (M^{-1}s^{-1})	4.0×10^6	1.5×10^6	5.6×10^5

[a]All catalase activity assays monitored O_2 production using a Clark-type O_2-sensitive electrode.
[b]All assays were carried out at 23 ^{o}C in 50 mM acetate buffer, pH 5.0.
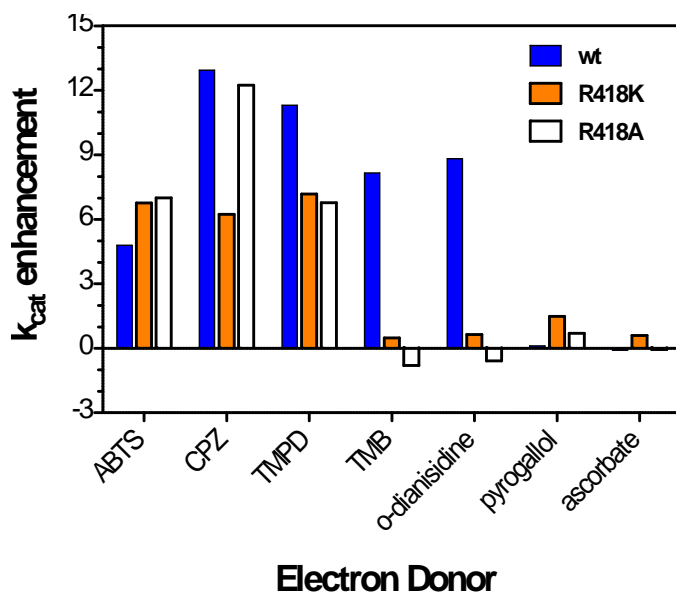
Figure 3.2. Effect of various peroxidatic electron donors on the apparent k_{cat} for the catalase activity of wild-type, R418K, and R418A MtKatG. Where the k_{cat} measured in the presence of the electron donor ($k_{cat(D)}$) was greater than that observed in its absence ($k_{cat(0)}$), the level of k_{cat} enhancement was calculated as $k_{cat(D)}/k_{cat(0)} - 1$. Where $k_{cat(D)}$ was less than $k_{cat(0)}$, the effect was calculated as $k_{cat(0)}/k_{cat(D)} - 1$. Accordingly, activation by the electron donor will be reflected in increasingly positive values, inhibition in increasingly negative values, and zero if the electron donor has no effect. A complete table of the effect of each electron donor on the kinetic parameters for the catalase activity of each variant is provided in Table 3.3. All activity measurements were on the basis of O_2 production as described in *Materials and Methods* and were carried out in 50 mM acetate buffer, pH 5.0, at 23 °C. All electron donors were present at a concentration of 0.1 mM.

The pH profiles for R418K and R418A catalase activity in the presence and absence of ABTS revealed an intriguing pattern (Fig. 3.3-panel A). Under both conditions, the R418K variant essentially mimicked the behavior of the wild-type enzyme. In the absence of ABTS, there was an optimum for catalase activity at pH 7.5. With decreasing pH, catalase activity diminished toward a plateau centered near pH 5.0, decreasing to negligible levels at pH 3.5. With ABTS present, the pH profile of R418K showed two optima. One (pH 7.5) was unaffected by ABTS, and the other (pH 5.0) was clearly dependent on the presence of ABTS.

In contrast, in the absence of ABTS, R418A KatG showed very little catalase activity near neutral pH; however, with decreasing pH, activity increased toward a maximum at pH 5.0. Indeed, below pH 6.0 the catalase activity for R418A converged with and was virtually indistinguishable from that of R418K. In the presence of ABTS, the R418A variant showed the same single-optimum profile (pH 5.0) as it did in the electron donor's absence, but with ABTS, an 8-fold greater catalase activity was observed. Subtracting the catalase activity observed in the absence of ABTS from that observed in the presence of ABTS, showed that the pH profile corresponding to ABTS-stimulated catalase activity was essentially the same for R418A and R418K KatG (Fig. 3.3-panel B).

The conditions that produced substantial catalase stimulation were commensurate with optimal peroxidase activity (i.e., pH 5.0, 0.1 mM ABTS, low concentrations of H_2O_2). As mentioned above, wild-type, R418K, and R418A KatG all showed very similar peroxidase kinetic parameters. Because both peroxidase activity and electron donor-stimulated O_2-production were likely to be occurring simultaneously, we evaluated the extent of $ABTS^{\bullet+}$ generated versus the quantity of H_2O_2 added. We have shown previously that wild-type KatG only produces ~0.005 equivalents of $ABTS^{\bullet+}$ for every equivalent of H_2O_2 consumed during
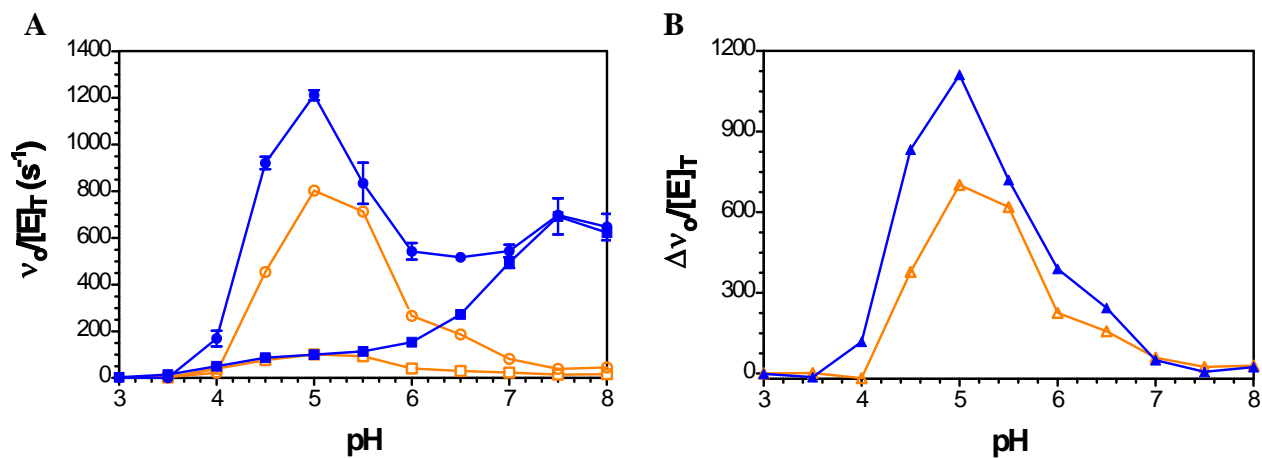
Figure 3.3. Effect of pH on the catalase activity of R418K and R418A KatG in the presence and absence of ABTS. The catalase activity of the R418K (closed symbols) and R418A (open symbols) was evaluated in the presence (circles) and absence (squares) of 0.1 mM ABTS (panel A). Panel B shows the $_o/[E]_T$ values obtained in the presence of ABTS minus those obtained in its absence for R418K ( ) and R418A ( ) MtKatG. All rates were determined on the basis of O_2 production as described in *Materials and Methods* at $23\,^oC$.

ABTS-stimulated catalatic turnover, and the phenomenon shows only limited dependence on H_2O_2 concentration (*177*). R418K KatG showed nearly identical behavior to the wild-type enzyme; however, R418A produced substantially greater quantities of $ABTS^{\bullet+}$ at all H_2O_2 concentrations tested (Fig. 3.4). Furthermore, the ratio of ABTS oxidized to H_2O_2 consumed was markedly H_2O_2 concentration dependent. At 5 mM H_2O_2, R418A KatG produced 0.015 equivalents $ABTS^{\bullet+}$, three-fold greater than that produced by either wild-type or R418K KatG. At 0.25 mM H_2O_2, R418A KatG produced 0.1 equivalents $ABTS^{\bullet+}$, 14-fold greater than the 0.007 equivalents produced by wild-type and R418K KatG. Using stopped-flow as described in *Experimental Procedures*, we evaluated $ABTS^{\bullet+}$ produced by R418A KatG in reactions ranging from 4 mM down to 3 µM H_2O_2. Strikingly, this approach produced precisely the same trend (Fig. 3.4). Indeed, reaction of R418A KatG with 3 µM H_2O_2 resulted in the generation of 1.95 µM (0.65 eq) $ABTS^{\bullet+}$.

We also used stopped-flow to evaluate the influence of R418 substitution and the presence of a peroxidatic electron donor on the dominant heme intermediate (s) observed during catalatic H_2O_2 consumption. Our previous studies with the wild-type enzyme had employed TMB as a model peroxidatic electron donor (*177*), but because the catalatic activity of neither R418A nor R418K KatG was stimulated by TMB, we used ABTS as a model peroxidatic electron donor instead. In the presence of 0.1 mM ABTS (and 0.1 mM ascorbate to scavenge the $ABTS^{\bullet+}$ radical), H_2O_2 produced a concentration-dependent increase in the time elapsed before the return of the ferric states of the wild-type (Fig. 3.5A) and R418A KatG (Fig. 3.6A). The behavior of the two proteins contrasted in two important ways. First, consistent with the kinetic parameters reported in Table 3.3, wild-type KatG required less time to consume a given concentration of H_2O_2 and return to its ferric state than the R418A variant. Second, for wild-type

89
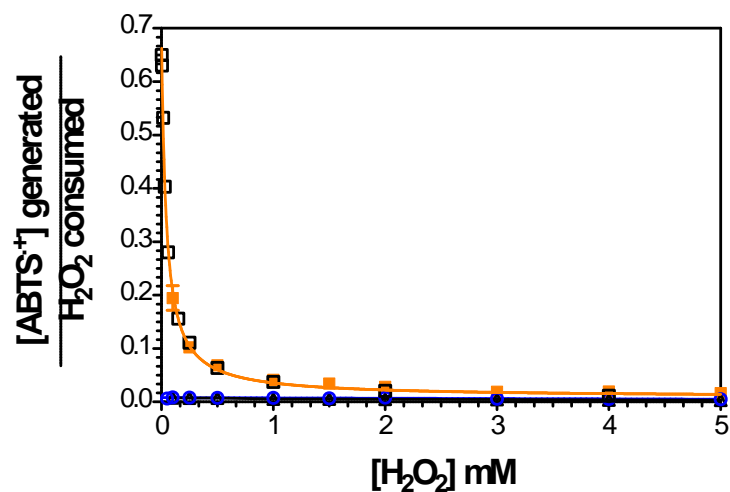
Figure 3.4. Effect of R418 substitution on the ratio of the extent of ABTS$^{\bullet+}$ generated to H$_2$O$_2$ concentration consumed. The extent of ABTS$^{\bullet+}$ production was determined for wild-type ( ), R418K ( ), and R418A ( ) following reaction with varying concentration of H$_2$O$_2$. All reactions were carried out at 23 $^{\circ}$C using 20 nM enzyme, 0.1 mM ABTS, and 50 mM acetate buffer, pH 5.0. The extent of ABTS$^{\bullet+}$ production by R418A KatG was also measured by stopped-flow ( ) according to the procedure described in *Materials and Methods* at 0.003, 0.006, 0.015, 0.03, 0.06, 0.15, 0.25, 0.5, 1.0, 2.0, and 4.0 mM H$_2$O$_2$.
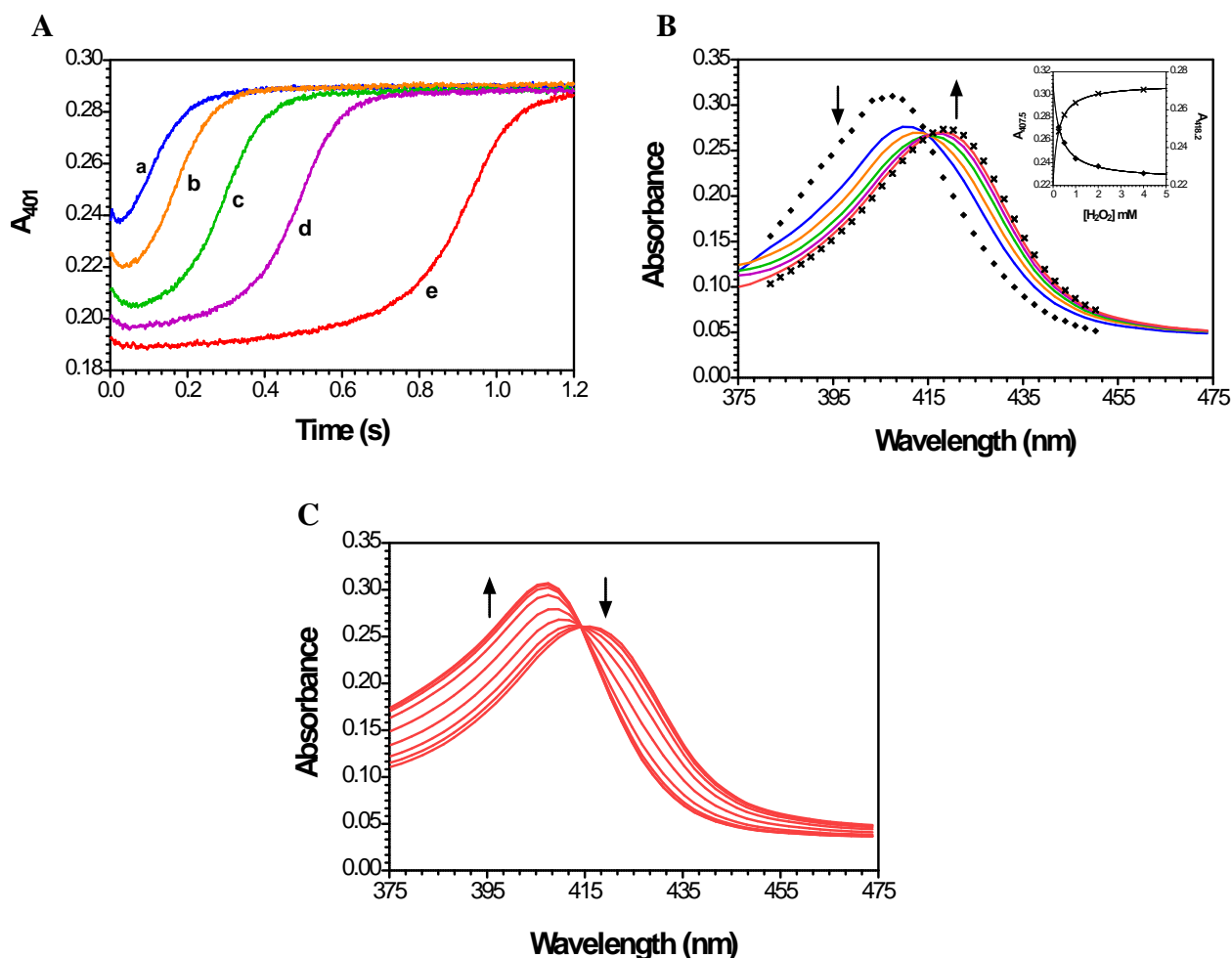
Figure 3.5. Effect of H_2O_2 concentration on ABTS-stimulated KatG catalatic turnover. The duration of a steady-state phase and the return of the ferric state (panel A) were evaluated in the presence of 0.1 mM ABTS, 0.1 mM ascorbate, and 0.25 (a), 0.5 (b), 1.0 (c), 2.0 (d), and 4.0 (e) mM H_2O_2. Spectra recorded at 40 ms for each H_2O_2 concentration tested are shown in panel B. The absorbance values for each wavelength as a function of H_2O_2 were plotted and fit using a hyperbolic function (407.5 and 418.2 nm data are shown in the inset). Absorbance values predicted for $[H_2O_2] = 0$ ( ) and $[H_2O_2] = \infty$ ($\times$) for each wavelength are shown. The direction of absorbance changes with H_2O_2 concentration are indicated by the arrows. Spectra recorded during the return of the ferric state (0.693 – 1.197 s, every 0.063 s) in the presence of 4 mM H_2O_2 are shown in panel C. The directions of absorbance changes with time are indicated by the arrows. The final concentration of enzyme in each reaction was 3 μM. All reactions were carried out in the presence of 50 mM acetate buffer, pH 5.0, at 4 °C.
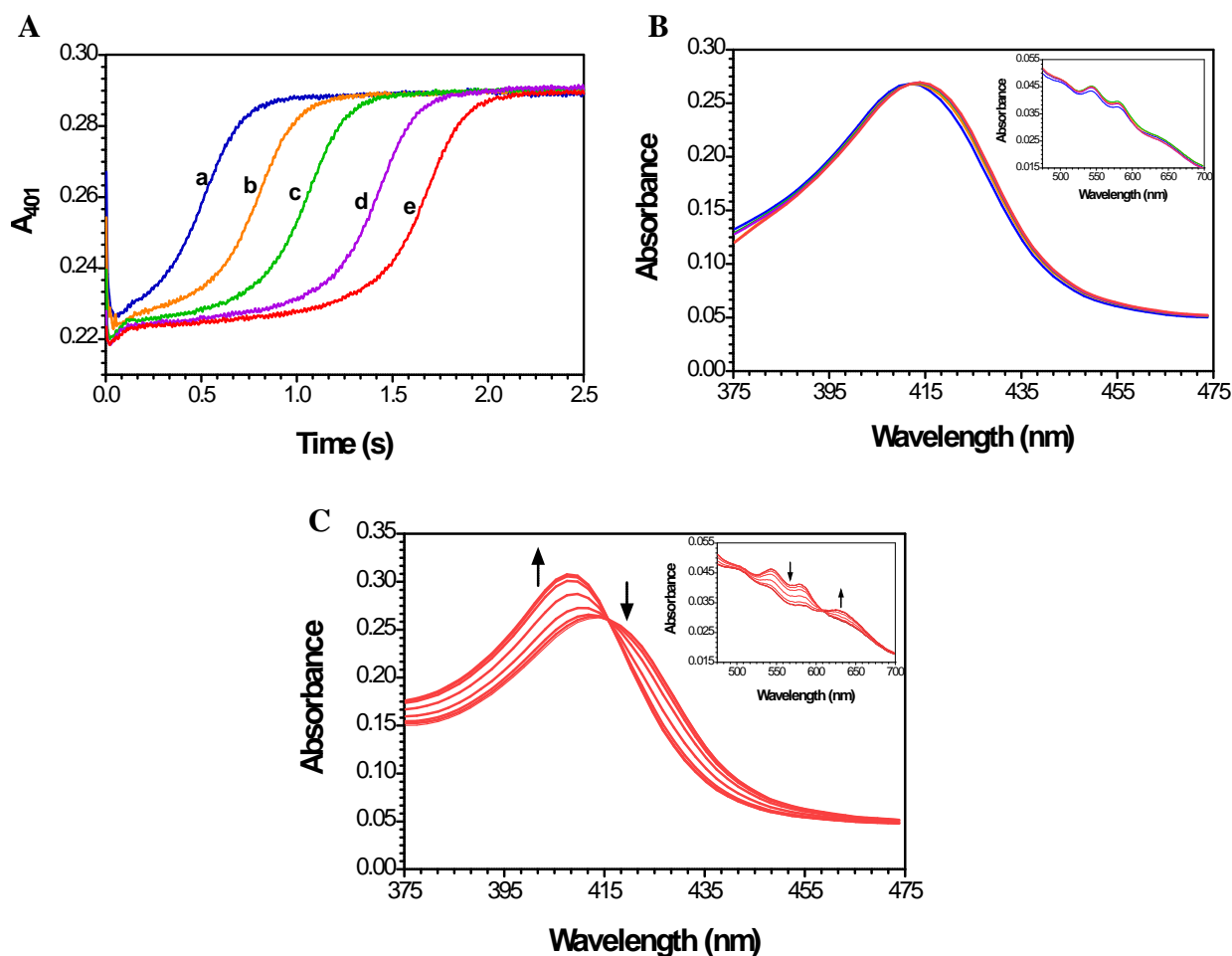
Figure 3.6. Effect of H_2O_2 concentration on ABTS-stimulated catalatic turnover of R418A KatG. The duration of a steady-state phase and the return of the ferric state (panel A) were evaluated in the presence of 0.1 mM ABTS, 0.1 mM ascorbate, and 0.015 (a), 0.03 (b), 0.06 (c), 0.15 (d), and 0.25 (e) mM H_2O_2. For comparison, the reaction of wild-type KatG (wt) with 0.25 mM H_2O_2 under the same conditions is also shown. Spectra recorded at 130 ms for each H_2O_2 concentration tested are shown in panel B. Spectra recorded during the return of the ferric state (1.13 – 2.08 s, every 0.095 s) in the presence of 0.25 mM H_2O_2 are shown in panel C. The directions of absorbance changes with time are indicated by the arrows. The final concentration of enzyme in each reaction was 3 µM. All reactions were carried out in the presence of 50 mM acetate buffer, pH 5.0, at 4 ^{o}C.

KatG the amplitudes of the traces were H_2O_2 concentration-dependent, whereas for R418A essentially the same amplitude was observed even to H_2O_2 concentrations as low as 15 µM (only 5 molar equivalents).

For wild-type KatG, a steady-state appeared to be established for each H_2O_2 concentration by ~40 ms (Fig. 3.5A). An overlay of the spectra recorded at this time point for each H_2O_2 concentration (Fig. 3.5B) showed a systematic progression of the Soret band from maximum at about 410 nm (0.25 mM H_2O_2) to 418 nm (4.0 mM H_2O_2) with an isosbestic point near 414 nm. This spectral transition was hyperbolic with respect to H_2O_2 concentration (Fig. 3.5B-inset). We fit the data at each wavelength to a hyperbolic equation and used the results to predict spectra for $[H_2O_2] = 0$ mM and $[H_2O_2] = $ mM. For the former, the predicted spectrum had an absorption maximum at 407.5 nm consistent with the ferric enzyme, and for the latter the absorption maximum was 418.2 nm. It was more difficult to obtain a clean result in the much weaker Q bands (500 – 650 nm), but it was clear that increasing concentrations of H_2O_2 produced more prominent absorption features at 540 and 578 nm.

In contrast, spectra recorded for R418A at the beginning of each steady-state phase (~130 ms) showed much less variability over a substantially wider H_2O_2 concentration range (Fig. 3.6B). Instead of the 8-nm Soret redshift observed for wild-type, R418A showed only a 4 nm redshift from ~412 nm (observed with 0.015 mM H_2O_2) to ~414 nm (observed with 0.25 mM H_2O_2) (Fig. 3.6B) to 416 nm (observed with 4 mM H_2O_2). Regardless of the concentration of H_2O_2 employed, the R418A KatG steady-state intermediate showed Q bands with absorption maxima at 540 and 578 nm consistent with a compound III-like species (Fig. 3.6B-inset).

The spectral features accompanying the return of the ferric state, including an isosbestic point at 414 nm, were nearly identical for wild-type (Fig. 3.5C) and R418A KatG (Fig. 3.6C).

Interestingly, these spectral transitions appeared to mirror the H_2O_2-dependent transition measured for wild-type enzyme in Figure 3.5B.

For wild-type KatG, our data indicated that the ferric and compound III-like heme states were both present during steady-state H_2O_2 consumption. Based on the hyperbolic shift toward the compound III-like state with increasing H_2O_2 concentration, we postulated a steady-state defined by equation **3.4**, where reaction of the ferric enzyme with H_2O_2 (governed by the rate constant k_a) must necessarily equal the H_2O_2-independent decomposition of the compound III-like state (governed by the first-order rate constant k_b).

$$k_a[Fe^{III}][H_2O_2] = k_b[Fe^{III}\text{-}O_2^{\bullet-}] \qquad (3.4)$$
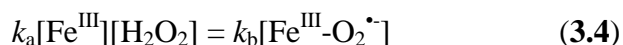
By this equation, k_b/k_a would represent the concentration of $[H_2O_2]$ where the steady-state is equally populated by the ferric and compound III-like states. According to the inset in Figure 3.5B-inset, k_b/k_a would be ~0.3 mM.

In order to estimate the rate constants (k_a and k_b) governing the donor-enhanced catalatic turnover, we reacted KatG against H_2O_2 in the presence of ABTS alone and monitored $ABTS^{\bullet+}$ at 645 nm. The turnover of KatG itself could be most clearly monitored when ascorbate was included with H_2O_2 and ABTS. Comparison of reactions carried out in the presence and absence of ascorbate showed that they ended simultaneously and that $ABTS^{\bullet+}$ production was linear over the period of steady-state H_2O_2 consumption (Fig. 3.7). The traces obtained at 645 nm in the absence of ascorbate not only allowed for the evaluation of $ABTS^{\bullet+}$ production rates, but also the *extent* of radical production for each reaction. In the example shown in Figure 3.7, it can be seen that a reaction including 2.0 mM H_2O_2 led to the production of 12.7 μM $ABTS^{\bullet+}$ ($[ABTS^{\bullet+}]/[H_2O_2]$ = 0.0064). Based on these data, we were able to infer enzyme H_2O_2 consumption rates from rates of $ABTS^{\bullet+}$ production and the $ABTS^{\bullet+}/H_2O_2$ ratios obtained for
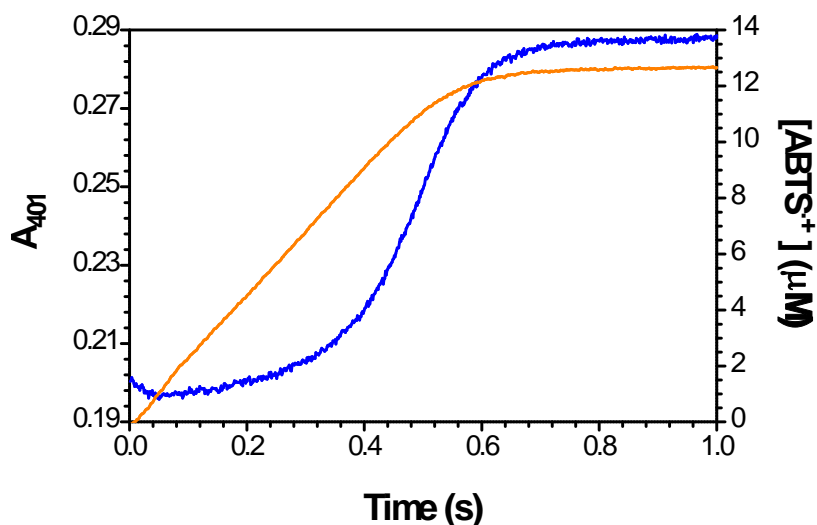
Figure 3.7. KatG return to its ferric state and production of ABTS$^{\bullet+}$ during reaction with 2 mM H_2O_2. MtKatG was reacted with 2 mM H_2O_2 in the presence of 0.1 mM ABTS alone (orange line) or 0.1 mM ABTS and 0.1 mM ascorbate (blue line). The former was monitored at 645 nm for the accumulation of ABTS$^{\bullet+}$ while the latter was monitored at 401 nm to observe the return of the KatG ferric state upon H_2O_2 depletion. The rate of ABTS$^{\bullet+}$ production (22.4 µM/s) is given by the slope of the fit line. Note that at the conclusion of the reaction 12.7 µM ABTS$^{\bullet+}$ had accumulated for the 2.0 mM H_2O_2 consumed, giving a ratio of 0.00634, and therefore, an estimated rate of H_2O_2 consumption of 3.53 mM/s. Accounting for stoichiometry and subtracting H_2O_2 consumption due to ABTS$^{\bullet+}$ production, an estimated rate of O_2 production of 1.76 mM s^{-1} was obtained.

each H_2O_2 concentration evaluated (Fig. 3.4). In the steady-state, both halves of equation **3.4** must necessarily be equal to the overall rate of reaction expressed here as the rate of H_2O_2 consumption, accounting for the stoichoimetry of the catalase reaction (equations **3.5** and **3.6**) and the minute concentration of H_2O_2 dedicated to ABTS$^{\bullet+}$ production.

$$-d[H_2O_2]/dt = 2k_a[Fe^{III}][H_2O_2] \qquad\qquad (\textbf{3.5})$$

$$-d[H_2O_2]/dt = 2k_b[Fe^{III}\text{-}O_2{}^{\bullet-}] \qquad\qquad (\textbf{3.6})$$

In the presence of 2 mM H_2O_2 this rate was 1.76 mM s^{-1}. Our stopped-flow studies also indicated that there was a H_2O_2 concentration-dependent distribution between the ferric and compound III-like states during electron donor-stimulated catalatic turnover of KatG (Fig. 3.5). From that hyperbolic dependence, we estimated that on reaching the steady-state there was a 0.14 : 0.86 ratio of ferric to compound III-like states (i.e., 0.42 μM : 2.58 μM). These data were used to solve equation **3.5** for k_a, producing a value of 2.1×10^6 M^{-1}s^{-1}. Likewise, equation **3.6** was solved to produce a value for k_b of 680 s^{-1}. The same exercise was carried out for each H_2O_2 concentration evaluated, and consistent values were obtained for both k_a ([2.1 ± 0.1] × 10^6 M^{-1} s^{-1}) and k_b (640 ± 30 s^{-1}). Accounting for the temperature used for our stopped-flow studies, these rate constants are in reasonable agreement with the parameters we obtained for ABTS-stimulated O_2 production (Table 3.3). Here the apparent second-order rate constant for O_2 production should correspond to k_a, and the k_{cat} should correspond to k_b, and k_b/k_a would be expected to be approximated by the apparent K_M.

The R418A variant stood in contrast to the wild-type enzyme in that H_2O_2 concentration had far less impact on the distribution between the ferric and compound III-like states. Two possible explanations for such a result would be, 1) a much larger value for k_a, or 2) a substantially smaller value for k_b. Evidence is overwhelming in favor of the latter rather than the

former. All evidence reported to date suggests that R418 (or its equivalent) substitution has no influence on the rate constant of compound I formation by H_2O_2. It has recently been reported that R418 substitution does not interfere with the formation of the compound III* state, but rather slows its decomposition to release O_2 in the final step of KatGs catalytic cycle (*176*). Finally, our own evidence shows that ABTS-enhanced catalatic activity (O_2 electrode) and the time required for H_2O_2 consumption and return to the ferric state (stopped-flow) are 3 – 4 fold slower for R418A KatG than for wild-type. These would not be accounted for by an enhanced k_a but rather a diminished k_b.

We also used stopped-flow to evaluate the reactions of wild-type and R418A KatG with H_2O_2 in the absence of ABTS or other peroxidatic electron donor. Both enzymes showed a much slower reemergence of the ferric state (i.e., > 100 s) following reaction with H_2O_2 (Fig. 3.8). Strikingly, for both proteins the bulk of H_2O_2 consumption occurred long before a full return of the ferric state was detected. Second, although consumption of 4 mM H_2O_2 was accomplished more rapidly with the wild-type enzyme (~8 s) than with R418A KatG (~20 s), both enzymes showed essentially the same slow accumulation of the ferric state.

The spectral transitions observed during reactions with H_2O_2 alone were nearly identical for wild-type and R418A KatG and were typified by those observed for R418A KatG upon its reaction with 1 mM H_2O_2 at pH 5.0 (Fig. 3.9). Spectra recorded at the earliest time points showed the familiar compound III-like character with absorption maxima at 542 and 578 nm (Fig. 3.9-panel A). As has been observed for wild-type KatG by our group (*177*) as well as others (*113, 115*), this was followed by a rapid (~ 0.5 s) and broad increase in absorption at wavelengths above 520 nm. From 0.2 to 9 s, there was little if any change in spectra (Fig. 3.9-panel B). From 9 to 50 s, the very slow return of the ferric state was observed (Fig. 3.9-panel C).
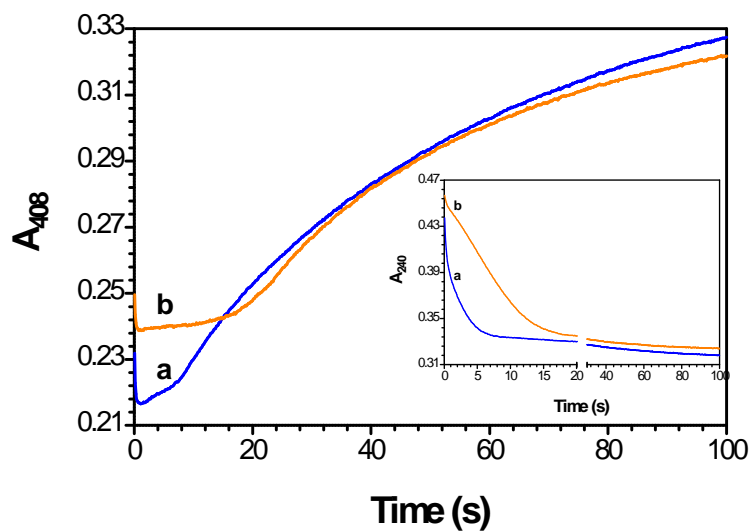
Figure 3.8. H_2O_2 consumption and return of the ferric state in the absence of electron donor for wild-type and R418A KatG. The return of the ferric form of wild-type (a) and R418A KatG (b) following reaction with 4 mM H_2O_2 was monitored at 408 nm. The consumption of H_2O_2 under identical reaction conditions (inset) was monitored for wild-type (a) and R418A KatG (b) at 240 nm. The final concentration of enzyme in each reaction was 3 µM, and all reactions were carried out in the presence of 50 mM acetate buffer, pH 5.0, at 4 ^{o}C.
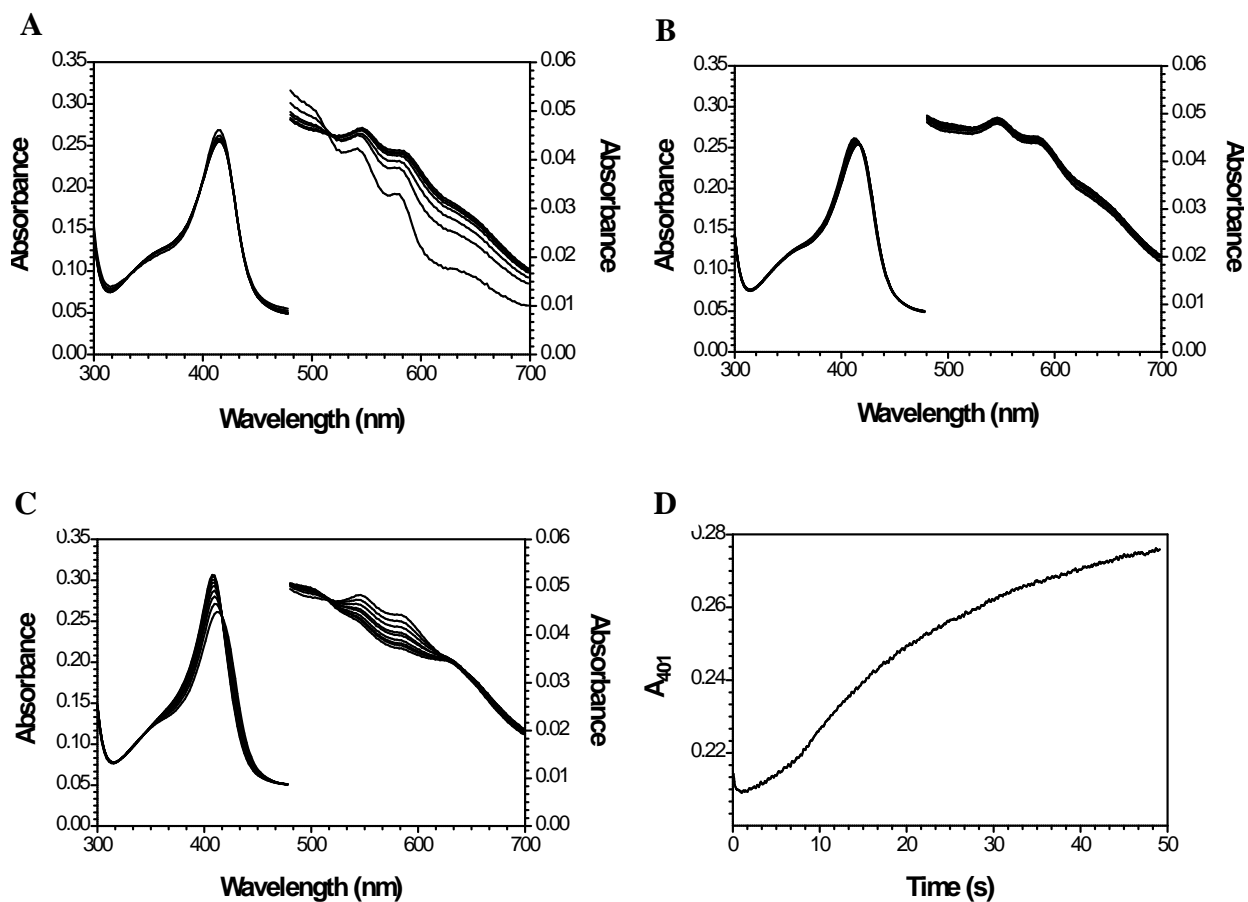
Figure 3.9. Spectra collected during reaction of R418A KatG with 1.0 mM H_2O_2. Spectra correspond to 8 – 220 ms (A), 0.22 – 9 s (B), and 9 – 50 s (C) following mixing of 3 μM enzyme with 1.0 mM H_2O_2. The change in absorbance at 401 nm over the entire course of the reaction (D) is also shown. This reaction was carried out using 50 mM acetate buffer, pH 5.0 at 4 °C.

The change in absorbance at 401 nm over the course of the entire reaction is shown in Figure 3.9-panel D.

3.4. Discussion

The stimulatory effect of electron donors on KatG catalatic activity and its pH dependence (*177*) prompted us to evaluate the effect of R418 substitution on the phenomenon. Building on the unique mechanism proposed for the catalase activity of KatG (*112-113*) and the data we have presented here, we postulate a model for the stimulatory effect of electron donors (Fig. 3.10). Generally, our model suggests that off-pathway intramolecular electron transfer leads to formation of catalase-inactive intermediate(s). Peroxidatic electron donors reduce these inactive intermediates to the ferric state, preventing their accumulation and thereby ensuring maximal catalatic turnover. Off-pathway reduction of compound I by a KatG-derived source other than the MYW adduct (path *a*) or reduction of the MYW radical itself at compound I* (path *b*) would presumably produce catalase-inactive states. In the presence of a suitable electron donor, reduction of these intermediates to the catalatically active ferric state would take place. However, in the absence of such a donor, these inactive ferryl intermediates would be expected to react further with H_2O_2 to form $Fe^{III}-O_2^{\bullet-}$ states. For all intents and purposes, these would be dead-end complexes in that they would have only limited ability to accomplish the final intramolecular electron transfer necessary for O_2 release.

As a side note, a late off-pathway reduction of the MYW radical of compound III* (path *c*) would also be expected to produce a dead-end $Fe^{III}-O_2^{\bullet-}$ complex, but we anticipate that peroxidatic electron donors would be of limited utility for addressing such a pathway.
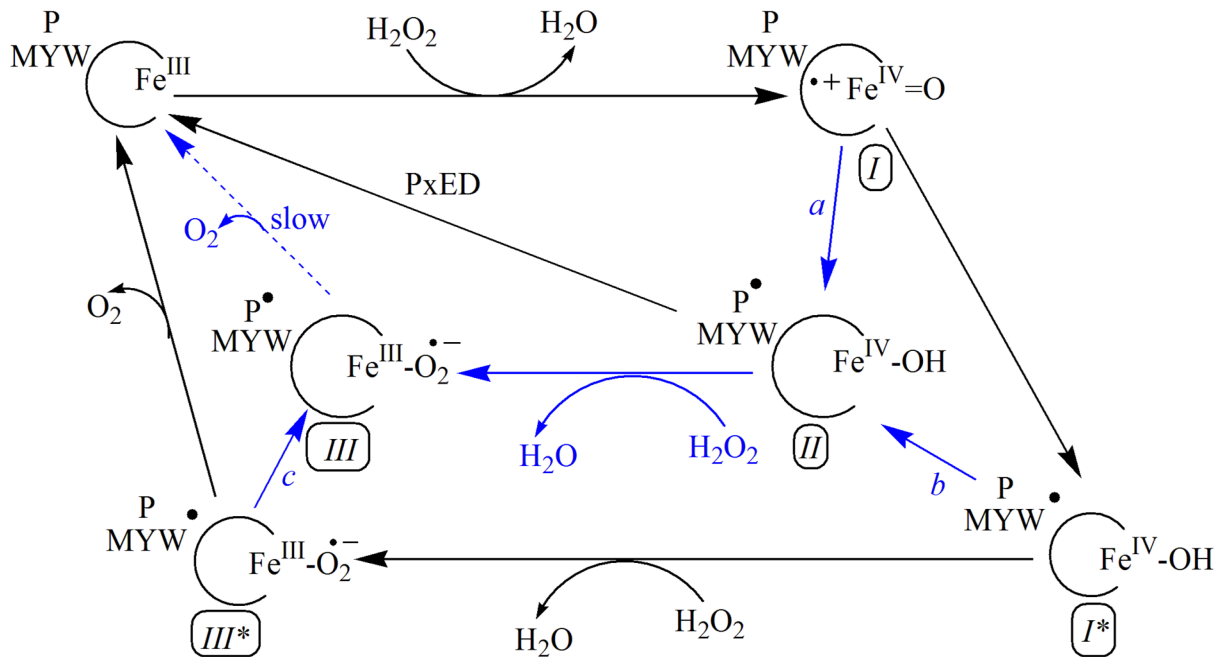
Figure 3.10. Scheme representing proposed mechanism for stimulation of KatG catalase activity by peroxidatic electron donors. The *catalatic* cycle proceeds by way of the ferric enzyme, compound I (I), compound I* (I*), and compound III* (III*). Off-pathway reduction of compound I (path *a*) or compound I* (path *b*) produces catalase-inactive compound II-like intermediate (II). Subsequent reaction of II with H_2O_2 produces a catalase-inactive compound III-like intermediate (III). The conversion of II to the active ferric state by a peroxidatic electron donor (PxED) is proposed. The Met-Tyr-Trp covalent adduct and its corresponding radical are represented by MYW and MYW$^\bullet$, respectively. An unspecified KatG oxidizable amino acid and its corresponding radical are represented by P and P$^\bullet$, respectively.

That catalase-inactive intermediates accumulated in the absence of a peroxidatic electron donor was apparent from the cessation of H_2O_2 consumption *prior to* the very slow reversion of enzyme to the ferric state. Though the slower catalatic turnover of the R418A variant was readily observable in the relative rates of H_2O_2 consumption, the spectra observed at the conclusion of H_2O_2 consumption and the kinetics of the return of the ferric state were indistinguishable between the two proteins. These data suggest that the inactive intermediate(s) formed by wild-type and R418A KatG and their reactivity were highly similar. Notably, spectra observed for both R418A and wild-type KatG at the conclusion of H_2O_2 consumption and prior to the return of the ferric state showed features consistent with a Fe^{III}-$O_2^{\bullet-}$ complex.

Our data show that ABTS does little to change the inherent difference in catalase activity of wild-type and R418K KatG on one hand and R418A KatG on the other. In the presence or absence of the donor a three to four-fold difference in activity persists. Furthermore, our stopped-flow data confirm this differential and indicate that the electron donor does little to change the underlying molecular cause for the diminished catalase activity of R418A. As Zhao et al. have recently shown, R418L KatG readily forms the compound III* state but demonstrates a diminished ability to complete the final step of the catalytic cycle (*176*). Our stopped-flow data indicate that ABTS does not change this catalytic disadvantage of the R418A variant. Consistent with these results, our model proposes that electron donors do not exert their stimulatory effect by direct interactions with catalatically active intermediates, but rather act indirectly to scavenge the off-pathway intermediates once they have been formed.

Given the size of many peroxidatic electron donors like ABTS and the aperture of channels leading to the KatG active site, simple steric considerations would suggest that these donors are unable to make direct contact with the heme edge for electron transfer. This sets KatG

apart from the monofunctional peroxidases of its superfamily (e.g., HRP). We suggest that the H_2O_2-dependent "peroxidase activity" of KatG amounts to nothing more than the failure of KatG to properly execute catalatic turnover. In this light, these events are relatively rare for wild-type and R418K KatG at all H_2O_2 concentrations. In contrast, for R418A KatG misdirected electron transfer appears to be a much more common event, and its frequency increases dramatically as H_2O_2 concentration decreases. Our model accounts for this behavior by suggesting that path *b* is the primary pathway for misdirected electron transfer for R418A KatG. The slow conversion of compound I* to III* imposed by low H_2O_2 concentration increases the likelihood that the MYW radical will be reduced by a KatG-derived electron source other than the $Fe^{III}-O_2^{\bullet-}$ that has yet to form. Conversely, the rapid rates of compound I* conversion to compound III* afforded by relatively high H_2O_2 concentrations would limit premature reduction of the MYW adduct radical. Interestingly, Zhao et al (*176*) have recently shown that R418L KatG is more susceptible than the wild-type enzyme to the oxidative formation of aggregates, a phenomenon associated with the misdirected oxidation of surface Trp/Tyr residues.

Thorough investigations of KatG enzymes from several organisms have identified pathways for transfer of oxidizing equivalents from the active site to distant tryptophan residues following reactions with peracetic acid (*104, 116-117, 154*). Of course, such studies are facilitated by the use of peracetic acid, a substrate with which KatG readily forms compound I but is incapable of completing catalytic turnover alone. The pathways for misdirected electron transfer during turnover in the presence of the physiological peroxide, H_2O_2, are less clear. Our data indicate that such events become much more prominent under circumstances where R418 is oriented away from the MYW adduct or is absent altogether. The question remains whether

R418 substitution simply increases utilization of a given route of off-pathway electron transfer, or whether the substitution opens a route that is otherwise unutilized by the wild-type enzyme.

Chapter four: Summary

The ability to rapidly degrade hydrogen peroxide is vital for all aerobic organisms, particularly pathogenic bacteria and fungi as they face large amounts of hydrogen peroxide secreted by the host-derived immune responses. As such, the survival of these pathogens during an encounter with the host requires that they possess enzymes that can efficiently degrade high amounts of hydrogen peroxide at the pH of the environment the host utilizes for its immune response.

Catalase-peroxidase (KatG) represents an important class of enzymes used by several bacteria and lower eukaryotes as a tool to rapidly degrade H_2O_2. The results of the research presented in this dissertation show that the peroxidatic and catalatic activities of KatG are synergistic. This is contrary to what has been the prevailing paradigm which holds these activities to be mutually antagonistic. Not only this, but our data also show that KatG is very nearly exclusively a catalase, and the peroxidase activity appears to arise whenever the enzyme fails to execute the catalase reaction. Our data indicate that under these circumstances, it oxidizes electron donors as a way to rescue catalatically inactive intermediates. This is supported by the fact that very little of the oxidized donor radicals accumulate under conditions which define the peroxidase activity. In addition, deletion or substitution variants devoid of catalase activity show robust peroxidase activity that even rivals that of horseradish peroxidase (*88*). In order words, in the absence of some dramatic modification that restores traditional peroxidase turnover, the peroxidase "activity" of KatG appears to fill an entirely alternate function.

4.1. Insights from the Heme Intermediates Involved in the Catalase Mechanism

A mechanism recently put forward in the literature suggests that a compound III-like intermediate (i.e., $Fe^{III}-O_2^{\bullet-}$) is central to the catalase mechanism of KatG. The results we presented in this dissertation lend support to this novel catalytic scheme. More so, we observed the accumulation of this same intermediate under conditions that defined catalase stimulation by peroxidatic electron donors. This suggests that peroxidatic electron donors play a central role in the catalase mechanism of KatG and center on a pathway that involves the cycling of the compound III-like intermediate. More details into the mechanism require the identification of the protein-based radical species that form when KatG undergoes active catalatic turnover in the presence of peroxidatic electron donors. Indeed, we have conducted initial rapid freeze quench EPR experiments with MtKatG and have observed a narrow doublet that has features similar to the putative MYW$^{\bullet}$-based radical intermediate. We suggest that the active compound III-like intermediate observed during catalatic turnover stimulated by electron donors is the $Fe^{III}-O_2^{\bullet-}$ [MYW$^{\bullet}$] species central to the proposed KatG mechanism (*112-113, 115, 121*). However, work is ongoing to identify this species and others that may be involved in the catalase mechanism of KatG.

4.2. Potential Binding Sites

Although we have provided sufficient data accounting for KatG stimulation by peroxidatic electron donors, very little is known about the binding site(s) for such compounds. The fact that R418 substitution affects the ability of some peroxidatic electron donors to stimulate the catalase activity suggests two possibilities. The first is that these donors bind at an

interface near the R418 side chain. The second is that they could bind in a cavity away from the R418 residue, and induce structural changes that facilitate electron transfer through interaction with the side chain of the R418 residue. Such speculations can only be verified through resolution of the crystal structure of KatG or the R418 substitution variants in the presence of peroxidatic electron donors. Work is also underway to evaluate such posibilities by X-ray crystallography and computational modeling.

4.3.   Physiological Implications

Finally, our research has shown for the first time that peroxidatic electron donors stimulate KatG catalase activity. This is counterintuitive relative to what one would normally expect, and it therefore raises several concerns. The most important points towards the implications of this novel catalatic mechanism and centers on whether or not there are any physiological advantages afforded by these compounds to organisms that carry KatG. For an organism like *Mycobacterium tuberculosis* which uses KatG as its only catalase-active enzyme, there might be several advantages afforded by the broadening of KatG catalase function at low pH, such as defense against hydrogen peroxide produced by the host-derived immune response. This is supported by the fact that the stimulatory effect is optimum at pH 5.0 which is the corresponding pH value observed in the phagolysosome of activated neutrophils.

In summary, the results presented in this dissertation have brought a great contribution toward understanding the mechanism of KatG catalase activity. We observed that the catalatic and peroxidatic activities of KatG are synergistic. Not only has this helped us to understand how nature efficiently built the coexistence of these two functions in a single active site, but it has

also helped us to understand how KatG catalase activity could be broadened, particularly under

conditions that coincide with antimicrobial defenses.

References

1. Messner, K. R., and Imlay, J. A. (1999) The identification of primary sites of superoxide and hydrogen peroxide formation in the aerobic respiratory chain and sulfite reductase complex of *Escherichia coli*, *J. Biol. Chem 274*, 10119-10128.

2. Imlay, J. A. (2008) Cellular defenses against superoxide and hydrogen peroxide, *Annu. Rev. Biochem 77*, 755-776.

3. Turrens, F. J. (2003) Mitochondrial formation of reactive oxygen species, *J. Physiol 552*, 335-344.

4. Bedard, K., and Krause, K. H. (2007) The NOX family of ROS-generating NADPH oxidases: Physiology and pathophysiology, *Physiol Rev 87*, 245-313.

5. Sharma, P., Jha, A. B., Dubey, R. S., and Pessarakli, M. (2012) Reactive oxygen species, oxidative damages, and antioxidative defense mechanism in plants under stressful conditions, *J. Botany 2012*, doi: 10.1155/2012/217037.

6. Gough, D. R., and Cotter, T. G. (2011) Hydrogen peroxide: a Jekyll and Hyde signaling molecule, *Cell Death and Disease 2*, doi:10.1038/cddis.2011.96.

7. Lambeth, J. D. (2007) Nox enzymes, ROS, and chronic disease: an example of antagonistic pleitropy, *Free. Radic. Biol. Med 43*, 332-347.

8. Bartz, R. R., and Piantadosi, C. A. (2010) Oxygen as a signaling molecule, *Critical Care* 14:234 doi:10.1186/cc9185.

9. Ushio-Fukai, M., Alexander, R. W., Akers, M., Yin, Q., Fujio, Y., Walsh, K., Griendling, K. K. (1999) Reactive oxygen species mediate the activation of Akt/protein kinase B by angiotensin II in vascular smooth muscle cells, *J. Biol. Chem 274*, 22699-22704.

10. Veal, E., and Day, A. (2011) Hydrogen peroxide as a signaling molecule, *Antioxid. Redox. Signal 15*, 147-151.

11. Halliwell, B., and Gutteridge, J. M. C. (1984) Oxygen toxicity, oxygen radicals, transition metals and disease, *Biochem. J 219*, 1-14.

12. Wood, P. M. (1974) The redox potential of the system oxygen-superoxidase, *FEBS Letters 44*, 22-24.

13.   Malmstrom, B. G. (1982) Enzymology of oxygen, *Ann. Rev. Biochem 51*, 21-59.

14.   Naqui, A., and Chance, B. (1986) Reactive oxygen intermediates in biochemistry, *Ann. Rev. Biochem 55*, 137-166.

15.   Miller, D. M., Buettner, G. R., and Aust, S. D. (1990) Transition metals as catalysts of "autoxidation" reactions, *Free. Radic. Biol. Med 8*, 95-108.

16.   Thannickal, V. J., and Fanburg, B. L. (2000) Reactive oxygen species in cell signaling, *Am J Physiol Lung Cell Mol Physiol 279*, L1005-L1028.

17.   Fridovich, I. (1995) Superoxide radical and superoxide dismutases, *Ann. Rev. Biochem 64*, 97-112.

18.   Rada, B., and Leto, T. L. (2008) Oxidative innate immune defenses by Nox/Duox family NADPH oxidases, *Contrib Microbiol 15*, 164-187.

19.   Hunter, P. (2005) Common defences, *EMBO Rep 6*, 504-507.

20.   Driessens, N., Versteyhe, S., Ghaddhab, C. et al. (2009) Hydrogen peroxide induces DNA single- and double-strand breaks in thyroid cells and is therefore a potential mutagen for this organ, *Endocr Relat Cancer 16*, 845-856.

21.   Beckman, K. B., and Ames, B. N. (1998) The free radical theory of aging matures, *Physiol Rev 78*, 547-581.

22.   Harman, D. (1956) Aging: a theory based on free radical and radiation chemistry, *J Gerontol 11*, 298-300.

23.   Zastawny, T. M., Altman, S.A., Randers-Eichhorn, L., Madurawe, R., Lumpkin, J. A., Dizdaroglu, M., and Rao, G. (1995) DNA base modifications and membrane damage in cultured mammalian cells treated with iron ions, *Free Radic Biol Med 18*, 1013-1022.

24.   Jaruga, P. W., Rodriguez, H., and Dizdaroglu, M. (2001) Measurement of 8-hydroxyl-2'-deoxyadenosine in DNA by liquid chromatography/mass spectrometry, *Free Radic Biol Med 31*, 336-344.

25.   Pym, A. S., Saint-Joanis, B., and Cole, S. T. (2002) Effect of katG mutations on the virulence of *Mycobacterium tuberculosis* and the implication for transmission in humans, *Infect Immun 70*, 4955-4960.

26.   Master, S., Zahrt, T. C., Song, J., and Deretic, V. (2001) Mapping of *Mycobacterium tuberculosis katG* promoters and their differential expression in infected macrophages, *J. Bacteriol 183*, 4033-4039.

27. Heym, B., Stavropoulos, E., Honoré, N., Domenech, P., Saint-Joanis, B., Wilson, T. M., Collins, M. J., and Cole, S. T. (1997) Effects of overexpression of the alkyl hydroperoxide reductase AhpC on the virulence and isoniazid resistance of *Mycobacterium tuberculosis*, *Infect Immun 65*, 1395-1401.

28. Brenot, A., King, K. Y., Janowiak, B., Griffith, O., and Caparon, M. G. (2004) Contribution of glutathione peroxidase to the virulence of *Streptococcus pyogenes*, *Infect Immun 72*, 408-413.

29. Missall, T. A., Cherry-Harris, J. F., and Lodge, J. K. (2005) Two glutathione peroxidases in the fungal pathogen *Cryptococcus neoformans* are expressed in the presence of specific substrates, *Microbiol 151*, 2573-2581.

30. Pineyro, M. D., Parodi-Talice, A., Arcari, T., and Robello, C. (2008) Peroxiredoxins from *Trypanosoma cruzi*: virulence factors and drug targets for treatment of Chagas disease? *Gene 408*, 45-50.

31. Wang, Y., Zhao, X., Jiang, X., Hua, X., and Xu, N. (2010) Molecular characterization of thyroid peroxidase gene in porcine (*sus scrofa*), *J. Genet. Genomics 37*, 381-388.

32. Lambeth, J. D. (2004) NOX enzymes and the biology of reactive oxygen, *Nat Rev Immunol 4*, 181-189.

33. Almagro, L., Gomez Ros, L. V., Belchi-Navarro, S., Bru, R., Ros Barcelo, A., and Pedreno, M. A. (2009) Class III peroxidases in plant defence reactions, *J. Exp. Bot 60*, 377-390.

34. Ralph, J., Bunzel, M., Marita, J. M., Hatfield, R. D., Lu, F., Kim, H., Schatz, P. F., Grabber, J. H., and Steinhart, H. (2004) Peroxidase-dependent cross-linking reactions of -hydroxycinnamates in plant cell walls, *Phytochem Rev 3*, 79-96.

35. Bacon, M. A., Thompson, D. S., and Davies, W. (1997) Can cell wall peroxidase activity explain the leaf growth response of *Lolium temulentum L.* during drought? *J. Exp. Bot 48*, 2075-2085.

36. Koua, D., Cerutti, L., Falquet, L., Sigrist, C. J. A., Theiler, G., Hulo, N., and Dunand, C. (2008) PeroxiBase: a database with new tools for peroxidase family classification, *Nucl Acids Res 37*, D261-D266.

37. Arthur, J. R. (2000) The glutathione peroxidases, *Cell. Mol. Life. Sci 57*, 1825-1835.

38. Toppo, S., Vanin, S., Bosello, V., and Tosatto, S. C. (2008) Evolutionary and structural insights into the multifaceted glutathione peroxidase (GPx) superfamily, *Antioxid. Redox. Signal 10*, 1501-1514.

39. Ursini, F., Maiorino, R., Brigelius-Flohe, R., Augman, K. D., Roveri, A., Schomburg, D., and Flohe, L. (1995) Diversity of glutathione peroxidases, *Methods. Enzymol 252*, 38-53.

40. Brigelius-Flohe, R., and Maiorino, M. (2012) Glutathione peroxidases, Biochim. Biophys. Acta, http://dxdoi.org/10.106/j.bbgen.2012.11.020.

41. Passardi, F., Bakalovic, N., Teixeira, F. K., Margis-Pinheiro, M., Penel, C, and Dunand, C. (2007) Prokaryotic origins of the non-animal peroxidase superfamily and organelle-mediated transmission to eukaryotes, *Genomics 89*, 567-579.

42. Daiyasu, H., and Toh, H. (2000) Molecular evolution of the myeloperoxidase family, *J. Mol. Evol 51*, 433-445.

43. Furtmuller, P. G., Zederbauer, M., Jantschko, W., Helm, J., Bogner, M., Jakopitsch, C., and Obinger, C. (2006) Active site structure and catalytic mechanisms of human peroxidases, *Arch. Biochem. Biophys 445*, 199-213.

44. Zamocky, M., Jakopitsch, C., Furtmuller, P. G., Dunand, C., and Obinger, C. (2008) The peroxidase-cyclooxygenase superfamily: reconstructed evolution of critical enzymes of the innate immune system, *Proteins 72*, 589-605.

45. Arnhold, J., Monzani, E., Furtmuller, P. G., Zederbauer, M., Casella, L., and Obinger, C. (2006) Kinetics and thermodynamics of halide and nitrite oxidation by mammalian heme peroxidases, *Eur. J. Inorg. Chem 19*, 3801-3811.

46. Zederbauer, M., Furtmuller, P. G., Brogioni, S., Jakopitsch, C., Smulevich, G., and Obinger, C. (2007) Heme to protein linkages in mammalian peroxidases: impact on spectroscopic, redox and catalytic properties, *Nat. Prod. Rep 24*, 571-584.

47. Brittain, T. (2008) Intra-molecular electron transfer in proteins, *Protein. Pept. Lett 15*, 556-561.

48. Welinder, K. G. (1992) Superfamily of plants, fungal and bacterial peroxidases, *Curr. Opin. Struct. Biol 2*, 388-393.

49. Reading, N. S., and Aust, S. D. (2001) Role of disulfide bonds in the stability of recombinant manganese peroxidase, *Biochemistry 40*, 8161-8168.

50. Mathe, C., Barre, A., Jourda, C., and Dunand, C. (2010) Evolution and expression of class III peroxidases, *Arch. Biochem. Biophys 500*, 58-65.

51. Fita, I., and Rossmann, M. G. (1985) The active center of catalases, *J. Mol. Biol 185*, 21-37.

52. Gajhede, M., Schuller, D. J., Henriksen, A., Smith, A. T., and Poulos, T. L. (1997) Crystal structure of horseradish peroxidase C at 2.5 resolution, *Nat. Struct. Biol 4*, 1032-1038.

53. Poulos, T. L., and Joseph, K. (1980) The stereochemistry of peroxidase catalysis, *J. Biol. Chem 255*, 8199-8205.

54. Vitello, L. B., Erman, J. E., Miller, M. A., Wang, J., and Kraut, J. (1993) Effect of arginine-48 replacement on the reaction between cytochrome *c* peroxidase and hydrogen peroxide. *Biochemistry 32*, 9807-9818.

55. Smith, A. T., and Veitch, N. C. (1998) Substrate binding and catalysis in heme peroxidases, *Curr. Opin. Chem. Biol 2*, 269-278.

56. Henriksen, A., Schuller, D. J., Meno, K., Welinder, K. G., Smith, A. T., and Gajhede, M. (1998) Structural interactions between horseradish peroxidase C and the substrate benzhydroxamic acid determined by X-ray crystallography, *Biochemistry 37*, 8054-8060.

57. Mogharrab, N., Ghourchian, H., and Amininasab, M. (2007) Structural stabilization and functional improvement of horseradish peroxidase upon modification of accessible lysine: Experiments and simulation, *Biophys. J 92*, 1192-1203.

58. Chelikani, P., Fita, I., and Loewen, P. C. (2004) Diversity of structures and properties among catalases, *Cell. Mol. Life. Sci 61*, 192-208.

59. Antonyuk, S V., Melik-Adamyan, V. R., Popov, A. N., Lamzin, V. S., Hempstead, P. D., Harrison, P. M., Artymyuk, P. J., and Barynin, V. V. (2000) Three-dimensional structure of the enzyme dimanganese catalase from *Thermus thermophilus* at 1 resolution, *Crystallogr. Rep 45*, 105-116.

60. Barynin, V. V., Whittaker, M. M., Antonyuk, S. V., Lamzin, V. S., Harrison, P. M., Artymiuk, P. J., and Whittaker, J. W. (2001) Crystal structure of manganese catalase from *Lactobacillus plantarum*, *Structure 9*, 725-738.

61. Whittaker, M. M., Barynin, V. V., Igarashi, T., and Whittaker, J. W. (2003) Outer sphere mutagenesis of *Lactobacillus plantarum* manganese catalase disrupts the cluster core. Mechanistic implications, *Eur. J. Biochem 270*, 1102-1116.

62. Whittaker, J. W. (2012) Non-heme manganese catalase - The 'other' catalase, *Arch. Biochem. Biophys 525*, 111-120.

63. Zamocky, M., Furtmuller, P. G., and Obinger, C. (2008) Evolution of catalases from bacteria to humans, *Antioxid. Redox. Signal 10*, 1527-1548.

64.	Zamocky, M., and Koller, F. (1999) Understanding the structure and function of catalases: clues from molecular evolution and in vitro mutagenesis, *Prog. Biophys. Mol. Biol 72*, 19-66.

65.	Diaz, A., Loewen, P. C., Fita, I., and Carpena, X. (2012) Thirty years of heme catalases structural biology, *Arch. Biochem. Biophys 525*, 102-110.

66.	Loewen, P. C., Switala, J., von Ossowski, I., Hillar, A., Christie, A., Tattrie, B., and Nicholls, P. (1993) Catalase HPII of *Escherichia coli* catalyzes the conversion of protoheme to *cis*-heme *d*, *Biochemistry 32*, 10159-10164.

67.	Obinger, C., Maj, M., Nicholls, P., and Loewen, P. (1997) Activity, peroxide compound formation, and heme *d* synthesis in *Escherichia coli* HPII catalase, *Arch. Biochem. Biophys 342*, 58-67.

68.	Hillar, A., Nicholls, P., Switala, J., and Loewen, P. C. (1994) NADPH binding and control of catalase compound II formation: comparison of bovine, yeast, and Escherichia coli enzymes, *Biochem. J 300*, 521-539.

69.	de Visser, S. P. (2006) What external perturbations influence the electronic properties of catalase compound I? *Inorg. Chem 45*, 9551-9557.

70.	Bravo, J., Fita, I., Ferrer, J. C., Ens, W., Hillar, A., Switala, J., and Loewen, P. C. (1997) Identification of a novel bond between a histidine and the essential tyrosine in catalase HPII of *Escherichia coli*, *Protein. Sci 6*, 1016-1023.

71.	Chelikani, P., Carpena, X., Fita, I., and Loewen, P. C. (2003) An electrical potential in the access channel of catalases enhances catalysis, *J. Biol. Chem 278*, 31290-31296.

72.	Kalko, S. G., Gelpi, J. L., Fita, I., and Orozco, M. (2001) Theoretical study of the mechanisms of substrate recognition by catalase, *J. Am. Chem. Soc 123*, 9665-9672.

73.	Klotz, G. M., and Loewen, P. C. (2003) The molecular evolution of catalatic hydroperoxidases: evidence for multiple lateral transfer of genes between prokaryota and from bacteria into eukaryota, *Mol. Biol. Evol 20*, 1098-1112.

74.	Zamocky, M., Furtmuller, P. G., and Obinger, C. (2010) Evolution of structure and function of Class I peroxidases, *Arch. Biochem. Biophys 500*, 45-57.

75.	Zamocky, M., and Obinger, C. (2010) in: Ayala, M., and Torres, E (Eds.), Biocatalysis based on heme peroxidases, *Springer-Verlag*, Berlin, pp. 7-35.

76.	Welinder, K. (1992) Superfamily of plant, fungal and bacterial peroxidases, *Curr. Opin. Struct. Biol 2*, 388-393.

77.   Bertrand, T., Eady, N. A. J., Jones, J. N., Nagy, J. M., Jamart-Gregoire, B., Raven, E. L., and Brown, K. A. (2004) Crystal structure of *Mycobacterium tuberculosis* catalase-peroxidase, *J. Biol. Chem 279*, 38991-38999.

78.   Carpena, X., Loprasert, S., Mongkolsuk, S., Switala, J., Loewen, P. C., and Fita, I. (2003) Catalase-peroxidase KatG of *Burkholderia pseudomallei* at 1.7   resolution, *J. Mol. Biol 327*, 475-489.

79.   Yamada, Y., Fujiwara, T., Sato, T., Igarashi, N., and Tanaka, N. (2002) The 2.0 angstrom crystal structure of catalase-peroxidase from *Haloarcula marismortui*, *Nat. Struct. Biol 9*, 691-695.

80.   Wada, K., Tada, T., Nakamura, Y., Kinoshita, T., Tamoi, M., Shigeoka, S., and Nishimura, K. (2002) Crystallization and preliminary X-ray diffraction studies of catalase-peroxidase from Synechococcus PCC 7942, *Acta Crystallogr. D Biol. Crystallogr 58*, 157-159.

81.   Santoni, E., Jakopitsch, C., Obinger, C., and Smulevich, G. (2004) Comparison between catalase-peroxidase and cytochrome *c* peroxidase. The role of the hydrogen-bond networks for protein stability and catalysis, *Biochemistry 43*, 5792-5802.

82.   Hillar, A., Peters, B., Pauls, R., Loboda, A., Zhang, H., Mauk, A. G., and Loewen, P. C. (2000) Modulation of the activities of catalase-peroxidase HPI of *Escherichia coli* by site-directed mutagenesis, *Biochemistry 39*, 5868-5875.

83.   Regelsberger, G., Jakopitsch, C., Ruker, F., Krois, D., Peschek, G. A., and Obinger, C. (2000) Effect of distal cavity mutations on the formation of compound I in catalase-peroxidases, *J. Biol. Chem 275*, 22854-22861.

84.   Jakopitsch, C., Auer, M., Regelsberger, G., Jantschko, W., Furtmuller, P. G., Ruker, F., and Obinger, C. (2003) The catalytic role of the distal site asparagine-histidine couple in catalase-peroxidases, *Eur. J. Biochem 270*, 1006-1013.

85.   Welinder, K. G. (1991) Bacterial catalase-peroxidases are gene duplicated members of the plant peroxidase superfamily, *Biochim. Biophys. Acta 1080*, 215-220.

86.   Carpena, X., Melik-Adamyan, W., Loewen, P. C., and Fita, I. (2004) Structure of the C-terminal domain of the catalase-peroxidase KatG from *Escherichia coli*, *Acta Crystallogr. D Biol. Crystallogr 60*, 1824-1832.

87.   Baker, R. D., Cook, C. O., and Goodwin, D. C. (2004) Properties of catalase-peroxidases lacking its C-terminal domain, *Biochem. Biophys. Res. Commun 320*, 833-839.

88.   Kudalkar, S. N., Campbell, R. A., Li, Y., Varnado, C. L., Prescott, C., and Goodwin, D. C. (2012) Enhancing the peroxidatic activity of KatG by deletion mutagenesis, *J. Inorg. Biochem 116*, 106-115.

89.   Wang, Y., and Goodwin, D. C. (2013) Integral role of the I'-helix in the function of the "inactive" C-terminal domain of catalase-peroxidase (KatG), *Biochim. Biophys. Acta 1834*, 362-371.

90.   Donald, L. J., Krokhin, O. V., Duckworth, H. W., Wiseman, B., Deemagarn, T., Singh, R., Switala, J., Carpena, X., Fita, I., and Loewen, P. C. (2003) Characterization of the catalase-peroxidase KatG from *Burkholderia pseudomallei* by mass spectrometry, *J. Biol. Chem 278*, 35687-35692.

91.   Jakopitsch, C., Kolarich, D., Petutschnig, G., Furtmuller, P. G., and Obinger, C. (2003) Distal side tryptophan, tyrosine and methionine in catalase-peroxidases are covalently linked in solution, *FEBS Lett 552*, 135-140.

92.   Zamocky, M., Droghetti, E., Bellei, M., Gasselhuber, B., Pabst, M., Furtmuller, P. G., Battistuzzi, G., Smulevich, G., and Obinger, C. (2012) Eukaryotic extracellular catalase-peroxidase from Magnaporthe grisea – Biophysical/Chemical characterization of the first representative from a novel phytopathogenic KatG group, *Biochimie 94*, 673-683.

93.   Ghiladi, R. A., Knudsen, G. M., Medzihradszky, K. F., and Ortiz de Montellano, P. R. (2005) The Met-Tyr-Trp cross-link in *Mycobacterium tuberculosis* catalase-peroxidase (KatG): Autocatalytic formation and effect on enzyme catalysis and spectroscopic properties, *J. Biol. Chem 280*, 22651-22663.

94.   Ghiladi, R. A., Medzihradszky, K. F., and Ortiz de Montellano, P. R. (2005) Role of the Met-Tyr-Trp cross-linking in *Mycobacterium tuberculosis* catalase-peroxidase (KatG) as revealed by KatG (M255I), *Biochemistry 44*, 15093-15105.

95.   Jakopitsch, C., Auer, M., Ivancich, A., Ruker, F., Furtmuller, P. G., and Obinger, C. (2003) Total conversion of bifunctional catalase-peroxidase (KatG) to monofunctional peroxidase by exchange of a conserved distal side tyrosine, *J. Biol. Chem 278*, 20185-20191.

96.   Yu, S., Girotto, S., Zhao, X., and Magliozzo, R. S. (2003) Rapid formation of compound II and a tyrosyl radical in the Y229F mutant of *Mycobacterium tuberculosis* catalase-peroxidase disrups catalase but not peroxidase function, *J. Biol. Chem 278*, 44121-44127.

97.   Regelsberger, G., Jakopitsch, C., Furtmuller, P. G., Ruker, F., Switala, J., Loewen, P. C., and Obinger, C. (2001) The role of distal tryptophan in the bifunctional activity of catalase-peroxidases, *Biochem. Soc. Trans 29*, 99-105.

98.   Singh, R., Wiseman, B., Deemagarn, T., Donald, L. J., Duckworth, H. W., Carpena, X., Fita, I., and Loewen, P. C. (2004) Catalase-peroxidases (KatG) exhibit NADH oxidase activity, *J. Biol. Chem 279*, 43098-43106.

99. Carpena, X., Wiseman, B., Deemagarn, T., Singh, R., Switala, J., Ivancich, A., Fita, I., and Loewen, P. C. (2005) A molecular switch and electronic circuit modulate catalase activity in catalase-peroxidases, *EMBO Rep 6*, 1156-1162.

100. Johnson, K., Froland, W. A., and Schultz, P. G. (1997) Overexpression, purification, and characterization of the catalase-peroxidase KatG from *Mycobacterium tuberculosis*, *J. Biol. Chem 272*, 2834-2840.

101. Jakopitsch, C., Ruker, F., Regelsberger, G., Dockal, M., Peschek, G. A., and Obinger, C. (1999) Catalase-peroxidase from the cyanobacterium *Synechocystis* PCC 6803: cloning, overexpression in *Escherichia coli*, and kinetic characterization, *Biol. Chem 380*, 1087-1096.

102. Kengen, S. W., Bikker, F J., Hagen, W. R., de Vos, W. M., and van der Oost, J. (2001) Characterization of a catalase-peroxidase from the hyperthermophilic archeon *Archaeoglobus fulgidus*, *Extremophiles 5*, 323-332.

103. Jakopitsch, C., Regelsberger, G., Furtmuller, P. G., Ruker, F., Peschek, G. A., and Obinger, C. (2002) Engineering the proximal heme cavity of catalase-peroxidase, *J. Inorg. Biochem 91*, 78-86.

104. Ivancich, A., Jakopitsch, C., Auer, M., Un. S., and Obinger, C. (2003) Protein-based radicals in the catalase-peroxidase of *Synechocystis* PCC 6803: a multifrequency EPR investigation of wild-type and variants on the environment of the heme active site, *J. Am. Chem. Soc 125*, 14093-14102.

105. Varnado, C. L., Hertwig, K. M., Thomas, R., Roberts, J. K., and Goodwin, D. C. (2004) Properties of a novel periplasmic catalase-peroxidase from *Escherichia coli* O157:H7, *Arch. Biochem. Biophys 421*, 166-174.

106. Li, Y., and Goodwin, D. C. (2004) Vital roles of an interhelical insertion in catalase-peroxidase bifunctionality, *Biochem. Biophys. Res. Commun 318*, 970-976.

107. Claiborne, A., and Fridovich, I. (1979) Purification of the o-dianisidine peroxidase from *Escherichia coli* B: physicochemical characterization and analysis of its dual catalatic and peroxidatic activities, *J. Biol. Chem 254*, 4242-4252.

108. Moore, R. L., Powell, L. J., and Goodwin, D. C. (2008) The kinetic properties producing the perfunctory pH profiles of catalase-peroxidases, *Biochim. Biophys. Acta 1784*, 900-907.

109. Alfonso-Prieto, M., Biarnes, X., Vidossich, P., and Rovira, C. (2009) The molecular mechanism of the catalase reaction, *J. Am. Chem. Soc 131*, 11751-11761.

110. Vlasits, J., Furtmuller, P. G., Jakopitsch, C., Zamocky, M., and Obinger, C. (2010) Probing hydrogen peroxide oxidation kinetics of wild-type *synechocystis* catalase-peroxidase (KatG) and selected variants, *Biochem. Biophys. Acta 1804*, 799-805.

111. Smulevich, G., Jakopitsch, C., Droghetti, E., and Obinger, C. (2006) Probing the structure and bifunctionality of catalase-peroxidase (KatG), *J. Inorg. Biochem 100*, 568-585.

112. Vlasits, J., Jakopitsch, C., Bernroitner, M., Zamocky, M., and Furtmuller, P. G. (2010) Mechanism of catalase activity of heme peroxidases, *Arch. Biochem. Biophys 500*, 74-81.

113. Suarez, J., Ranguelova, K., Jarzecki, A. A., Manzerova, J., Krymov, V., Zhao, X., Yu, S., Metlitsky, L., Gerfen, G. J., and Magliozzo, R. S. (2009) An oxyferrous heme/protein-based radical intermediate is catalytically competent in the catalase reaction of *Mycobacterium tuberculosis* catalase-peroxidase (KatG), *J. Biol. Chem 284*, 7017-7029.

114. Deemagarn, T., Wiseman, B., Carpena, X., Ivancich, A., Fita, I., Loewen, P. C. (2007) Two alternative substrate paths for compound I formation and reduction in catalase-peroxidase KatG from *Burkholderia pseudomallei*, *Proteins 66*, 219-228.

115. Jakopitsch, C., Vlasits, J., Wiseman, B., Loewen, P. C., and Obinger, C. (2007) Redox intermediates in the catalase cycle of catalase-peroxidases from *Synechocystis* PCC 6803, *Burkholderia pseudomallei*, and *Mycobacterium tuberculosis*, *Biochemistry 46*, 1183-1193.

116. Colin, J., Wiseman, B., Switala, J., Loewen, P. C., and Ivancich, A. (2009) Distinct role of specific tryptophans in facilitating electron transfer or as [Fe(IV)=O Trp•] intermediates in the peroxidase reaction of *Burkholderia pseudomallei* catalase-peroxidase: a multifrequencyEPR spectroscopy investigation, *J. Am. Chem. Soc 131*, 8557-8563.

117. Singh, R., Switala, J., Loewen, P. C., and Ivancich, A. (2007) Two [Fe(IV)O Trp•] intermediates in *M. tuberculosis* catalase-peroxidase discriminated by multifrequency (9-285 GHz) EPR spectroscopy: reactivity toward isoniazid, *J. Am. Chem. Soc 129*, 15954-15963.

118. Carpena, X., Wiseman, B., Deemagarn, T., Herguedas, B., Ivancich, A., Singh, R., Loewen, P. C., and Fita, I. (2006) Roles for Arg426 and Trp111 in the modulation of NADH oxidase activity of the catalase-peroxidase KatG from *Burkholderia pseudomallei* inferred from pH-induced structural changes, *Biochemistry 45*, 5171-5179.

119. Vidossich, P., Alfonso-Prieto, M., Carpena, X., Fita, I., Loewen, P. C., and Rovira, C. (2010) The dynamic role of distal side residues in heme hydroperoxidase catalysis. Interplay between X-ray crystallography and ab initio MD simulations, *Arch. Biochem. Biophys 500*, 37-44.

120. Vidossich, P., Alfonso-Prieto, M., Carpena, X., Loewen, P. C., Fita, I., and Rovira, C. (2007) Versatility of the electronic structure of compound I in catalase-peroxidases, *J. Am. Chem. Soc 129*, 13436-13446.

121. Zhao, X., Suarez, J., Khajo, A., Yu, S., Metlitsky, L., and Magliozzo, R. S. (2010) A radical on the Met-Tyr-Trp modification required for catalase activity in catalase-peroxidase is established by isotopic labeling and site-directed mutagenesis, *J. Am. Chem. Soc 132*, 8268-8269.

122. Jakopitsch, C., Wanasinghe, A., Jantschko, W., Furtmuller, P. G., and Obinger, C. (2005) Kinetics of interconversion of ferrous enzymes, compound II and compound III, of wild-type *Synechocystis* catalase-peroxidase and Y249F: proposal for the catalatic mechanism, *J. Biol. Chem 280*, 9037-9042.

123. Zhao, X., Yu, S., Ranguelova, K., Suarez, J., Metlitsky, L., Schelvis, J. P. M., and Magliozzo, R. S. (2009) Role of the oxyferrous heme intermediate and distal side adduct radical in the catalase activity of *Mycobacterium tuberculosis* KatG revealed by the W107F mutant, *J. Biol. Chem 284*, 7030-7037.

124. Dunford, H. B. Heme Peroxidases, Wiley-VCH, New York, 1999.

125. Hiner, A. N. P., Hernandez-Ruiz, J., Rodriguez-Lopez, J. N., Garcia-Canovas, F., Brisset, N. C., Smith, A. T., Arnao, M. B., and Acosta, M. (2002) Reactions of the Class II peroxidases, lignin peroxidase and *Arthromyces ramosus* peroxidase, with hydrogen peroxide: catalase-like activity, compound III formation, and enzyme inactivation, *J. Biol. Chem 277*, 26879-26885.

126. Hiner, A. N. P., Hernandez-Ruiz, J., Williams, G. A., Arnao, M. B., Garcia-Canovas, F., and Acosta, M. (2001) Catalase-like oxygen production by horseradish peroxidase must predominantly be an enzyme-catalyzed reaction, *Arch. Biochem. Biophys 392*, 295-302.

127. Jittawuttipoka, T., Buranajitpakorn, S., Vattanaviboon, P., and Mongkolsuk, S. (2009) The catalase-peroxidase KatG is required for virulence of *Xanthomonas campestris* pv. campestris in a host plant by providing protection against low levels of H_2O_2, *J. Bacteriol 191*, 7372-7377.

128. Chromy, B. A., Choi, M. W., Murphy, G. A., Gonzales, A. D., Corzett, C. H., Chang, B. C., Fitch, J. P., and McCutchen-Maloney, S. L. (2005) Proteomic characterization of *Yersinia pestis* virulence, *J. Bacteriol 187*, 8172-8180.

129. Thulasiraman, V., McCutchen-Maloney, S. L., Motin, V. L., and Garcia, E. (2001) Detection and identification of virulence factors in *Yersinia pestis* using SELDI ProteinChip system, *BioTechniques 30*, 428-432.

130. Brunder, W., Schmidt, H., and Karch, H. (1996) KatP, a novel catalase-peroxidase encoded by the large plasmid of enterohaemorrhagic *Escherichia coli* O157:H7, *Microbiol 142*, 3305-3315.

131. Gerrish, R. G., Lee, J. E., Reed, J., Williams, J., Farrell, L. D., Spiegel, K. M., Sheridan, P. P., and Shields, M. S. (2007) PCR versus hybridization for detecting virulence genes of enterohemorrhagic *Escherichia coli*, *Emerg Infect Dis 13*, 1253-1255.

132. Bandyopadhyay, P., Byrne, B., Chan, Y., Swanson, M. S., and Steinman, H. M. (2003) *Legionella pneumophila* catalase-peroxidases are required for proper trafficking and growth in primary macrophages, *Infect. Immun 71*, 4526-4535.

133. Zamocky, M., Droghetti, E., Bellei, M., Gasselhuber, B., Pabst, M., Furtmuller, P. G., Battistuzzi, G., Smulevich, G., and Obinger, C. (2012) Eukaryotic extracellular catalase-peroxidase from *Magnaporthe grisea* – Biochemical/chemical characterization of the first representative from a novel phytopathogenic KatG group, *Biochimie 94*, 673-683.

134. Zhang, Y., Heym, B., Allen, B., Young, D., and Cole, S. (1992) the catalase-peroxidase gene and isoniazid resistance of *Mycobacterium tuberculosis*, *Nature 358*, 591-593.

135. Chouchane, S., Lippai, I., and Magliozzo, R. S. (2000) Catalase-peroxidase (*Mycobacterium tuberculosis* KatG) catalysis and isoniazid activation, *Biochemistry 39*, 9975-9983.

136. Lei, B., Wei, C. J., and Tu, S. C. (2000) Action mechanism of antitubercular isoniazid. Activation by *Mycobacterium tuberculosis* KatG, isolation, and characterization of InhA inhibitor, *J. Biol. Chem 275*, 2520-2526.

137. Rattan, A., Kalia, A., and Ahmad, N. (1998) Multidrug-resistant *Mycobacterium tuberculosis*: molecular perspectives, *Emerg. Infect. Dis 4*, 195-209.

138. Cade, C. E., Dlouhy, A. C., Medzihradszky, K. F., Salas-castillo, S. P., and Ghiladi, R. A. (2010) Isoniazid-resistance conferring mutations in *Mycobacterium tuberculosis* KatG: catalase, peroxidase, and INH-NADH adduct formation activities, *Protein Sci 19*, 458-474.

139. Poulos, T. L., Edwards, S. L., Wariishi, H., and Gold, M. H. (1993) Crystallographic refinement of lignin peroxidase at 2 , *J. Biol. Chem 268*, 4429-4440.

140. Switala, J., and Loewen, P. C. (2002) Diversity of properties among catalases, *Arch. Biochem. Biophys 401*, 145-154.

141. Singh, R., Wiseman, B., Deemagarn, T., Jha, V., Switala, J., and Loewen, P. C. (2008) Comparative study of catalase-peroxidases (KatGs), *Arch. Biochem. Biophys 471*, 207-214.

142.   Varnado, C. L., and Goodwin, D. C. (2004) System for the expression of recombinant hemoproteins in *Escherichia coli*, *Protein. Expr. Purif 35*, 76-83.

143.   Maniatis, T., Fritsch, E. F., and Sambrook, J. Molecular cloning: a laboratory manual, Cold Spring Habor Laboratory, Cold Spring Harbor, N.Y., 1982.

144.   Falk, J. K. in: Smith, K. M (Ed.), Porphyrins and Metalloporphyrins, Elsevier Publishing, New York, 1964, pp. 804-807.

145.   Scott, S. L., Chen, W. J., Bakac, A., and Espenson, J. H. (1993) Spectroscopic parameters, electrode potentials, acid ionization constants, and electron exchange rates of the 2,2'-azinobis(3-ethylbenzothiazoline-6-sulfonate) radicals and ions, *J. Phys. Chem 97*, 6710-6714.

146.   Josephy, P. D., Eling, T., and Mason, R. P. (1982) The horseradish peroxidase-catalyzed oxidation of 3,5,3',5'-tetramethylbenzidine. Free radical and charge-transfer complex intermediates, *J. Biol. Chem 257*, 3669-3675.

147.   Nelson, D. P., and Kiesow, L. A. (1972) Enthalpy of decomposition of hydrogen peroxide by catalase at 25 $^{\circ}$C (with molar extinction coefficient of H_2O_2 solutions in the UV), *Anal. Biochem 49*, 474-478.

148.   Goodwin, D. C., and Hertwig, K. M. (2003) Peroxidase-catalyzed oxidation of capsaicinoids: steady-state and transient-state kinetic studies, *Arch. Biochem. Biophys 417*, 18-26.

149.   Goodwin, D. C., Yamazaki, I., Aust, S. D., and Grove, T. A. (1995) Determination of rate constants for rapid peroxidase reactions, *Anal. Biochem 231*, 333-338.

150.   Wengenack, N. L., Todorovic, S., Yu, L., and Rusnak, F. (1998) Evidence for differential binding of isoniazid by *Mycobacterium tuberculosis* KatG and the isoniazid-resistant mutant KatG (S315T), *Biochemistry 37*, 15825-15834.

151.   Chouchane, S., Girotto, S., Kapetanaki, S., Schelvis, J. P. M., Yu, S., and Magliozzo, R. S. (2003) Analysis of heme structural heterogeneity in *Mycobacterium tuberculosis* catalase-peroxidase (KatG), *J. Biol. Chem 278*, 8154-8162.

152.   Kirkman, H. N., Galiano, S., and Gaetani, G. F. (1987) The function of catalase-bound NADPH, *J. Biol. Chem 262*, 660-666.

153.   Kirkman, H. N., and Gaetani. (2007) Mammalian catalase: a venerable enzyme with new mysteries, *Trends. Biochem. Sci 32*, 44-50.

154.   Jakopitsch, C., Obinger, C., Un, S., and Ivancich, A. (2006) Identification of Trp106 as the tryptophanyl radical intermediate in *Synechocystis* PCC6803 catalase-peroxidase by

multifrequency Electron Paramagnetic Resonance spectroscopy, *J. Inorg. Biochem 100*, 1091-1099.

155.   Hernandez-Ruiz, J., Arnao, M. B., Hiner, A. N. P., Garcia-Canovas, F., and Acosta, M. (2001) Catalase-like activity of horseradish peroxidase: relationship to enzyme inactivation by H_2O_2, *Biochem. J 354*, 107-114.

156.   Buckova, M., Godocikova, J., Zamocky, M., and Polek, B. (2010) Screening of bacteria isolates from polluted soils exhibiting catalase and peroxidase activity and diversity of their responses to oxidative stress, *Curr. Microbiol 61*, 241-247.

157.   Bearson, S., Bearson, B., and Foster, J. M. (1997) Acid stress responses in enterobacteria, *FEMS. Microbiol. Lett 147*, 173-180.

158.   Audia, J. P., Webb, C. C., and Foster, J. W. (2001) Breaking through the acid barrier: an orchestrated response to proton stress by enteric bacteria, *Int. J. Med. Microbiol 291*, 97-106.

159.   Bruno-Barcena, J. M., Azcarate-Peril, M. A., and Hassan, H. M. (2010) Role of antioxidant enzymes in bacterial resistance to organic acids, *Appl. Environ. Microbiol 76*, 2747-2753.

160.   Wiseman, B., Carpena, X., Feliz, M., Donald, L. J., Pons, M., Fita, I., and Loewen, P. C. (2010) Isonicotinic acid hydrazide conversion to isonicotinyl-NAD by catalase-peroxidases, *J. Biol. Chem 285*, 26662-26673.

161.   Zamocky, M., and Obinger, C. (2010) Molecular phylogeny of heme peroxidases. in *Biocatalysis Based on Heme Peroxidases* (Ayala, M., and Torres, E. eds.), Springer-Verlag, Berlin. pp 7-35.

162.   Mishra, S., and Imlay, J. (2012) Why do bacteria use so many enzymes to scavenge hydrogen peroxide? *Arch. Biochem. Biophys 525*, 145-160.

163.   Tanabe, S., Ishii-Minami, N., Saitoh, K., Otake, Y., Kaku, H., Shibuya, N., Nishizawa, Y., and Minami, E. (2011) The role of catalase-peroxidase secreted by *Magnaporthe oryzae* during early infection of rice cells, *Molecular plant-microbe interactions: MPMI 24*, 163-171.

164.   Uhlich, G. A. (2009) KatP contributes to OxyR-regulated hydrogen peroxide resistance in *Escherichia coli* serotype O157:H7, *Microbiology 155*, 3589-3598.

165.   Uhlich, G. A., Chen, C. Y., Cottrell, B. J., Irwin, P. L., and Philips, J. G. (2012) Peroxide resistance in *Escherichia coli* serotype O157:H7 biofilms is regulated by both RpoS-dependent and –independent mechanisms, *Microbiology 158*, 2225-2234.

166. Passardi, F., Zamocky, M., Favet, J., Jakopitsch, C., Penel, C., Obinger, C., and Dunand, C. (2007) Phylogenic distribution of catalase-peroxidases: Are there patches of order in chaos? *Gene 397*, 101-113.

167. Zhang, Y., Vilcheze, C., and Jacobs, W. R., Jr. (2005) Mechanisms of drug resistance in *Mycobacterium tuberculosis*. in *Tuberculosis and the Tubercle Bacillus, 2nd Ed.* (Cole, S. T., Eisenach, K. D., Jacobs, W. R., Jr., and McMurray, D. N. eds.), American Society for Microbiology, Washington, D.C. pp 155-140.

168. Guo, H., Seet, Q., Denkin, S., Parsons, L., and Zhang, Y. (2006) Molecular characterization of isoniazid-resistant clinical isolates of *Mycobacterium tuberculosis* from the USA, *J. Med. Microbiol 55*, 1527-1531.

169. Suarez, J., Ranguelova, K., Schelvis, J. P., and Magliozzo, R. S. (2009) Antibiotic resistance in *Mycobacterium tuberculosis*: Peroxidase intermediate bypass causes poor isoniazid activation by the S315G mutant of *M. tuberculosis* catalase-peroxidase (KatG), *J. Biol. Chem 284*, 16146-16155.

170. Patterson, W. R., and Poulos, T. L. (1995) Crystal structure of recombinant pea cytosolic ascorbate peroxidase, *Biochemistry 34*, 4331-4341.

171. Poulos, T. L., Freer, S. T., Alden, R. A., Edwards, S. L., Skogland, U., Takio, K., Eriksson, B., Xuong, N., Yonetani, T., and Kraut, J. (1980) The crystal structure of cytochrome *c* peroxidase, *J. Biol. Chem 255*, 575-580.

172. Zamocky, M., Regelsberger, G., Jakopitsch, C., and Obinger, C. (2001) The molecular peculiarities of catalase-peroxidases, *FEBS Lett. 492*, 177-182.

173. Jakopitsch, C., Kolarich, D., Petutschnig, G., Furtmuller, P. G., and Obinger, C. (2003) Distal side tryptophan, tyrosine and methionine in catalase-peroxidases are covalently linked in solution, *FEBS Lett. 552*, 135-140.

174. Jakopitsch, C., Droghetti, E., Schmuckenschlager, F., Furtmuller, P. G., Smulevich, G., and Obinger, C. (2005) Role of the main access channel of catalase-peroxidase in catalysis, *J. Biol. Chem 280*, 42411-42422.

175. Ator, M. A., and Ortiz de Montellano, P. R. (1987) Protein control of prosthetic heme reactivity. Reaction of substrates with the heme edge of horseradish peroxidase, *J. Biol. Chem 262*, 1542-1551.

176. Zhao, X., Khajo, A., Jarrett, S., Suarez, J., Levitsky, Y., Burger, R. M., Jarzecki, A. A., and Magliozzo, R. S. (2012) Specific function of the Met-Tyr-Trp adduct radical and residues Arg-418 and Asp-137 in the atypical catalase reaction of catalase-peroxidase KatG, *J. Biol. Chem 287*, 37057-37065.

177. Ndontsa, E. N., Moore, R. L., and Goodwin, D. C. (2012) Stimulation of KatG catalase activity by peroxidatic electron donors, *Arch. Biochem. Biophys 525*, 215-222.

178. Jakopitsch, C., Ivancich, A., Schmuckenschlager, F., Wanasinghe, A., Poltl, G., Furtmuller, P. G., Ruker, F., and Obinger, C. (2004) Influence of the unusual covalent adduct on the kinetics and formation of radical intermediates in *Synechocystis* catalase-peroxidase. A stopped-flow and EPR characterization of the Met^{275}, Tyr^{249}, and Arg^{429} variants, *J. Biol. Chem 279*, 46082-46095.

179. Ghiladi, R. A., Medzihradszky, K. F., Rusnak, F. M., and Ortiz de Montellano, P. R. (2005) Correlation between isoniazid resistance and superoxide reactivity in *Mycobacterium tuberculosis* KatG, *J. Am. Chem. Soc 127*, 13428-13442.

180. Moore, S. (Accessed January 2008) 'Round-the-horn site-directed mutagenesis – OpenWetWare. In http://openwetware.org/wiki/'Round-the-horn_site-directed_mutagenesis.

181. Marcinkeviciene, J. A., Magliozzo, R. S., and Blanchard, J. S. (1995) Purification and characterization of the Mycobacterium smegmatis catalase-peroxidase involved in isoniazid activation, *J. Biol. Chem 270*, 22290-22295.